The Dissertation Committee for Brandon Trent Certifies that this is the approved version of the following Dissertation:

Pulmonary vascular malfunction and inflammation during *Orientia tsutsugamushi* infection

Committee:

Lynn Soong

Dr. Lynn Soong, Supervisor

David H Walker

Dr. David Walker

Sanjeev K. Sahni

Dr. Sanjeev Sanhi

Dr. Alfredo Torres

nahed ismail 7/31/2019

Dr. Nahed Ismail

Dissertation

Presented to the Faculty of the Graduate School of

The University of Texas Medical Branch

in Partial Fulfillment

of the Requirements

for the Degree of

Doctor of Philosophy

The University of Texas Medical Branch

July, 2019

Dedication

Dedicated to my Grandpa, Dr. Dennis Trent.

Acknowledgements

There are so many people I have to thank for getting me to this point. First and foremost, the individuals at UTMB who have helped me generously with this project. To my mentor Dr. Soong, thank you for the opportunity to study and explore my research interests in your lab. You provided guidance and help to me even when I had my own stubborn, and often wrong, ideas about the direction my projects should take. You have taught me invaluable lessons in science, experimental design, writing, and how to keep your head up during difficult experiments.

I have had helpful guidance throughout my entire dissertation work by my committee members. Drs. David Walker, Alfredo Torres, Sanjeev Sanhi, and Nahed Ismail. Your input has always been welcome advice that has allowed me to push through obstacles in my project (and to let me know when to drop a project direction!). Thank you for your help.

I've been very lucky to work with incredibly generous and patient fellow students, staff, and post-docs here at UTMB. Almost everything I know about *Orientia* I learned first from Dr. Tom Shelite. Tom – you have been not only a great friend, but also my sounding board for all my ideas and complaints and gave me invaluable training that allowed me to do all of this project. I would also like to thank Dr. Yuejin Liang, who is the hardest working scientist I know. Without his training, flow cytometry experience, and assistance in manuscript writing this dissertation would not have been possible. Dr. Donald Bouyer and members of his lab, especially Nicole Mendell have been incredibly generous with their lab space, reagents, and *Orientia* expertise. Their contributions are noted in almost all of my projects, thank you for allowing me to be a pseudo-part of your lab. Generous assistance was provided by a cast of visiting scientists, especially Drs. Peter Liu,

Wei Yang, and Yan Xing. Their contributions to figures and data, especially in regard to IFA staining, were important parts of this project and I thank them from the bottom of my heart for their hard work and patience with me.

I want to thank my family who have supported me through this whole process. To my Mom – you showed me how to love learning and to be happy even during difficult times. To my Dad – you showed me how to work hard, even when it's hard work. Thank you, I love you guys. To my wife Camille, it's hard to express how much your support and love have buoyed me through this dissertation. You sacrificed so much to help me attain this goal and have been so supportive. Thank you so much. I love you. To my son, Teddy – you make the hard days worth it. Thanks, bud.

Lastly, I want to thank my Grandpa, Dennis Trent. His love of science and microbiology was inspiring to me from a young age. I was fascinated by his knowledge of microbiology and the impact it had on the world, and I knew that I wanted to do what he did. Love you, Grandpa.

Pulmonary vascular malfunction and inflammation during *Orientia tsutsugamushi* infection

Publication No._____

Brandon Trent, Ph.D.

The University of Texas Medical Branch, 2019

Supervisor: Lynn Soong

Scrub typhus is a potentially lethal illness caused by infection with the bacterium, *Orientia tsutsugamushi*. Scrub typhus remains a neglected tropical disease, despite being a tremendous burden in endemic areas. Lung injury is one of the most common pathologies that arise from severe cases of scrub typhus, but the underlying mechanisms are unclear. Development of relevant animal models allow for investigation into the cellular populations that are contributing to the observed lung pathology during *O. tsutsugamushi* infection.

The first objective of this work was to characterize the activation of the pulmonary endothelium during infection. Although *O. tsutsugamushi* is considered an endotheliotropic bacterium, no research has been conducted to evaluate changes in the endothelium *in vivo* during infection. Prolonged activation and loss of barrier integrity in pulmonary endothelium are initial steps to the development of lung injury during infection. To this end, we analyzed the increase of expression of the activation markers and decrease of barrier proteins on pulmonary endothelial cells. Activation of endothelial cells results in

the recruitment of circulating immune cells, especially neutrophils; however, excessive neutrophil recruitment can exacerbate lung injury and endothelial damage. Neutrophils were recruited in significant numbers by late infection and developed an activated phenotype. Further, depletion of neutrophils at various points of infection attenuated either weight loss or mortality of infected mice and modulated the macrophage and T cell populations in the lungs. These data suggest a pathogenic and regulatory role of neutrophils during scrub typhus.

In addition to endothelial cells, *O. tsutsugamushi* has been shown to replicate in macrophages *in vitro* and *in vivo*. The second objective of this study was to determine the state of macrophage polarization in the lungs of mice lethally infected with *O. tsutsugamushi* and determine how this polarization affects bacterial growth. Macrophages were recruited in high numbers to the lung at both day 6 and day 9 of infection, and they were almost entirely polarized to an inflammatory, "M1", phenotype. The M1 polarization was also shown to be capable of slowing bacterial growth *in vitro* in comparison to macrophages polarized to an "M2" phenotype. Mechanisms of macrophage activation and restriction of *O. tsutsugamushi* growth are unknown.

TABLE OF CONTENTS

List of Tables

List of Figures

List of Abbreviations

ALCAM	Activated Leukocyte Cell Adhesion Molecule
Ang	Angiopoietin
ARDS	Acute Respiratory Distress Syndrome
Arg-1	Arginase 1
CD	Cluster of Differentiation
CLP	Cecal Ligation Puncture
CXCL	Chemokine (C-X-C motif)
DAMP	Danger Associated Molecular Pattern
DAPI	4′,6-diamidino-2-phenylindole
DNA	Deoxyribonucleic Acid
Fpr2	Formyl Peptide Receptor 2
HUVEC	Human Umbilical Vein Endothelial Cell
I.V.	Intravenous
IBA-1	Ionized Calcium-Binding Adaptor Molecule 1
ICAM	Intracellular Adhesion Molecule
IFN-γ	Interferon Gamma
IL	Interleukin
LPS	Lipopolysaccharide
MPO	Myeloperoxidase
MΦ	Macrophage
NET	Neutrophil Extracellular Trap

NLR	Nod-like Receptor
NOS2	Nitric Oxide Synthesis Gene 2
PAMP	Pathogen Associated Molecular Pattern
RNA	Ribonucleic Acid
siRNA	Silencing Ribonucleic Acid
SOCS	Suppression of Cytokine Signaling
Tie2	TEK Tyrosine Kinase
TLR	Toll-like Receptor
TNFα	Tumor Necrosis Factor Alpha
VCAM	Vascular Cell Adhesion Molecule
VE-Cadherin	Vascular Endothelial Cadherin
VEGF	Vascular Endothelial Growth Factor
VEGFR2	Vascular Endothelial Growth Factor Receptor 2
WRAIR	Walter Reed Army Institute of Research

Chapter 1: Introduction to *Orientia tsutsugamushi*

Orientia tsutsugamushi is an obligate intracellular bacterium and the causative agent of the life-threatening disease, scrub typhus [5]. The bacterium is transferred to mammalian hosts via the bite of a larval *Leptotrombidium* mite (also known as chiggers). Following an incubation period of 6-21 days infected individuals may develop signs of general of illness, such as fever, headache, cough, and malaise. During this incubation time, *O. tsutsugamushi* can spread systemically, resulting in infections in the lung, liver, heart, and other organs [6]. If left untreated, scrub typhus can manifest as interstitial pneumonia, myocardial and hepatic inflammation, and meningoencephalitis [7]. Severe cases of scrub typhus can progress to life-threatening clinical manifestations, including acute renal failure, acute respiratory distress syndrome (ARDS), and multiple organ dysfunction syndrome [7-9]. These complications lead to poor patient prognosis and, in the pre-antibiotic era, some endemic areas were reporting mortality rates as high as 40-45% during outbreaks [10]. Multiple risk factors including age of the infected individual and delayed antibiotic treatment contribute to the severity and outcome of the infection [9, 11].

O. tsutsugamushi is endemic to an area known as the "tsutsugamushi triangle". Geographically, the triangle encompasses areas from northern Australia to Japan to West India (**Fig. 1.1**)[1].

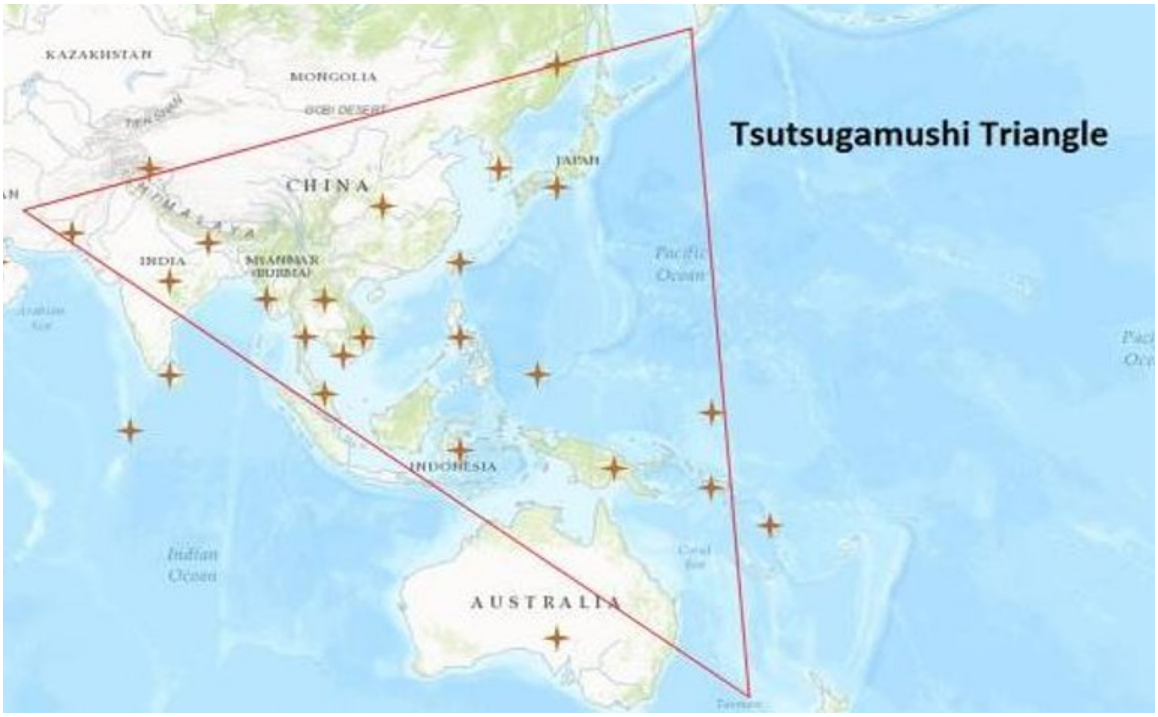

Fig.1.1: Geographic area of the "tsutsugamushi triangle." Scrub typhus is endemic to a large portion of Southeast Asia and Northern Australia, encompassing not only a large geographic region, but also billions of individuals [1].

Although somewhat geographically limited, more than one billion individuals reside in the tsutsugamushi triangle, and there are a suspected one million new cases of scrub typhus each year [5]. Due to underreporting, incorrect diagnoses, and early symptoms that compare to various diseases, scrub typhus has long been considered a neglected pathogen, despite the fact that within endemic areas, scrub typhus is reported to cause a substantial proportion (approximately 15-23%) of reported febrile illness [12, 13]. Recent reports indicate that a number of countries, including India and South Korea, experienced an increase of scrub typhus outbreaks [14, 15]. The reason for the increase in cases is unknown. However, it is speculated to be due to increased surveillance and reporting, improvements in diagnoses, and deforestation and warming climates leading to increased contact with the mite vector [5, 14]. Interestingly, as the prevalence and disease burden of scrub typhus is being more fully appreciated in endemic areas, a recent report has also

identified scrub typhus cases in South America, a continent previously believed to be free from the disease [16].

Scrub typhus, was first described in 1878 by Baelz and Kawakami, calling the disease ‘blood fever’ or ‘river fever’ as reported in 1926 by Rinya Kawamura[17]. In his 1926 report, Kawamura also describe that Australia and countries in Southeast Asia were reporting similar cases of ‘tsutsugamushi disease’. Scrub typhus became a particular concern to the U.S. and the Allied military force in the Pacific theater during World War II as thousands of troops began to fall ill with the disease during deployment, with reports of one British battalion losing 5% of its men to scrub typhus [18]. Rickettsial diseases have long played a significant role in shaping the outcomes of military campaigns from ancient Greece to modern day warfare [19]. Louse borne typhus (caused by *Rickettsia prowazekii*), which had caused tremendous illness and hospitalizations in previous wars was almost entirely prevented among allied troops with the employment of a *R. prowazekii* vaccine and use of DDT powder [18]. Unfortunately, DDT powder did not prevent mite feedings and thus by the end of the war there were an estimated 18,000 scrub typhus cases among allied troops [20]. Antibiotics available at the time did not affect the disease and thus scrub typhus plagued both Allied and Japanese troops till the end of World War II. It was not until late 1947 that a team of U.S. army doctors led by Dr. Joseph Smadel tested a new antibiotic, chloromycetin, in scrub typhus patients and began to see improvement in patient health [19]. This group would later be designated the “Walter Reed Army Institute of Research, or WRAIR, which is still active to this day in scrub typhus research [19]. Despite the availability of effective antibiotics, scrub typhus was one of the leading causes of fevers of unknown origin in U.S. troops during the Vietnam War [21, 22]. One military report

from 1967 recounted that between indigenous and U.S. fighting forces, roughly 13% of deployed forces were reporting back to base with scrub typhus [23]. The report also mentions the high probability that scrub typhus cases were significantly underreported due to misdiagnoses or lack of reporting [23].

Present day cases of scrub typhus are due to contact with infected mites in rural, developing, or urban areas, although studies taken from the general population of endemic areas reveal that a substantial number of individuals are seropositive to *O. tsutsugamushi* antigen [1]. Furthermore, a review by Xu *et al*. documented the numerous scrub typhus outbreaks in endemic regions both past and present [1]. Coupled with the growing case reports in South Korea and India and the newly discovered *Orientia* infection cases in Chile, studies to elucidate the pathogenesis and immune response during scrub typhus are of the utmost importance.

PULMONARY INVOLVEMENT DURING *O. TSUTSUGAMUSHI* INFECTION

Lung infection is a common occurrence during scrub typhus, and patients typically develop mild interstitial pneumonitis during self-resolving or promptly treated scrub typhus [24]. However, in severe cases, pulmonary pathology includes lung hemorrhage, pulmonary edema, damage to pulmonary vasculature, and diffuse cellular infiltration resulting in ARDS [2, 25](**Fig. 1.2**).

ARDS is a serious clinical syndrome that is characterized by lung injury leading to dyspnea, hypoxemia, and pulmonary infiltration [26]. Pathophysiology of ARDS begins with damage to lung endothelial cells leading to accumulation of protein- rich edema in the interstitial and alveolar spaces. Damage to the vasculature results in the production of proinflammatory cytokines (i.e., CXCL8, TNFα), leading to recruitment of leukocytes, especially neutrophils that in turn secrete their own chemokines and effector proteins, contributing to the proinflammatory microenvironment and cellular damage. Without resolution of inflammation and/or prompt treatment, atelectasis and eventual death may occur [26].

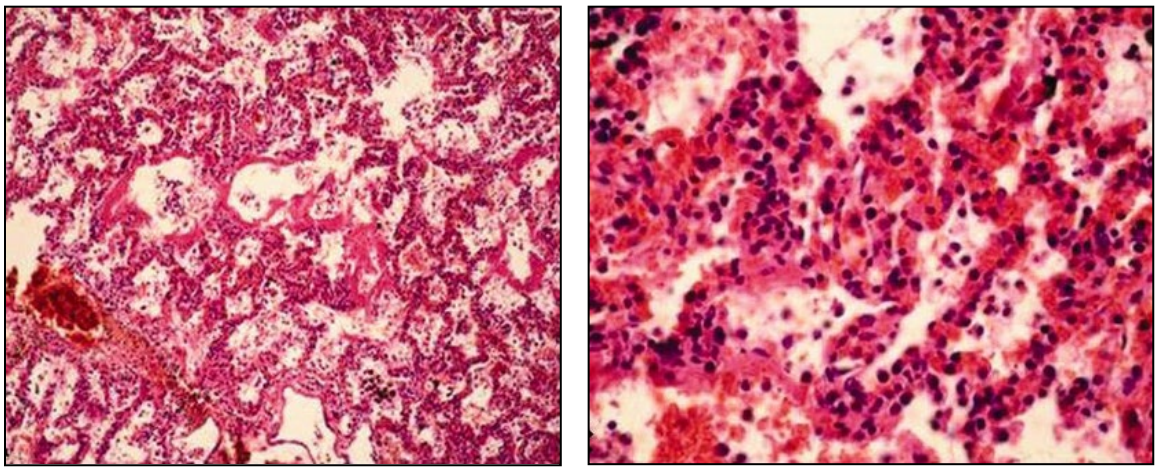

Fig.1.2: Human pulmonary pathology from scrub typhus induced ARDS. Taken from Hsu *et al.*, these images display the cellular infiltration, alveolar damage, and hyaline membrane formation that occur in ARDS development from scrub typhus. 100x (left) and 400x (right) [2].

ARDS development during scrub typhus is reported to occur in 6–44% of cases [7, 8, 11, 27]; risk factors of scrub typhus patients to develop ARDS include septic shock, hypoalbuminemia, high circulating white blood cell counts, delayed antibiotic treatment, and advanced age [11, 28]. Scrub typhus patients who developed ARDS presented with various clinical features, including pleural effusion, peribronchial thickening, hyaline membrane formation, and occasionally, pulmonary edema [2, 29, 30]. Recent studies from

our group and others have established murine models of *O. tsutsugamushi* infection that mimic various severities of scrub typhus observed in humans [4, 31, 32]. These models, coupled with known human infection data, are now being used to answer questions regarding tissue pathology and immune response during the infection (**Table 1.1**). Work in this dissertation has been principally focused on investigating the lung immune response and role of several cell types during *O. tsutsugamushi* infection that play key roles in ARDS, focusing on endothelial cells, neutrophils, and macrophages (MΦs). While activation and interaction of these innate cells are well documented for other infectious and non-infectious lung injury models, similar studies have been lagged behind for animal models of scrub typhus. A better understanding of how these three types of immune cells interact with and respond to *O. tsutsugamushi* infection, and how they contribute to disease progression, is critical for the development of effective methods for the management of severe scrub typhus.

Endothelial Cells

Endothelial cells are a cellular target of *O. tsutsugamushi* infection, during systemic infection. Using autopsy tissues from U.S. soldiers who died of scrub typhus, Moron and colleagues have reported in 2001 that *O. tsutsugamushi* is readily observed in endothelial cells in infected tissues, including the lung, late in infection [6]. Immunohistochemical analyses of patient lung samples further suggest ARDS development in severe scrub typhus cases [2]. While there are lines of *in vitro* evidence for *O. tsutsugamushi*-induced activation of human endothelial cells and subsequent cell death [33-35], there are no detailed reports for the mechanisms determining acute lung injury and ARDS development in scrub typhus.

It is well documented from other severe diseases that EC activation and damage are hallmarks of acute lung injury and ARDS development [36, 37]. Endothelial activation can be triggered directly via pathogen replication and the recognition of pathogen-associated molecular pattern molecules, or indirectly via recognition of damage-associated molecular pattern (DAMP) molecules or inflammatory cytokines. While EC activation promotes leukocyte adhesion/transmigration, antigen presentation, and cytokine production [38, 39], uncontrolled endothelial activation and cell death can alter vascular function, resulting in excessive influx of neutrophils and MΦs/monocytes to the lung interstitium, increased vascular permeability leading to edema buildup, tissue hypoxemia, and ARDS [40-42].

For *O. tsutsugamushi* infection models, only a few *in vivo* studies document endothelial activation and injury, but such studies have provided important insights into the pathogenesis of this endothelial-tropic pathogen. Since 2014, our group has documented pulmonary endothelial cellular tropism in C57BL/6 mice infected with *O. tsutsugamushi* Karp strain via the intravenous (i.v.) route [31], or the intradermal route [4, 43]. Regardless of the routes of inoculation, the mouse lungs carry the highest bacterial loads compared with the liver, spleen, kidney, and brain [4, 31, 43]. Likewise, Keller and colleagues used a footpad inoculation of *O. tsutsugamushi* Karp strain in BALB/c mice and confirmed that the lungs carry the highest bacterial loads, but bacteria were interpreted to be localized within pulmonary MΦs, rather than in pulmonary endothelial cells [32]. At present, it is unclear whether *O. tsutsugamushi* preferentially replicates within endothelial cells or phagocytes at different stages or severities of diseases in these mouse models.

Sublethal infection via intradermal inoculation of mice with *O. tsutsugamushi* strains Karp, Gilliam, or Woods resulted in increased circulation of the endothelial markers

such as soluble VCAM-1 and soluble ICAM-1 [44], indicating increased endothelial activation during infection. The sICAM-1 levels were also significantly increased following intradermal inoculation of rhesus macaques [45]. Supporting the data from the animal models, circulating markers of endothelial activation, sVCAM-1 and sALCAM (soluble activated leukocyte cell adhesion molecule) were found to be increased in human patients with scrub typhus compared to healthy controls and correlated with levels of organ dysfunction [46].

Previous work in our lab has shown that *O. tsutsugamushi* infection of endothelial cells can induce the expression of IL-33, a nucleus-located alarmin molecule that belongs to the IL-1 superfamily, and that exogenous addition of recombinant IL-33 during murine infection results in a more severe disease course [47]. While the mechanism of action of IL-33 in scrub typhus pathogenesis remains unclear, IL-33 is released from damaged endothelial cells and other host cells is processed and activated via phagocyte-derived enzymes, acting as a DAMP molecules on nearby endothelium [48, 49]. Investigation of human scrub typhus patients will allow us to determine circulating IL-33 levels during various stages of disease and help to understand the inflammatory response to *O. tsutsugamushi* infection.

Our studies in mouse models also revealed the potential use of the angiopoietin 2 (Ang2) to angiopoietin 1 (Ang1) ratio as biomarkers for severe *O. tsutsugamushi* infection [3]. Ang2 and Ang1 are ligands of the predominantly endothelial-expressed receptor, Tie2 [50]. Ang1 is constitutively expressed by cells to promote endothelial quiescence and effective barrier function [51], while Ang2 is released/produced by endothelial cells during endothelial damage or activation to bind to Tie2 and act as an antagonist [51]. Ang2

increase and Ang1 decrease have been shown to correlate with ARDS development in humans and animal models [52, 53]. Additionally, decrease in Tie2 expression and angiopoietin imbalance have been noted in several diseases often manifesting lung injury and ARDS including, malaria [54, 55], influenza [54], and sepsis [54, 56, 57].

Neutrophils

Often considered as the "first responders" during tissue injury or infection, neutrophils are the most abundant leukocyte in circulation [58] and they are a critical component of the innate immune response. Neutrophil recruitment plays an important function in early control of human pathogens [59, 60]; however, prolonged neutrophil involvement can be detrimental to host health [59, 61], contributing to the development of acute lung injury and ARDS [62-64]. Neutrophil effector functions include phagocytosis and killing of bacteria, release of antimicrobial granule contents, and release of neutrophil extracellular traps (NETs). These latter two functions work to combat pathogens, but can also damage host tissues [63].

Few studies have been conducted to address the role of neutrophils during scrub typhus. Early *in vitro* work revealed that after incubating *in vitro*, *O. tsutsugamushi* could be found within neutrophils in both phagosomes and also in the extracellular space [65]. Chemokines for neutrophil recruitment, CXCL1 and CXCL2, are increased at a transcriptional level by 6 dpi in the liver, spleen, and lungs of i.v. infected mice [3]. These chemokines are critical for transendothelial migration of neutrophils from the circulation to areas of infection [66] via interaction with the receptor CXCR2. Human patient data mirror mouse studies, as scrub typhus patients display an increase of circulating CXCL8,

a potent neutrophil chemoattractant in humans that, like CXCL1 and CXCL2, signals through the receptor CXCR2 [67]. CXCL8 is increased in individuals with ARDS and is believed to contribute to ARDS pathology via neutrophil recruitment, inhibiting neutrophil apoptosis, and activating lung endothelium [68, 69]. CXCL8 increase in scrub typhus patients has been shown to correlate with disease severity and mortality [70]. Investigation of neutrophil expression of the receptor of these neutrophil chemoattractants, CXCR1 and CXCR2, has not been examined in either humans or experimental animal studies, but may provide important details on whether recruited and circulating neutrophils are protective or deleterious at various points of infection as they are for bacterial sepsis [71].

Neutrophil pulmonary recruitment and activity during *O. tsutsugamushi* infection have been primarily studied in murine models (Table 1.1). Immunohistochemical studies in both the footpad and i.v. infection models demonstrated neutrophil infiltration of the pulmonary interstitium [3, 32]. Lung tissues from infected mice also stained positive for myeloperoxidase (MPO), a peroxidase enzyme abundantly present in neutrophil primary granules that catalyzes hydrogen peroxide to hypochlorous acid as an antimicrobial mechanism (**Fig. 1.3**)[3].

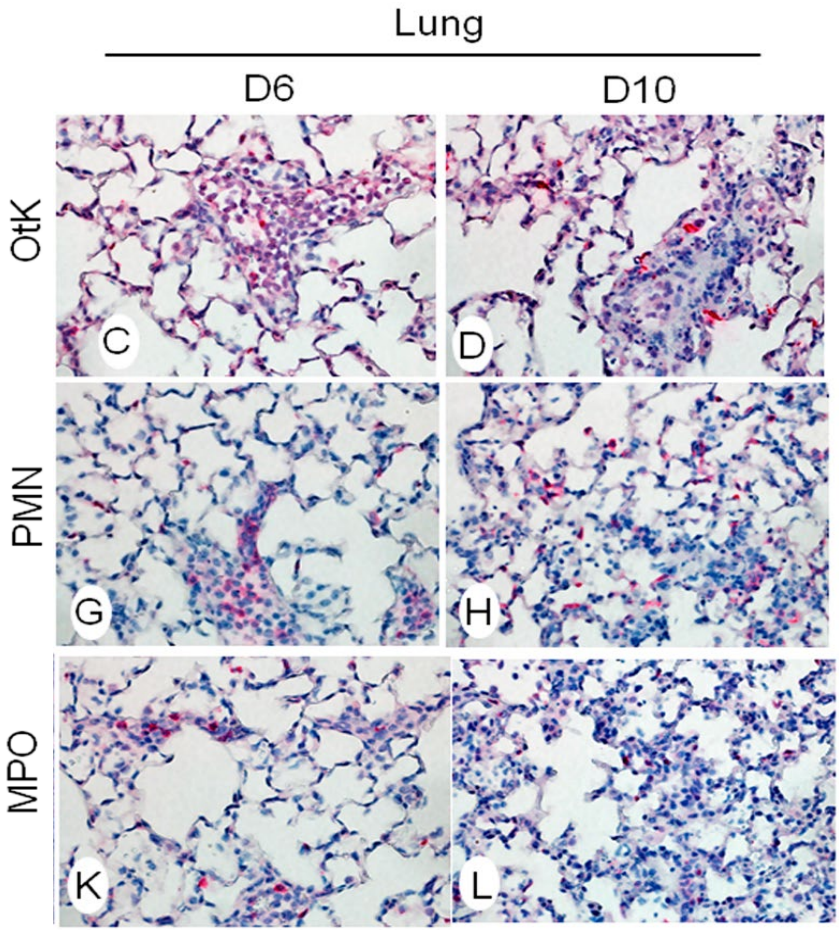

Fig.1.3: Immunohistochemical (IHC) staining of *Orientia* (OtK) neutrophils (PMN) and MPO$^+$ cells in the lungs of mice lethally infected with *O. tsutsugamushi*. Early work in our lab used IHC to demonstrate the appearance of neutrophils and MPO$^+$ cells at 6 and 10 dpi. [3]. Importantly, large cellular infiltrates are observed in our mouse model as is seen in severe human cases as well (**Fig.1.2**).

In one of the few human studies regarding neutrophil activation during *O. tsutsugamushi* infection, Paris *et al.* showed that markers of neutrophil activation and possible NET formation were also significantly upregulated in the plasma of severe human scrub typhus patients compared to less severe scrub typhus cases and patients with murine typhus [72, 73]. NET formation in the lung from neutrophils could be linked to ARDS development as NET formation is known to contribute to epithelial and endothelial cytotoxicity, a common hallmark of ARDS [61]. Further highlighting the importance of NET formation during ARDS, treatment of mice with DNase I or deletion of the *PADI4*

gene was shown to reduce lung injury during bacterial pneumonia induced ARDS [74], although these models have yet to be studied during *O. tsutsugamushi* infection. Despite recruitment and activation in significant numbers and correlation with disease severity, the role of neutrophils in scrub typhus pathogenesis has not been fully investigated. Contribution of specific neutrophil processes such as degranulation, NET formation, and production of reactive oxygen species to control of *O. tsutsugamushi* growth and dissemination requires further investigation given the pulmonary recruitment of neutrophils in animal models of scrub typhus. Whether neutrophils are critical for host protection or play a role in the pathogenesis of scrub typhus remains to be determined.

Macrophages

Both resident alveolar MΦs and recruited circulating monocytes have important roles in the development and resolution of acute lung injury and ARDS in other infections [75]. The *in vivo* MΦ depletion models have demonstrated that MΦs promote either a pathogenic or protective role during ARDS, depending on the method of lung injury induction and time of disease progression [76-78]. MΦs recruited to the lungs during ARDS have been shown to adopt an initial M1 MΦ profile required for generation of an acute inflammatory response and combating pathogens such as *Mycobacterium tuberculosis, Streptococcus pneumoniae,* and *Pseudomonas aeruginosa* [79-81]. Inflammatory M1 polarization is believed to be, in part, responsible for initiation of ARDS via secretion of inflammatory cytokines and chemokines and production of reactive oxygen and nitrogen species [80, 82]. Shifting of the pulmonary MΦ population from a

predominantly M1 phenotype to an alternative M2 phenotype is understood to be important for resolution of lung inflammation and tissue healing [80, 81, 83].

During *O. tsutsugamushi* infection, MΦs can serve not only as a cellular target of bacterial replication but also as an initiator of the inflammatory response [6, 84]. Studies of eschars in both human [5] and rhesus macaques [44] demonstrated the localization of *O. tsutsugamushi* in antigen-presenting cells (including MΦs). Early uptake/infection of *O. tsutsugamushi* MΦs in the eschar lesion may propagate the lymphogenous dissemination of the bacteria from the skin to regional lymph nodes. The *in vitro* infection of MΦs by *O. tsutsugamushi* has been shown to generate inflammasome activation [85], initiate inflammatory signaling cascades [86], and generate production of chemokines for recruiting T cells, neutrophils, and monocytes [84]. Many of the preceding MΦ-*O. tsutsugamushi* interaction studies have been discussed in detail in the recent review by Diaz *et al*. [87], and recent *in vitro* studies as to how *O. tsutsugamushi* establish infection in MΦs and modulate the immune response are important topics of investigation [88, 89].

The recruitment and role of pulmonary MΦs during systemic *O. tsutsugamushi* infection have been investigated using various *in vivo* murine models of infection. Footpad inoculation generates a systemic but sublethal infection that promotes MΦ recruitment in the lungs of infected mice. Work by Keller *et al*. using this model demonstrated that lung recruited MΦs were observed in the pleura and bronchus-associated lymphatic tissue after infection [32]. Furthermore, *O. tsutsugamushi* was present in pulmonary MΦs, and there was evidence of iNOS (inducible nitric oxide) production that correlated with recruitment of MΦs to the lungs of infected mice [32]. iNOS production has also been observed in human alveolar MΦs, from patients who succumbed to ARDS during severe scrub typhus

[2]. Generation of iNOS to combat invading pathogens is a product of MΦ activation and associated with M1 polarization. Further *in vitro* studies showed that mouse MΦs activated with IFN-γ were able to limit *O. tsutsugamushi* growth compared to untreated MΦs, but this growth inhibition was ablated when an the IFN-γ-treated MΦs were given the iNOS inhibitor, N-monomethylarginine [32]. *In vivo* evidence of inflammatory M1 polarization is confirmed by transcriptome analysis of human monocytes as well as peripheral blood mononuclear cells from human scrub typhus patients [90]. While M1 polarization has been shown to contribute to lung injury and ARDS development [80], the contribution of M1-polarized MΦs to lung injury during scrub typhus is still unclear. Furthermore, the presence/role of M2 MΦs during *O. tsutsugamushi* infection has not been explored. M2 MΦs are critical for inflammation resolution and removal of apoptotic cells, particularly neutrophils, thus helping to prevent ARDS development [80]. As both a cellular target of *O. tsutsugamushi* infection and as a coordinator of inflammation and lung injury, MΦ polarization and antibacterial mechanisms such as iNOS production present vital areas of research in scrub typhus to better understand bacterial dissemination and disease progression.

Table 1.1: Endothelial cell, neutrophil, and macrophage presence and function in the lungs during scrub typhus

Lung				
Cell Type	Host	Infection Route	Phenotype	References
Macrophage	Mouse	Footpad	Recruitment of macrophages to lung pleura and bronchus-associated lymphatic tissue (BALT). *Orientia* present in alveolar macrophages. Evidence of pulmonary iNOS production. Immunofluorescent staining confirmed the presence of infected macrophages in BALT. $B_2m^{-/-}$ (MHC I deficient) mice have decreased macrophage recruitment to BALT during infection.	Keller 2014 Xu 2017
		Intradermal	Increase in macrophage activating cytokines and chemokines including TNF-α, MCP-1, MIP-1α, and MIP-1β.	Soong 2016
		Intravenous	Increase in protein pulmonary protein and transcript levels of TNF-α and IFN-γ.	Soong 2014, Soong 2016
	Human	Natural Infection	$iNOS^+$ macrophages in lung interstitium that colocalized with Orientia antigen. M1 transcriptome present in circulating PBMCs.	Hsu 2008 Tantibhedhyangkul 2011
Neutrophils	Mouse	Footpad	Neutrophils recruited heavily to inflammatory foci and the pleura of infected mouse lungs.	Keller 2014
		Intradermal	Increased KC (analogous to CXCL8) chemokine production in lungs during infection.	Soong 2016
		Intravenous	Neutrophil recruitment to lungs by D6-D9 of infection. Large portions of recruited leukocytes stain MPO^+ (IHC) indicating activation of neutrophil populations.	Soong 2014

			Increased lung transcript production of neutrophil chemokines CXCL1 and CXCL2.	
Endothelial Cells	Mouse	Footpad	*O. tsutsugamushi* was found to colocalize closely with, but not infect, lung endothelium during infection.	Keller 2014
		Intradermal	Infection of pulmonary endothelium confirmed via IHC.	Soong 2016
		Intravenous	Infection of lung endothelium confirmed via electronmicroscopy. Imbalance of Ang2/Ang1 transcript ratios at D6 of infection.	Shelite 2014
	Human	Natural Infection	Orientia identified in pulmonary endothelial cells. Endothelial damage and hyaline membrane noted in some severe cases.	Moron 2001, Hsu 2008 Hsu 2008

GAPS IN KNOWLEDGE

Due to the difficult nature of cultivating and genetically manipulating *O. tsutsugamushi*, many basic questions regarding disease pathogenesis and host immune response have gone unanswered thus far. As mentioned, despite being considered an endotheliotropic pathogen, very little is known about endothelial activation and function *in vivo*. The *in vitro* experiments have demonstrated the ability of *O. tsutsugamushi* to not only activate endothelial cells, but also induce apoptosis [33, 35]. Pulmonary endothelial activation, breakdown of barrier function, and death all directly contribute to acute lung injury during infection [37]. The Tie2/Angiopoietin signaling axis controls many of these functions, and Ang2/Ang1 transcript production has been shown to be altered during *in vivo* infection with *O. tsutsugamushi*, suggesting its involvement in disease pathogenesis, as observed in other diseases [3].

Activation of endothelial cells is part of the early innate immune response and results in recruitment of innate immune cells such as neutrophils and monocytes/macrophages. Neutrophils have been shown in multiple scrub typhus murine models to be recruited to the lungs of infected mice [3, 32]. The recruitment of these neutrophils is correlated with an increase in transcripts of the neutrophil chemoattractants CXCL1 and CXCL2; however, the specific activation states of these neutrophils and their role during *O. tsutsugamushi* have not been addressed [3]. Neutrophils are important cells in combating extracellular pathogens such as fungi and extracellular bacteria, but whether the role of neutrophils is protective or pathogenic during infection with intracellular pathogens such as viruses and obligate intracellular bacterial pathogens is less defined [91]. Furthermore, neutrophil activation states are important in the pathogenesis of severe

systemic disease, such as bacterial sepsis, and contribute directly to lung tissue damage during acute lung injury [63, 92]. We sought to determine neutrophil recruitment and activation in infected lung tissues during severe *O. tsutsugamushi* infection, and whether the recruitment of neutrophils during *O. tsutsugamushi* to infected tissues contributes to control of the pathogen or to immunopathology and host mortality.

MΦ activation and polarization during scrub typhus have been investigated by several groups in both a mouse model and with human patients [32, 90, 93]. The consensus is that circulating monocytes/MΦ adopt an inflammatory profile during scrub typhus and this activation is also recapitulated *in vitro*. There is some debate in the field as to whether this activation acts to restrict bacterial growth or actually serves in favor of bacterial replication [32, 94]. We sought here to determine the polarization (both M1 and M2) and recruitment of macrophages in the lung during *O. tsutsugamushi* infection. Additionally, we investigated the effects of M1 and M2 polarization on *O. tsutsugamushi* growth.

By addressing these gaps in knowledge, we elucidated many of the early innate immune responses to *Orientia* infection to understand how the strong type-1 inflammatory response generated to *O. tsutsugamushi* infection acts to protect or damage the host.

HYPOTHESIS AND SPECIFIC AIMS

Previous work in Dr. Lynn Soong's lab focused on defining the strong type-1 immune response that we see in our murine model and the DAMPs that could be associated with this strong immune response [3, 47]. The lack of research regarding the immune response and *O. tustsugamshi* have led us to the **long term goal** to elucidate specifics of the immune response to severe *Orientia* infection and determine how elements of this strong inflammatory immune response affect disease pathogenesis and outcome. After

observing strong neutrophil recruitment visualized via immunohistochemistry in our murine model of scrub typhus, we hypothesized that sustained and uncontrolled neutrophil recruitment and activation exacerbate dysregulation of the endothelial functions, leading to tissue damage and lethality. To this end we developed specific aims that address this central hypothesis.

Specific Aim 1: Determine vascular dysregulation and neutrophil-mediated pathogenesis during infection. To address this specific aim, we utilized *in vivo* approaches using a newly developed murine model of severe scrub typhus. Past reports have demonstrated the endotheliotropic specificity of *Orientia* in human patients and have examined general circulating markers of endothelial activation during murine infection [6, 44]. Here we examined specific markers of endothelial angiogenesis, activation, and cell-cell adhesion in the lungs of infected mice. We demonstrated the disruption in the Tie2/Ang signaling axis that occurs during *Orientia* infection, and surprising effect of Ang1 recombinant protein administration or blocking of Ang2 during infection *in vivo.* Furthermore, we determined neutrophil recruitment and activation kinetics in the lungs of infected mice. We also evaluated the ability of neutrophil depletion to ameliorate disease and modulate immune populations during infection. These experiments are the first to investigate specific endothelial activation *in vivo* and to investigate the role of neutrophils during infection.

Specific Aim 2: Determine the kinetics of pulmonary macrophage polarization during infection and the role of macrophage polarization in *O. tsutsugamushi* replication. In addition to understanding the early innate immune responses of pulmonary endothelium and recruited neutrophils, we investigated the recruitment and polarization of

macrophages in the lung of infected mice. Macrophages are targets of infection but have been shown *in vitro* to have the capability to restrict growth of *O. tsutsugamushi* after IFN-γ stimulation [6, 32]. We determined the recruitment and polarization kinetics of macrophages in the lung during severe infection. Additionally, we investigated the effect of M1 or M2 polarization on bacterial growth *in vitro*.

Chapter 2: Materials and Methods

MOUSE INFECTION AND ETHICS STATEMENT

Female C57BL/6 mice were purchased from Envigo (Huntingdon, United Kingdom), maintained under specific pathogen-free conditions and used at 6-9 weeks of age, following protocols approved by the Institutional Animal Care and Use Committee (protocols # 9007082B and 1302003) at the University of Texas Medical Branch (UTMB) in Galveston, TX. All mouse infection studies were performed in the ABSL3 facility in the Galveston National Laboratory located at UTMB; all tissue processing and analysis procedures were performed in the BSL3 or BSL2 facilities. All procedures were approved by the Institutional Biosafety Committee, in accordance with Guidelines for Biosafety in Microbiological and Biomedical Laboratories. UTMB operates to comply with the USDA Animal Welfare Act (Public Law 89-544), the Health Research Extension Act of 1985 (Public Law 99-158), the Public Health Service Policy on Humane Care and Use of Laboratory Animals, and the NAS Guide for the Care and Use of Laboratory Animals (ISBN-13). UTMB is a registered Research Facility under the Animal Welfare Act, and has a current assurance on file with the Office of Laboratory Animal Welfare, in compliance with NIH Policy.

O. tsutsugamushi Karp strain was used herein; all infection studies were performed with the same bacterial stocks prepared from Vero cell infection, for which infectious organisms were quantified via a qPCR viability assay [4, 31]. Mice were inoculated intravenously (i.v.) with ~1.325×10^6 viable bacteria (a lethal dose in 200 µl), ~1.0×10^5 (a sublethal dose), 1.5×10^5 (a predominantly sublethal dose) or PBS and monitored daily for weight loss and

signs of disease. In most cases, tissue samples (4-5 mice/group) were collected at indicated days post-infection and inactivated for immediate or subsequent analyses.

Ethical approval for human samples used in this work was granted by the Institutional Review Board of both Seoul National University Hospital (IRB NO 1603-136-751) and Chungnam National University Hospital (IRB NO 2014-12-006). All patients and healthy volunteers provided written informed consent prior to sample collection

IMMUNOFLUORESCENCE MICROSCOPY

Mouse lung tissues were processed for immunofluorescent staining, as in our previous report [95]. Briefly, 6-μm frozen sections were blocked and incubated with the following rat or rabbit anti-mouse antibodies (1:200, purchased from Abcam, Cambridge, MA, USA, unless specified): anti-ICAM-1, anti-Ang1, anti-Ang2 (R&D Systems/Biotechne, McKinley Place NE, Minnesota), anti-Tie2, anti-VE-Cadherin (adherence junctions), anti-occludin (epithelial tight junctions), anti-MPO, anti-CD41 (platelets), anti-Ly6G (neutrophils), anti-IBA-1 (ionised calcium binding adapter molecule-1, a MΦ marker), anti-CD45 (BD Bioscience, San Jose, CA, USA), or anti-Ang2 (R&D Systems, Minneapolis, MN, USA). Staining endothelium in sections was done with FITC-conjugated *Griffonia Simplicifolia* lectin I (1:100, GSL I-B_4 lectin, Vector Lab, Burlingame, CA, USA). Bacteria were stained in various sections using rabbit anti-*O. tsutsugamushi* Karp serum (1:500) [31]. Bound antibodies were visualized by using Alexa Fluor 488- or 555-conjugated, goat anti-rat or anti-rabbit IgG (H+L, 1:1,000-1:2,000, Life Technologies, Grand Island, NY, USA). All sections were stained with DAPI (1:5,000, Sigma-Aldrich, St. Louis, MO, USA). Infected sections stained with secondary Abs and

DAPI only served as negative controls to optimize staining conditions. For each section, at least 6 low- and 6 high-magnification fields of the lung sections were imaged on a Carl Zeiss Axio Observer fluorescence microscope (Carl Zeiss Microscopy LLC, Thornwood, NY, USA) equipped with ApoTome and Zen imaging software. Acquisition settings were identical among samples of different experimental groups. Representative images at each time point are presented.

For *in vitro* studies, cells were seeded onto coverslips in 24-well plates (Falcon Corning, Corning, NY, USA). At indicated times of infection, slides were washed, fixed with 4% PFA for 20 min, and permeabilized with Triton X-100 for 15 min. After blocking with 10% BSA/3% goat serum for 1 h, cells were incubated with serum collected from *Orientia* infected mice (1:1,500) or rabbit anti-IBA-1 (1:250, Abcam) (1:50) at 4°C overnight and then with a secondary Ab: goat anti-mouse Alexa Fluor 488 (Thermo Fisher Scientific, Waltham, MA, USA) or donkey anti-rabbit Alexa Fluor 594 (Invitrogen/Thermo Fisher Scientific) and DAPI (1:1000, Thermo Fisher Scientific). The cover slips were mounted on slides by using an Antifade Mountant solution (Invitrogen/Thermo Fisher Scientific). Images were taken using an Olympus IX51 microscope (Olympus Corporation, Tokyo, Japan).

FLOW CYTOMETRY

Equivalent portions of lung tissues were harvested from infected and control mice, minced, and digested with 0.05% collagenase type IV (Gibco/Thermo Fisher Scientific) in Dulbecco's Modified Eagle's Medium (DMEM, Sigma-Aldrich, St. Louis, MO) for 30 mins at 37°C. Minced tissues were loaded into Medicons and homogenized using a BD

Mediamachine System (BD Biosciences, Franklin Lakes, NJ). Lung single-cell suspensions were made by passing lung homogenates through 70-µm cell strainers. Spleen homogenates were made by passing tissue through a 70-µm strainer. Lymphocytes were enriched by using Lympholyte-M Cell Separation Media (Burlington, NC). Red blood cells were removed by using Red Cell Lysis Buffer (Sigma-Aldrich). Leukocytes were stained with the Fixable Viability Dye (eFluor 506) (eBioscience/Thermo Fisher Scientific, Walthalm, MA) for live/dead cell staining, blocked with FcγR blocker, and stained with fluorochrome-labeled antibodies (Abs). The following Abs purchased from Thermo Fisher Scientific, BioLegend (San Diego CA), and BD Biosciences: PE-Cy7-anti-CD3ε (145-2C11), Pacific Blue-anti-CD4 (GK1.5), APC-Cy7-anti-CD8a (53-6.7), APC-anti-Ly6G (1A8-Ly6G), PE-anti-CD63 (NVG-2), APC-anti-CD31 (390), PE-anti-VEGFR2 (Avas12a1), FITC-anti-ICAM-1 (YN1/1.7.4), Pacific Blue-anti-CD45 (30-F11), PE-anti-CD80 (16-10A1), BV421-anti-CD206 (CO68C2), FITC-anti-CD64 (X54-5/7.1), PerCP-Cy5.5-anti-CD11b (M1/70), PE-anti-CD69 (H1.2F3), FITC-anti-CD103 (2E7), PerCP-Cy5.5-anti-CD49a (Ha31/8), Alexafluor 700-anti-B220 (RA3-6B2), PerCP-Cy5.5-anti-CD138 (281-2). Cells were fixed in 2% paraformaldehyde overnight at 4°C before cell analysis. Data were collected by a BD LSRFortessa (Becton Dickinson, San Jose, CA) and analyzed using FlowJo software version 8.86 (Tree Star, Ashland, OR). As previously reported for mouse lung tissues [96] $CD45^{+}CD31^{-}$ and $CD45^{-}CD31^{+}$ cells were considered hematopoietic cells and endothelial cells by flow cytometry, respectively.

WESTERN BLOT

Protein from lung tissues was extracted with RIPA lysis buffer (Cell Signaling Technology, Danvers, MA) and quantified with BCA Protein Assay kit (Thermo Fisher Scientific). Protein samples (40 μg/lane) were loaded onto 4-20% SDS-PAGE gels (Bio-Rad Laboratories, Hercules, CA, USA) and separated via electrophoresis before being transferred onto nitrocellulose membranes (Bio-Rad Laboratories). After blocking non-specific binding sites, membranes were respectively incubated with rabbit Abs specific to mouse Tie2 (1:500, Abcam), phospho-Tie2 (1:400, R&D System, USA), and GAPDH (1:15000, Novus Biologicals, USA), and an anti-rabbit secondary antibody (SouthernBiotech, Birmingham, AL, USA). After treatment with the Maximum Sensitivity Substrate (Thermo Fisher Scientific) for 1 min, the light signals were captured by Luminescent Image Analyzer (ImageQuant LAS 4000, GE Healthcare Bio-Sciences AB, Sweden). Protein bands were quantified by using image analysis software (ImageJ). Three independent experiments were performed.

INFECTION OF MOUSE NEUTROPHILS AND BONE MARROW-DERIVED MACROPHAGES

Bone marrow cells were collected from mouse femur and tibia and treated with red cell lysis buffer (Sigma). Neutrophils were purified by using an anti-Ly6G Microbead kit (Miltenyi Biotec, Auburn, CA), counted, and seeded in 48-well plates (Falcon Corning) in complete RPMI-1640 medium (Gibco). Neutrophils were innoculated with *O. tsutsugamushi* (1 MOI) for 4 h and compared with uninfected controls. For MΦ generation, bone marrow cells were grown in DMEM (Gibco) with 10% FBS, penicillin/streptomycin antibiotics, and 40 ng/ml M-CSF (BioLegend) and incubated at 37°C. Medium was changed at day 3, and cells were collected at day 7 and seeded onto 6- or 24-well plates for overnight. MΦs were treated with either 100 ng/ml LPS (for M1 polarization) or 10 ng/ml

mouse rIL-4 (for M2 polarization, Peprotech, Rocky Hill, NJ) for 24 h. Cells were then infected with *O. tsutsugamushi* (5 MOI) and centrifuged at 450 x g for 5 min to synchronize infection of the cells.

HUMAN UMBILICAL VEIN ENDOTHELIAL CELL (HUVEC) INFECTION

HUVECs (Cell Application, San Diego, CA) were maintained in complete Prigrow I medium supplemented with 3% heat-inactivated FBS (Applied Biological Materials, Vancouver, Canada) in 5% CO_2 at 37°C. All *in vitro* experiments were performed between cell passages 5 and 7, as described previously [47, 97]. For infection, HUVECs were cultivated in Prigrow I medium with 10% FBS and seeded onto 6-well plates (Corning Inc., Corning, NY). Confluent monolayers were infected with *Orientia* (3 and 10 MOI) for 24 h and compared with uninfected controls.

HUMAN SERUM COLLECTION AND MEASUREMENT OF ANG2 BY ELISA

Human serum samples were collected from healthy volunteers (n = 8) and scrub typhus patients (n = 32) after obtaining informed consent at the Chungnam National University Hospital in Daejeon, South Korea. Scrub typhus diagnosis was confirmed based on clinical symptoms and a positive serology: a 4-fold or greater rise in the titer of paired plasma or single cut-off titer of an IgM antibody ≥ 1:160 by an indirect immunofluorescence antibody assay (IFA) against *O. tsutsugamushi* antigens or passive hemagglutination assay (PHA) during hospital admission. Healthy volunteers had never been previously diagnosed with scrub typhus, and their sera were negative when examined by IFA. Patient plasma samples were classified into four groups based on their IFA titers. Ang2 concentration was

determined by using a commercial ELISA kit (Abcam), according to manufacturer's instructions.

HUMAN ANTIBODY TITER MEASURED BY IFA

L929 cells infected with three strains of *O. tsutsugamushi* (Boryong, Karp, and Gilliam strains) were harvested, mixed in equal amounts, and used as antigens to measure total IgG titers against *O. tsutsugamushi* via IFA. Briefly, infected L929 cells were harvested, washed with PBS, seeded onto Teflon-coated spot slides, and fixed with cold acetone for 10 min. The slides were stored at -70°C until use. Two-fold serially diluted (1:40 to 1:1280 in PBS) patient sera was added to the antigen-coated spot on the slide and incubated for 30 min in a wet chamber at room temperature. An Alexa Fluor 488-conjugated goat anti-human IgG (diluted 1:1000 in PBS, Molecular Probes, Waltham, MA, USA) was used as the secondary antibody. The stained slides were examined under an Olympus FV1000 laser scanning confocal microscope (Olympus, Tokyo, Japan). The endpoint titer of IFA was defined as the highest titer showing a fluorescence signal above the background.

QUANTITATIVE PCR AND REVERSE TRANSCRIPTASE PCR (QPCR AND QRT-PCR)

To determine bacterial loads, bone marrow-derived MΦs were collected at 3, 24, 48, and 72 hpi by using a DNeasy kit (Qiagen) and used for qPCR assays, as previously described [3]. Bacterial loads were normalized to total nanogram (ng) of DNA per μL for the same sample, and data are expressed as the gene copy number of 47-kDa protein per picogram (pg) of DNA. The copy number for the 47-kDa gene was determined by known

concentrations of a control plasmid containing single-copy insert of the gene. Gene copy numbers were determined via serial dilution (10-fold) of the control plasmid.

To measure host gene expression, mouse tissues or *in vitro*-infected cells were respectively collected in RNA*Later* (Ambion, Austin, TX) or Trizol solution at 4°C overnight to inactivate infectious bacteria and stored at -80°C for subsequent analyses. Total RNA was extracted by using RNeasy mini kits (Qiagen) and digested with RNase-free DNase (Qiagen); cDNA was synthesized with the iScript cDNA synthesis kit (Bio-Rad Laboratories, Hercules, CA). The quantitative RT-PCR (qRT-PCR) assays were performed with iTaq SYBR Green Supermix and a CFX96 Touch Real-Time PCR Detection System (Bio-Rad). PCR assays were denatured for 3 min at 95°C, followed by 40 cycles of 10s at 95°C and 30s at 60°C. Melt-curve analysis was also used to check the specificity of the amplification reaction. Relative abundance of transcripts was calculated by using the $2^{-\Delta\Delta CT}$ method and compared to housekeeping genes glyceraldehyde-3-phosphate dehydrogenase (GAPDH) or β-actin. Primers used in these analyses are listed in Table S1.

NEUTROPHIL DEPLETION

Female C57Bl/6 mice were infected with ~$2.5x10^5$ of *O. tsutsugamushi* Karp strain and treated intraperitoneally with anti-Ly6G antibody alone (50μg/mouse, Bio X Cell, West Lebanon, NH) at one day prior to infection (D-1) or at 4 days post infection (D4). Mice were monitored for weight, disease score, and survival. At D6 of infection lungs and spleens were collected for flow cytometry and bacterial load analysis.

SIMVASTATIN TREATMENT

Female C57Bl/6 mice were infected with ~1.0x10^6 of *O. tsutsugamushi* Karp strain and treated with Simvastatin (Millipore Sigma, Burlington, MA) intraperitoneally (1μg/g) at -1, 3, 6, and 9 dpi. Mice were monitored for weight and survival.

ANTI-ANG2/RECOMBINANT ANG1 TREATMENT

Female C57Bl/6 mice were infected with ~1.0x10^5 of *O. tsutsugamushi* Karp strain and treated intraperitoneally with anti-Ang2 antibody alone (5μg/g, REGN910, Regeneron, Tarrytown, NY) or a combination of anti-Ang2 and recombinant Ang1 (25μg/g, REGN108, Regeneron). Mice were treated with anti-Ang2 antibody every 4 days starting at -1 dpi (-1, 3, 7 dpi) and recombinant Ang1 mice were treated every 3 days starting at -1 dpi as well (-1, 2, 5, 8 dpi). Mice were monitored for weight, disease score, and survival.

Table 2.1: Primers for qRT-PCR and q-PCR analyses			
	Gene	Forward	Reverse
Human	GAPDH	5’-ACAACTTTGGTATCGTGGAAGG-3’	5’- GCCATCACGCCACAGTTTC-3’
	ICAM-1	5’-ATGCCCAGACATCTGTGTCC-3’	5’-GGGGTCTCTATGCCCAACAA-3’
	IL-8	5’-TTTTGCCAAGGAGTGCTAAAGA	5’-AACCCTCTGCACCCAGTTTTC-3’
Mouse	β-actin	5’-CGAGGCCCAGAGCAAGAGAG-3’	5’-CGGTTGGCCTTAGGGTTCAG-3’
	Fpr2	5’-GAGCCTGGCTAGGAAGGTG-3’	5’-TCGTGAAACCAATAAGGAACCTG-3’
	CD38	5’-TCTCTAGGAAAGCCCAGATCG-3’	5’-GTCCACACCAGGAGTGAGC-3’
	NOS2	5’-GTTCTCAGCCCAACAATACAAGA-3’	5’-GTGGACGGGTCGATGTCAC-3’
	IFN-γ	5’-AACGCTACACACTGCATCTTGG-3’	5’-GCCGTGGCAGTAACAGCC-3’
	CD206	5’-CTCTGTTCAGCTATTGGACGC-3’	5’-CGGAATTTCTGGGATTCAGCTTC-3’
	Egr2	5’-GCCAAGGCCGTAGACAAAATC-3’	5’-CCACTCCGTTCATCTGGTCA-3’
	Arg1	5’-CTCCAAGCCAAAGTCCTTAGAG-3’	5’-AGGAGCTGTCATTAGGGACATC-3’
	IL-10	5’-GCTCTTACTGACTGGCATGAG-3’	5’-CGCAGCTCTAGGAGCATGTG-3’
	PADI4	5’-TCTGCTCCTAAGGGCTACACA-3’	5’- GTCCAGAGGCCATTTGGAGG-3’

	Elastase	5’-CCCATCACAACTGCTGAACGA-3’	5’- AGACATGGAGTTCTGTCACCC-3’
	SOCS1	5’-GATTCTGCGTGCCGCTCT-3’	5’-TGCGTGCTACCATCCTACTC-3’
	SOCS3	5’-TGCGCCTCAAGACCTTCAG-3’	5’-GCTCCATGAGAATCCGCTCTC-3’
Bacteria	*Orientia* 47-kDa	5’-AACTGATTTTATTCAAACTAATGCTGCT-3’	5’-TATGCCTGAGTAAGATACTGTAATGGA-3’

Table 2.2: Animal illness scoring chart for Orientia tsutsugamushi infection

Animal illness scoring chart for *Orientia tsutsugamushi* infection	
Score	Symptoms
0	Normal behavior (typically seen with uninfected mice)
1	Active, some weight loss (<5%), but eat and/or drink normally (daily observations in the morning or afternoon)
2	Score 1 + additional weight loss (6-10%), some ruffled fur (limited to between shoulders), but eat and/or drink normally (daily observations in the morning or afternoon)
3	Score 2 + additional weight loss (11-19%), more pronounced ruffled fur, hunched posture, erythema, reduced food/water taken.
4	Score 3 + additional weight loss (20-25%), decreased activity, bilateral conjunctivitis, incapable to reaching food/water.
5	Score 4 + non-responsive (or weight loss of greater than 25%)

Chapter 3: Pulmonary Vascular Dysregulation and Neutrophil Recruitment during Severe *O. tsutsugamushi* Infection

PULMONARY ENDOTHELIAL ACTIVATION AND TIGHT JUNCTION DISRUPTION DURING INFECTION IN MICE

Given that the lung is a major site of *O. tsutsugamushi* infection in humans and animal models [2, 3] and that EC activation and disruption of vascular barrier integrity are principal steps for acute lung injury in sepsis and pneumonia models [37], we sought to investigate pulmonary endothelial cell activation in C57BL/6 mice following i.v. inoculation with a lethal dose of *O. tsutsugamushi* (~1.325×10^6 viable bacteria in 200 µl of PBS). Inoculation using this route establishes bacterial replication in the lungs accompanied by interstitial pneumonitis and alveolar thickening [31](**Fig. 1.3**). Immunofluorescent staining of frozen lung sections revealed increased ICAM-1-positive (green) vascular staining on days 2 (D2) to 9, as well as a close association of bacteria (red) with activated endothelium at D9 (**Fig 3.1**, boxed area). To examine endothelial structure and adherens junctions, we co-stained lung sections with GSL I-B_4 lectin (specific for α-galactose residues enriched on the surface of endothelium) and anti-VE-cadherin/CD144 (an adherens junction protein, red), as described in our previous report for neuroinflammation [95]. The VE-cadherin staining was intense and homogenous in the control tissues, but markedly reduced in D2 samples; VE-cadherin staining was nearly absent in some foci of D6 and D9 samples (**Fig. 3.2**), implying the reduction of junction proteins. In conjunction with the endothelial junction proteins, we co-stained the epithelial junction protein, occludin, and GSL I-B_4 lectin. Consistently, we found a near absence of staining in D9 samples (**Fig. 3.5**). IFA results were quantified from different tissue sections

for ICAM-1 and VE-cadherin, displaying the increase in ICAM-1 expression and loss of VE-cadherin as infection progressed (**Fig.3.3**) These data suggest a progressive and severe loss of vascular barrier integrity in the infected lungs, especially at late stages of acute infection prior to host death (D9) [3].

To support our immunofluorescent results, we prepared single-cell suspensions from mouse lung tissues and used flow cytometry to examine the frequency of recovered $CD31^{+}CD45^{-}$ endothelial cells and their surface ICAM-1 expression. We found that compared with the mock infected controls, infected lung tissues contained a significant increase in the frequencies of ICAM-$1^{+}CD31^{+}CD45^{-}$ endothelial cells at D6 and D9, respectively ($p < 0.001$, $p < 0.01$, **Fig. 3.4**), while there was approximately a 5-fold reduction in the detection of pulmonary endothelial cells at D6 and D9 ($p < 0.001$, **Fig. 3.6**). We also examined endothelial expression of vascular endothelial growth factor receptor 2 (VEGFR2), a critical factor controlling vascular permeability and barrier function [98]. Compared with the mock controls, there was an approximately 6-fold increase in the frequencies of $VEGFR2^{+}CD31^{+}CD45^{-}$ endothelial cells in the lung tissues at D6 and D9 (**Fig 3.4**). These flow cytometry data reinforced the immunofluorescent results, indicating marked endothelial activation and damage at D6 (the onset of disease) and D9 (prior to host demise). To validate these findings in human cells, we infected HUVECs with different doses of *O. tsutsugamushi* (3 and 10 MOI) and found a dose-dependent increase in *ICAM1* and *IL8/CXCL8* transcripts at 24 h post-infection (**Fig. 3.4**). Collectively, these data indicate infection-triggered endothelial stress and activation, accompanied by tight junction disruption during the course of infection.

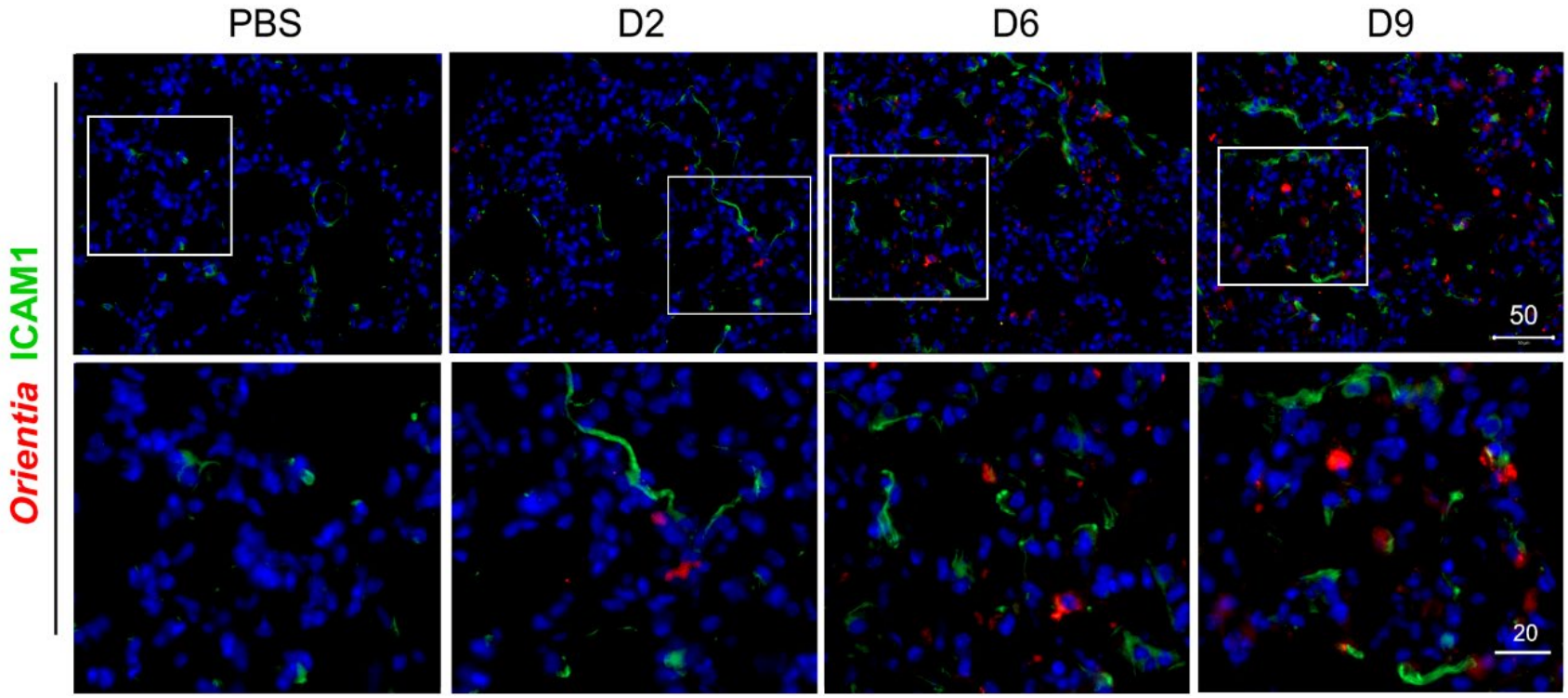

Fig. 3.1: Endothelial cell activation and vascular damage in the lungs of *O. tsutsugamushi*-infected mice. Female C57BL/6J mice were inoculated with 1.325 x 10^6 of *O. tsutsugamushi* Karp strain (4-5 mice/group) or PBS (3-4 mice/group). At days 2, 6, or 9 post-infection, equivalent lung portions were collected for analyses. Frozen lung sections were co-stained for *Orientia* bacteria (red) and ICAM-1 (green, top row, scale bar = 50 µm), with close-up views of the boxed areas in the bottom row (bar = 20 µm).

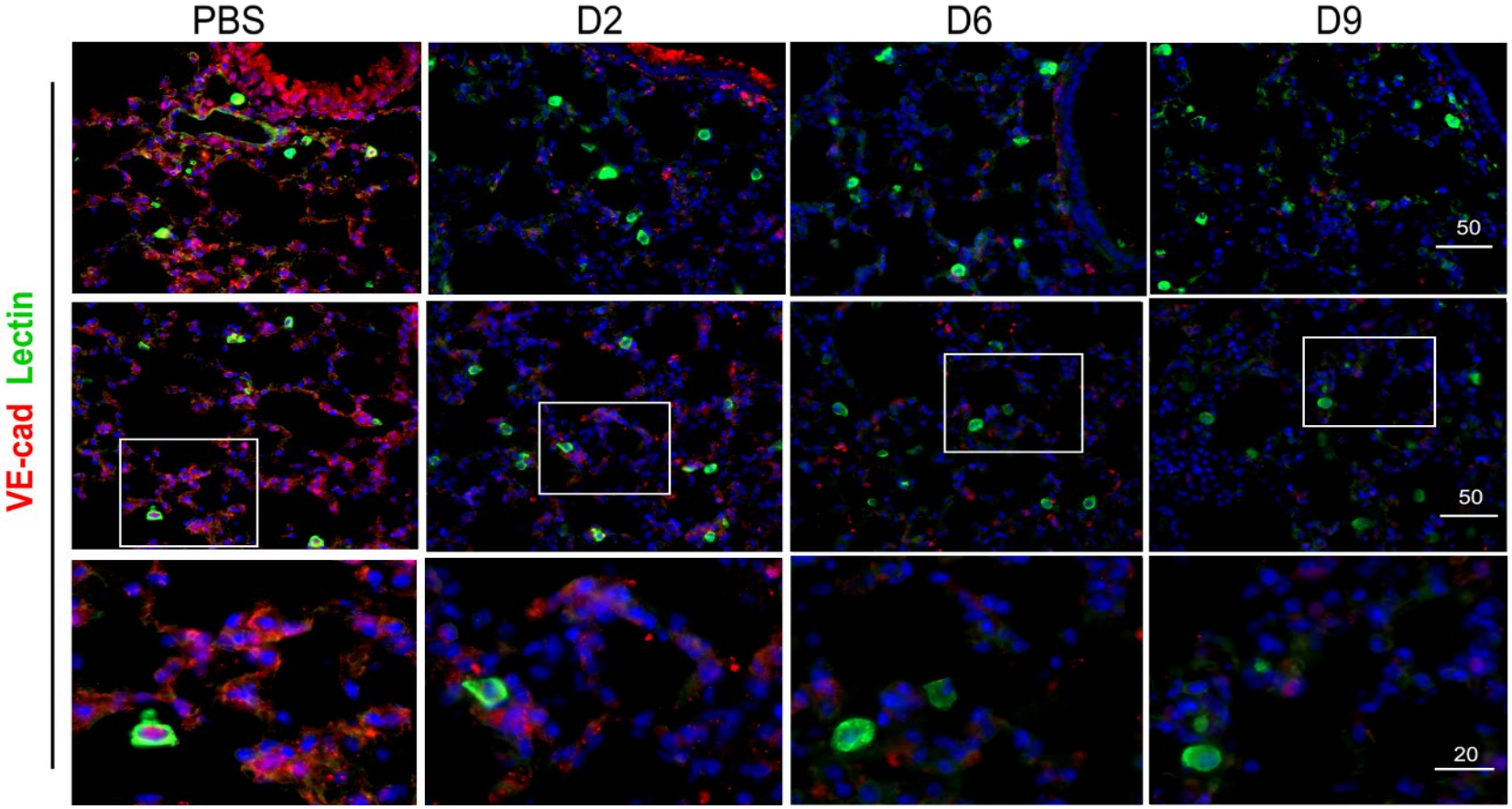

Fig. 3.2: Endothelial cell barrier protein expression in the lungs of *O. tsutsugamushi*-infected mice. Female C57BL/6J mice were inoculated with 1.325 x 10^6 of *O. tsutsugamushi* Karp strain (4-5 mice/group) or PBS (3-4 mice/group). At days 2, 6, or 9 post-infection, equivalent lung portions were collected for analyses. Lung sections were co-stained for VE-cadherin (adherens junctions, red) and FITC-labeled I-B_4 lectins (green, top row, bars = 50 μm), with close-up views of the boxed areas in the bottom row (bar = 20 μm).

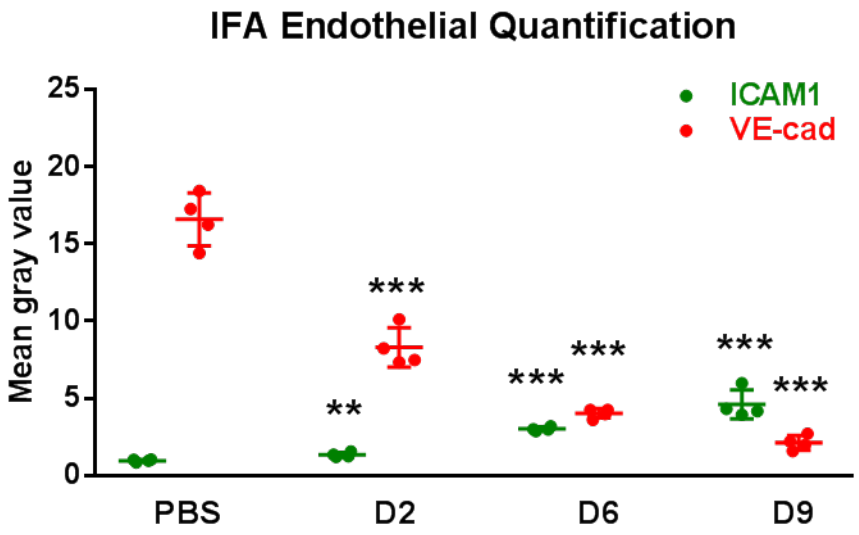

Fig. 3.3: Quantification of pulmonary IFA staining of VE-Cadherin and ICAM-1. Four representative images for each day mice were collected and were analyzed for fluorescence intensity of ICAM-1 (green) and VE-Cadherin (red) and quantified on a gray scale. *, $p < 0.05$; **, $p < 0.01$; and ***, $p<0.001$ compared to PBS controls. Graphs are shown as mean +/- SEM. Each group was compared to PBS control using student's T-test.

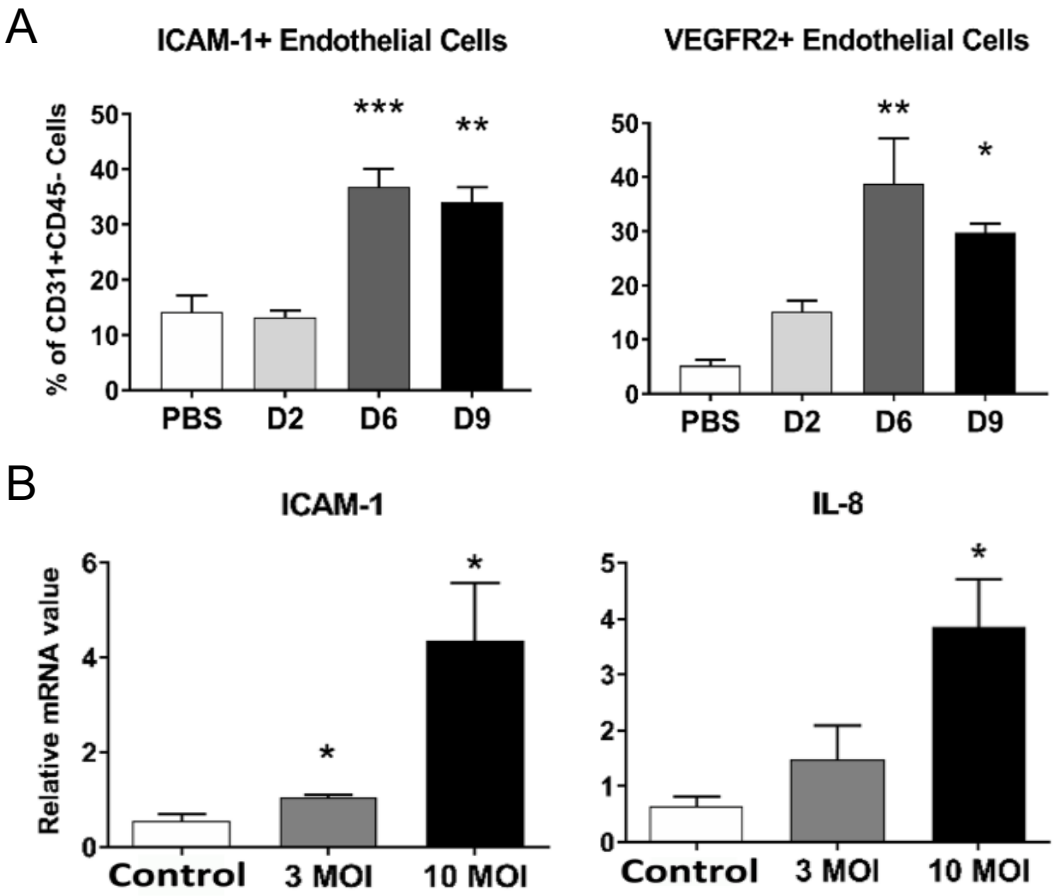

Fig. 3.4: Endothelial cell (EC) activation in *O. tsutsugamushi*-infected mice and in infected HUVECs *in vitro*. (A) Lung-derived cells were analyzed via flow cytometry for the percentage of ICAM-1^+ and $VEGFR2^+$ cells among gated $CD31^+CD45^-$ ECs (5 mice/group in infected groups; 3 mice/group in PBS groups). (B) Cultured HUVECs were infected with bacteria at 3 or 10 multiplicity of infection (MOI, 4 samples/group) and analyzed via qRT-PCR for gene expression at 24 h post-infection. Data are presented as relative to GAPDH values. *, $p < 0.05$; **, $p < 0.01$; and ***, $p<0.001$ compared to PBS controls. Graphs are shown as mean +/- SEM. Flow cytometric and qRT-PCR data were analyzed by using one-way ANOVA with Tukey's Post Hoc. At least 2 independent mouse infection experiments and 2 independent *in vitro* experiments were performed with similar trends and shown are representative data.

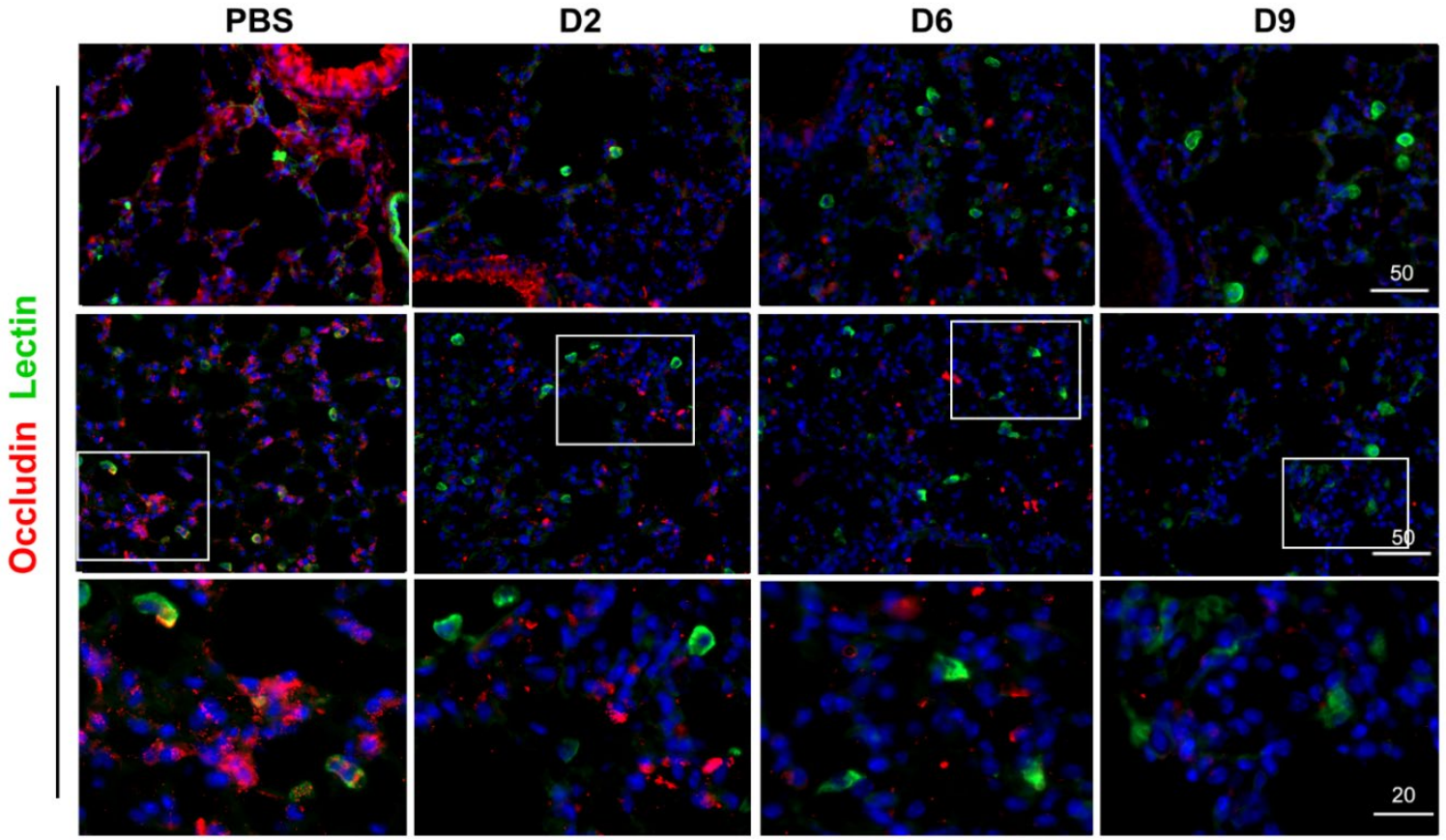

Fig. 3.5: Pulmonary pathology progression and reduced expression of occludin tight junction proteins in infected lung tissues. Female C57BL/6J mice (4-6 mice/group) were inoculated with 1.325 x 10^6 of *O. tsutsugamushi* Karp strain. At indicated days of infection, equivalent lung portions were collected. Frozen sections were processed for immunofluorescent staining and co-stained for occludin (cell-cell tight junctions, red) and FITC-labeled GSL I-B_4 lectins (green, top rows, scale bars = 50 μm). The close-up views of the boxed areas are shown in the lower row (bar = 20 μm).

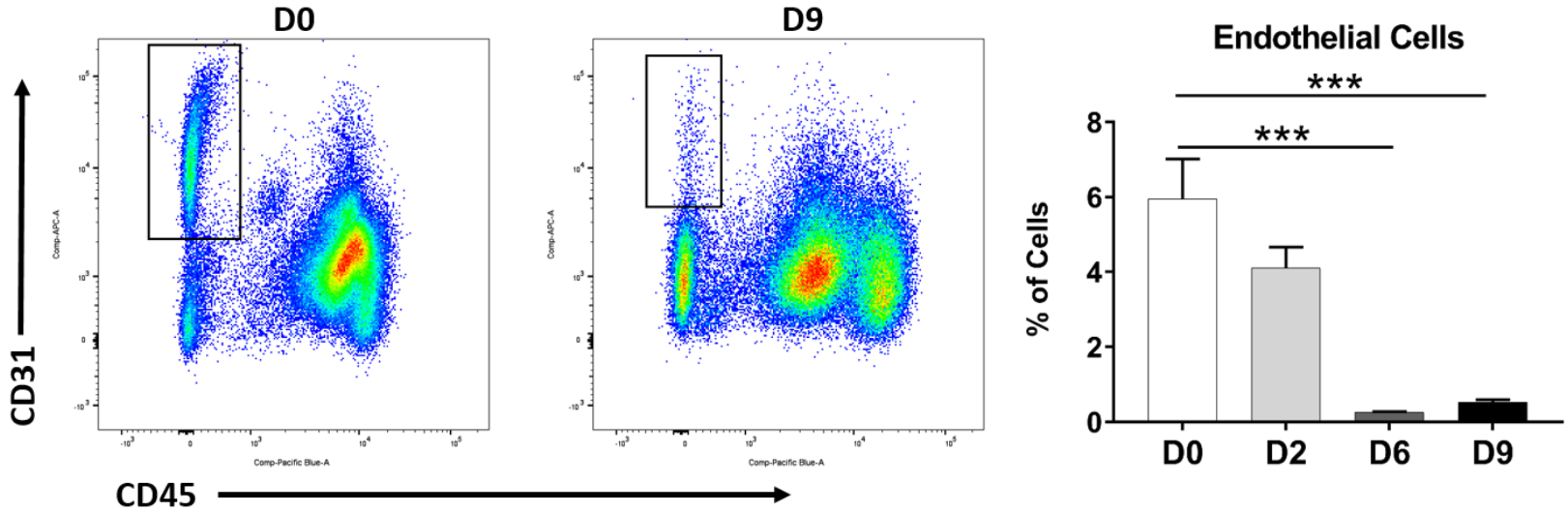

Fig. 3.6: Reduction in pulmonary endothelial staining during infection. Female C57BL/6J mice (4-6 mice/group) were inoculated with 1.325 x 10^6 of *O. tsutsugamushi* Karp strain. At indicated days of infection, equivalent lung portions were collected and single cell suspensions were made for flow cytometry staining. Endothelial cells were determined as $CD31^+CD45^-$ labeled cells (left panels). Total percentages of these cells were quantified (right panel). Graphs are shown as +/- SEM and were analyzed using one-way ANOVA with Tukey's Post Hoc. ***, $p<0.01$.

ALTERATIONS IN THE ANGIOPOIETIN-TIE2 SYSTEM DURING *ORIENTIA* INFECTION

There are no reported *in vivo* studies to define molecular mechanisms underlying *O. tsutsugamushi* infection-associated vascular damage. For other severe and systemic infections caused by bacteria or viruses, alterations in angiopoietin proteins or their functional Tie2 receptor is considered as one of the key mechanisms for vascular dysfunction [54, 99]. Given elevated *ANG2/ANG1* mRNA ratios in mice with severe scrub typhus and in *O. tsutsugamushi*-infected HUVECs [47], we considered that impairment in Tie2 function occurs in severe scrub typhus [100]. To test this hypothesis, we examined Ang1, Ang2, and Tie2 protein levels in the lung tissues via immunofluorescent staining (**Fig. 3.7**). While the mock controls contained relatively high levels of Ang1 (green) and Tie2 (red), with low levels of Ang2 (red), we found a modest decrease in Ang1-positive staining, a remarkable reduction in Tie2 staining, and a steady increase in Ang2 staining, during the course of infection. The Tie2 staining was nearly absent in some foci of D6 and D9 samples. Using Western blot analyses of lung tissues, we confirmed a striking reduction of phosphorylated Tie2 (pTie2) and total Tie2 levels at both D6 and D9, as compared with either the mock or D2 samples (**Fig. 3.8**), implying impairments at the translational and functional levels. The qRT-PCR analyses further validated a statistically significant decrease in *TIE2* mRNA levels in the lungs at D6 and D10 ($p < 0.01$, compared with the mock controls, **Fig. 3.8**), implying impairment at the transcriptional level. These data, together with our previous studies [3, 47], indicate that marked Ang2 production, accompanied with severe impairment in the Tie2 functions, are pathogenic mechanisms of severe vascular damage in *O. tsutsugamushi* infection. To validate this, we measured scrub typhus patient sera via specific ELISA assays and found a statistically significant increase

in circulating Ang2 levels that correlated with their bacterium-specific antibody titers, an indication of the duration of infection ($p < 0.05$ and $p < 0.01$, comparing IFA titers of 1:640 and 1:1280 with the controls, **Fig. 3.9**). These human data support findings obtained in mouse tissues, indicating increasing serum Ang2 levels during scrub typhus.

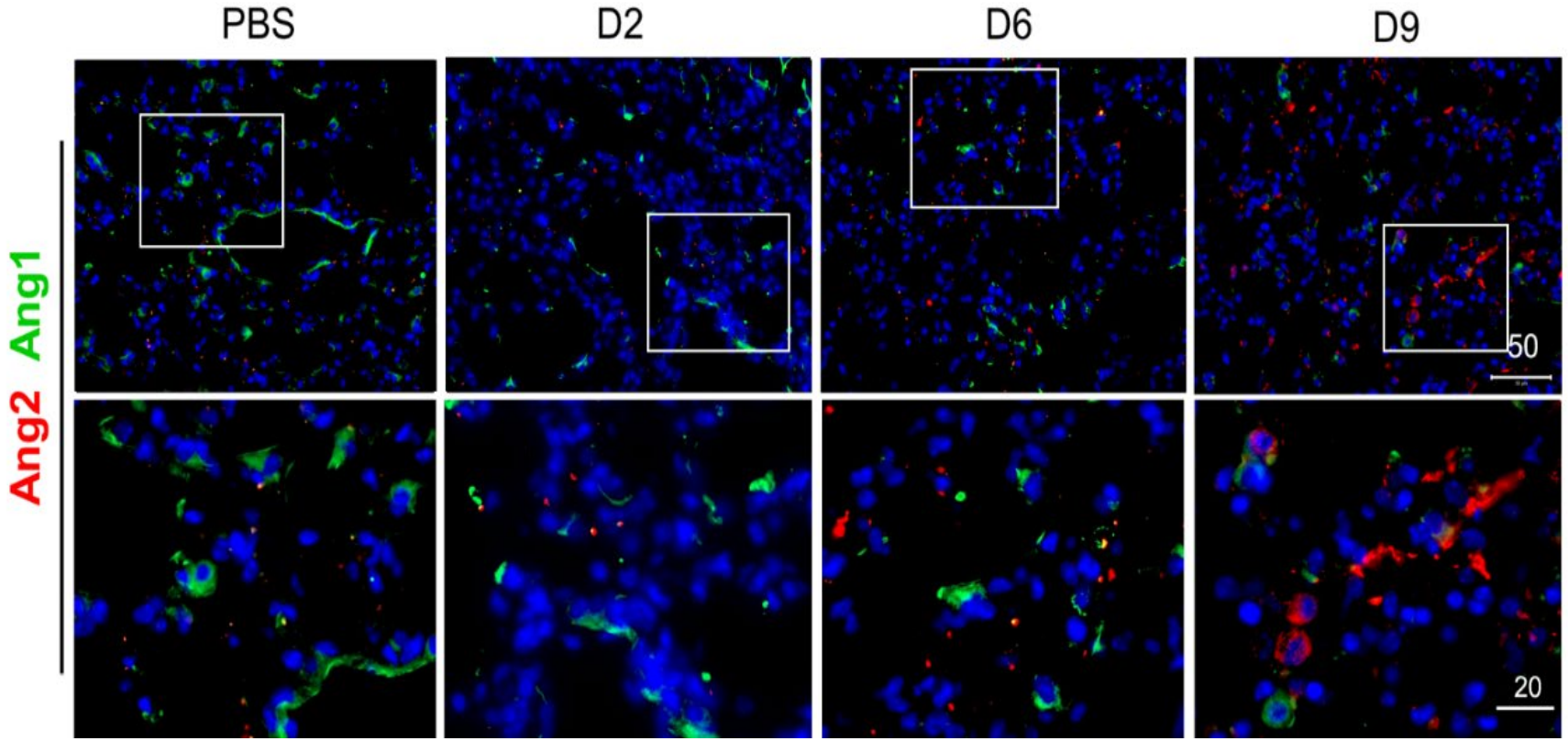

Fig. 3.7: Elevated Ang2 expression in the lungs of infected mice during *O. tsutsugamushi* infection. Mice were infected as in *Fig. 1*. Frozen lung sections were co-stained for Ang1 (a marker for endothelial quiescence, green) and Ang2 (an endothelial stress marker, red), showing images at a low magnification (top row, scale bar = 50 μm) and close-up views of the boxed areas (bottom row, bar = 20 μm).

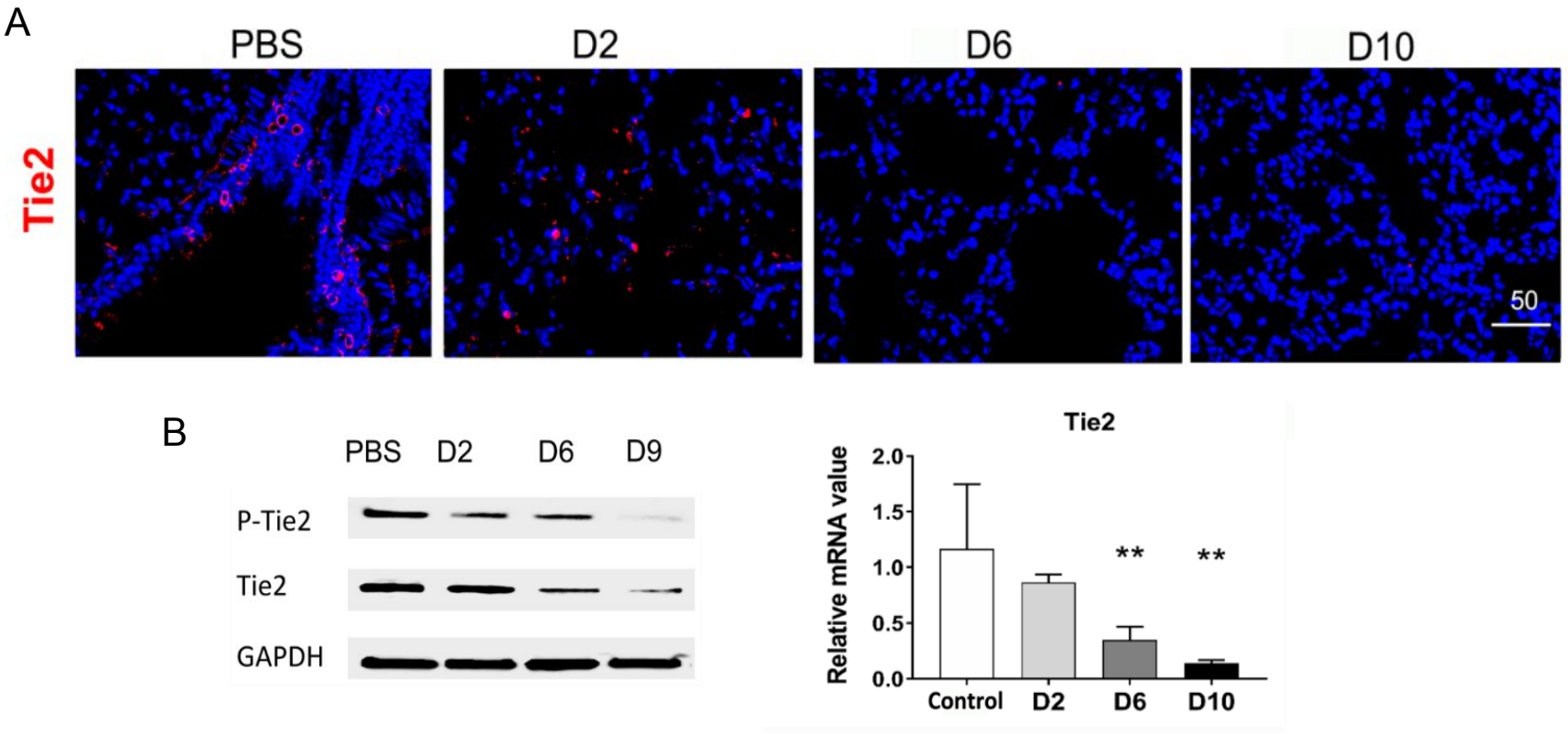

Fig. 3.8: Decreased Tie2 expression and signaling during *O. tsutsugamushi* infection. Mice were infected as in *Fig. 1*. (A) Frozen lung sections were stained for the Tie2 receptor (red, bar = 50 μm). (B) Lung tissue homogenates (40 μg/lane) were measured by Western blots for the levels of phospho-Tie2 (pTie2) and total Tie2 proteins and compared with the GAPDH controls. (C) *TIE2* mRNA levels in mouse lungs were measured via qRT-PCR; data are presented as relative mRNA values normalized to GAPDH. . Graphs are shown as mean +/- SEM. Serum ELISA and qRT-PCR groups were analyzed via one-way ANOVA with Tukey's Post Hoc.

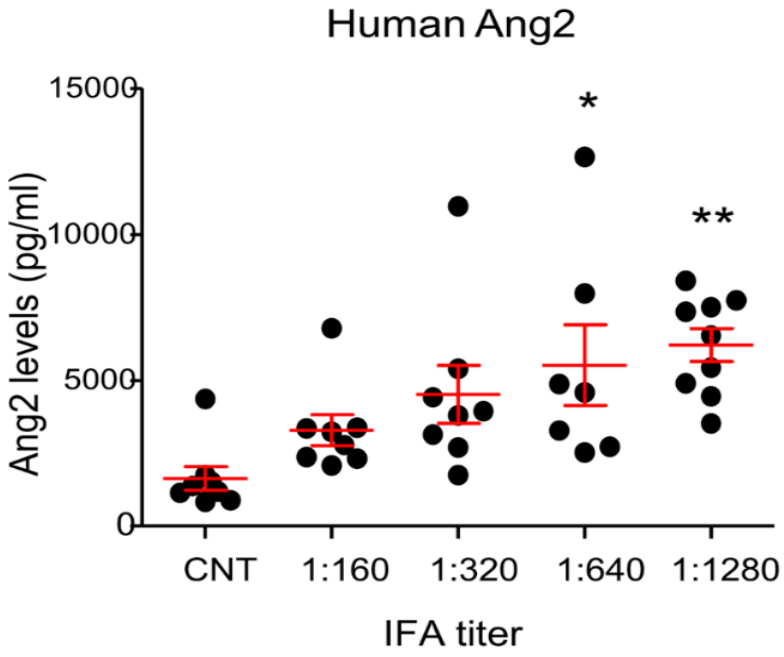

Fig. 3.9: Elevated Ang2 in the serum of scrub typhus patients. Human serum Ang2 proteins in the control subjects (CNT) or scrub typhus patients (8/group) with different anti-*Orientia* IFA antibody titers were measured by ELISA. *, $p<0.05$; **, $p<0.01$ compared to control subjects. Graphs are shown as mean +/- SEM. Serum ELISA and qRT-PCR groups were analyzed via one-way ANOVA with Tukey's Post Hoc.

MIXED MYELOID CELL RESPONSES AND NEUTROPHIL ACTIVATION AT LATE STAGES OF INFECTION

Having documented progressive endothelial activation and alterations in endothelium-specific biomarkers following *O. tsutsugamushi* infection, we then examined the timing and magnitude of leukocyte recruitment and activation. Although some reports described leukocyte involvement in *O. tsutsugamushi*-infected mouse spleen and brain [1, 95], there are no detailed studies of innate immune responses in infected lungs. Using immunofluorescent staining, we found $CD45^+$ leukocytes and $CD3^+$ T cells accumulated around Ang2-positive foci in the lungs at D6 and D10, and that CD45-Ang2 or CD3-Ang2 co-stained foci were readily detectable at D10 (yellow, **Fig. 3.10**). Flow cytometric

analyses revealed a 20-fold increase in total numbers of $CD4^+$ T cells at D10, but a statistically significant decrease in percentages of these cells at D6 and D10, respectively ($p < 0.0001$, compared with mock controls, **Fig. 3.11**). In contrast, there was a 50-fold increase in total numbers and 2.3-fold increase in percentages of $CD8^+$ T cells at D10 (**Fig. 3.11**). These findings were consistent with the known importance of $CD8^+$ T cells in infection with *O. tsutsugamushi* in mice [1, 101].

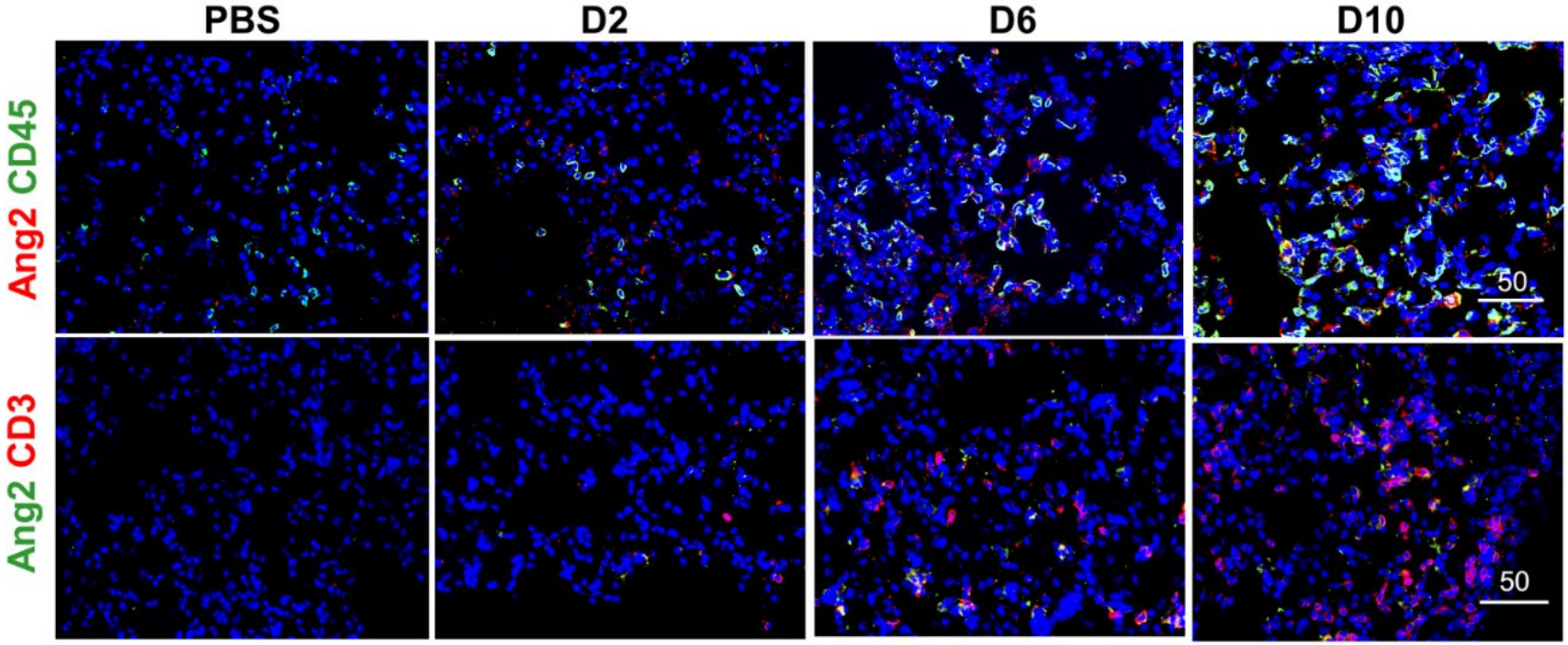

Fig. 3.10: T cell recruitment and endothelial cell activation in the lungs of lethally challenged mice. Female C57BL/6J mice (3-5 mice per group) were inoculated with 1.325 x 10^6 of *O. tsutsugamushi* Karp strain. At indicated days of infection, equivalent lung portions were collected and processed for immunofluorescent staining. Frozen sections were either co-stained for Ang2 (red) and CD45 (a leukocyte marker, green), or Ang2 (green) and CD3 (a T cell marker, red, bars = 50 μm).

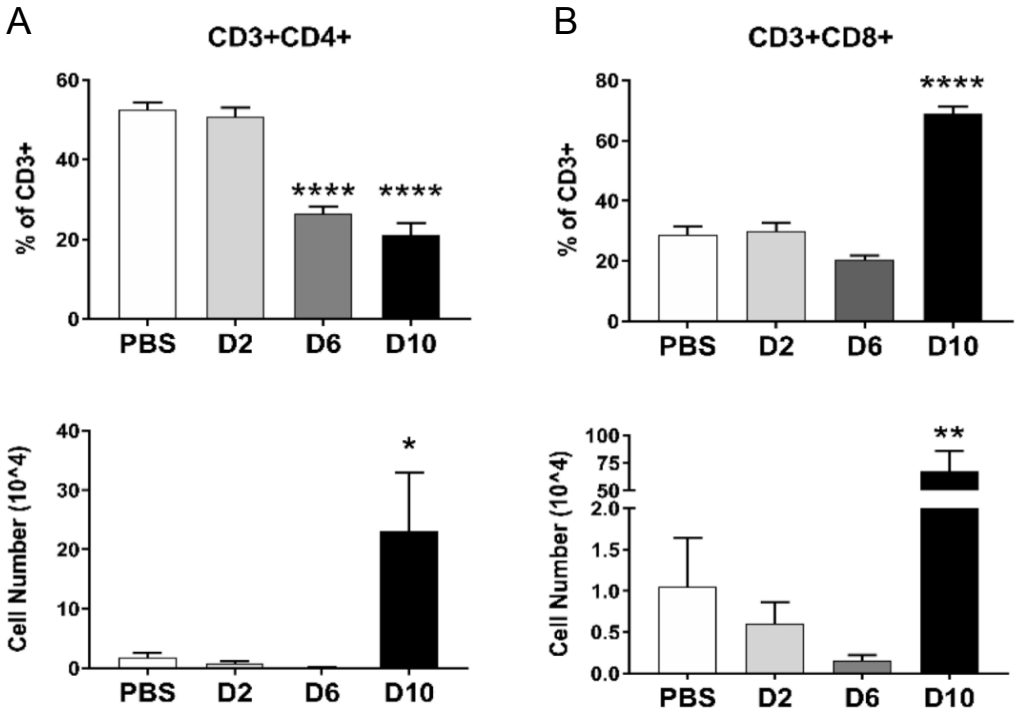

Fig. 3.11: CD4 and CD8 T cell populations in the lungs of lethally infected mice. Female C57BL/6J mice (3-5 mice per group) were inoculated with 1.325 x 10^6 of *O. tsutsugamushi* Karp strain. At indicated days of infection, equivalent lung portions were collected and processed for flow cytometric analysis. The percentage and absolute number of (A) $CD3^+CD4^+$ T cells, as well as (B) $CD3^+CD8^+$ T cells, were quantified and compared to non-infected controls (*, $p<0.05$; **, $p<0.01$; ****, $p<0.0001$). Graphs are shown as +/- SEM. Flow cytometry groups were analyzed using one-way ANOVA with Tukey's Post Hoc.

For innate immune cells, we and others have suggested a pathogenic role for neutrophils and neutrophil-chemoattractants *CXCL1* and *CXCL2* in scrub typhus patients and mouse models [3, 72]. To investigate neutrophil activation and their functions, we isolated neutrophils from the bone marrow of naïve mice, exposed cells to live *O. tsutsugamushi* (1 MOI) for 4 h and analyzed expression levels of elastase (an effector molecule) and peptidyl arginine deiminase type-4 (PADI4, an essential factor for forming neutrophil extracellular traps or, NET). As shown in **Fig. 3.12**, bacterial exposure

stimulated the expression of both *ELASTASE* and *PADI4* genes ($p < 0.05$ compared with the mock controls). In flow cytometric analyses of lung neutrophils (**Fig. 3.12**), we found a statistically significant increase in both frequency and total number of $CD11b^+Ly6G^+$ neutrophils at D6 and D9, but not at D2 (**Fig. 3.12**). Likewise, the D6 and D9 lung samples contained ~7-fold increase in frequency and ~40-fold increase in the total number of activated ($CD63^+CD11b^+Ly6G^+$) neutrophils, when compared to the mock controls (**Fig. 3.12**). To validate these findings, we analyzed neutrophil activities in the spleen and confirmed significant increases in neutrophil influx and activation at late stages of infection, although some tissue-specific differences in the neutrophil influx were also noticed (**Fig. 3.15**). Nevertheless, our data suggested that pulmonary neutrophil influx and activation coincided with the onset of weight loss and was sustained until the severe stages of disease.

To examine neutrophil-bacterial interactions in the lungs, we used immunofluorescent staining and confirmed increased detection of $Ly6G^+$ neutrophils (green, **Fig. 3.13**), as well as activated neutrophils that expressed high levels of myeloperoxidase (MPO, green, **Fig. 3.14**), at D6 and D9. The co-localization of *Orientia* (red) with $Ly6G^+$ neutrophils was most evident at D9 (yellow in boxed areas, **Fig. 3.13**). To visualize neutrophil interactions with activated endothelial cells, we performed MPO- and Ang2 co-staining and found a positive correlation between increased MPO- and Ang2-positive staining, as well as increased detection and patterns of MPO-Ang2 co-localization at D9 (**Fig. 3.16**), implying a close contact of activated neutrophils and activated/damaged ECs. Our results were consistent with clinical findings of neutrophil activation in scrub

typhus patients [72, 102]. Together, these data indicate infection-triggered neutrophil activation and degranulation.

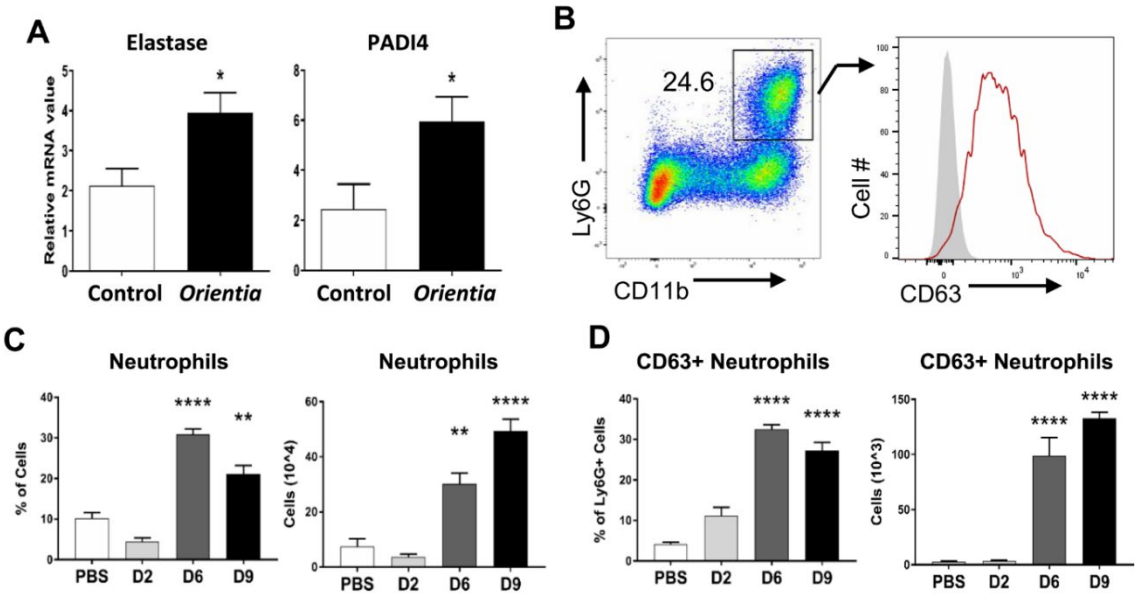

Fig. 3.12: Neutrophil recruitment and activation during infection *in vitro* and in the lungs of lethally-infected mice. (A) Bone marrow-derived neutrophils were exposed to *O. tsutsugamushi* (MOI = 1, 4 samples/group) for 24 h and examined for the indicated transcripts of mRNA for *ELASTASE* and *PADI4* via qRT-PCR. Data are presented as relative mRNA values normalized to β-actin. (B-F) Mice were infected as in Fig. 1. At indicated days of infection, lung tissues were collected to prepare a single-cell suspension for flow cytometry and frozen sections for immunofluorescent analyses. (B) Flow cytometry gate of $CD11b^{+}Ly6G^{+}$ neutrophils and activated ($CD63^{+}CD11b^{+}Ly6G^{+}$) neutrophils was shown for D9 samples. The percentages and total numbers of pulmonary neutrophils (C) and activated neutrophils (D) during the course of infection were presented and compared to the PBS controls. *, $p<0.05$; **, $p<0.01$; and ****, $p<0.0001$ compared with the PBS controls. Graphs are shown as mean +/- SEM. Data for qRT-PCR were analyzed via a two-tailed Student's t-test. Flow cytometry data were analyzed via one-way ANOVA with Tukey's Post Hoc.

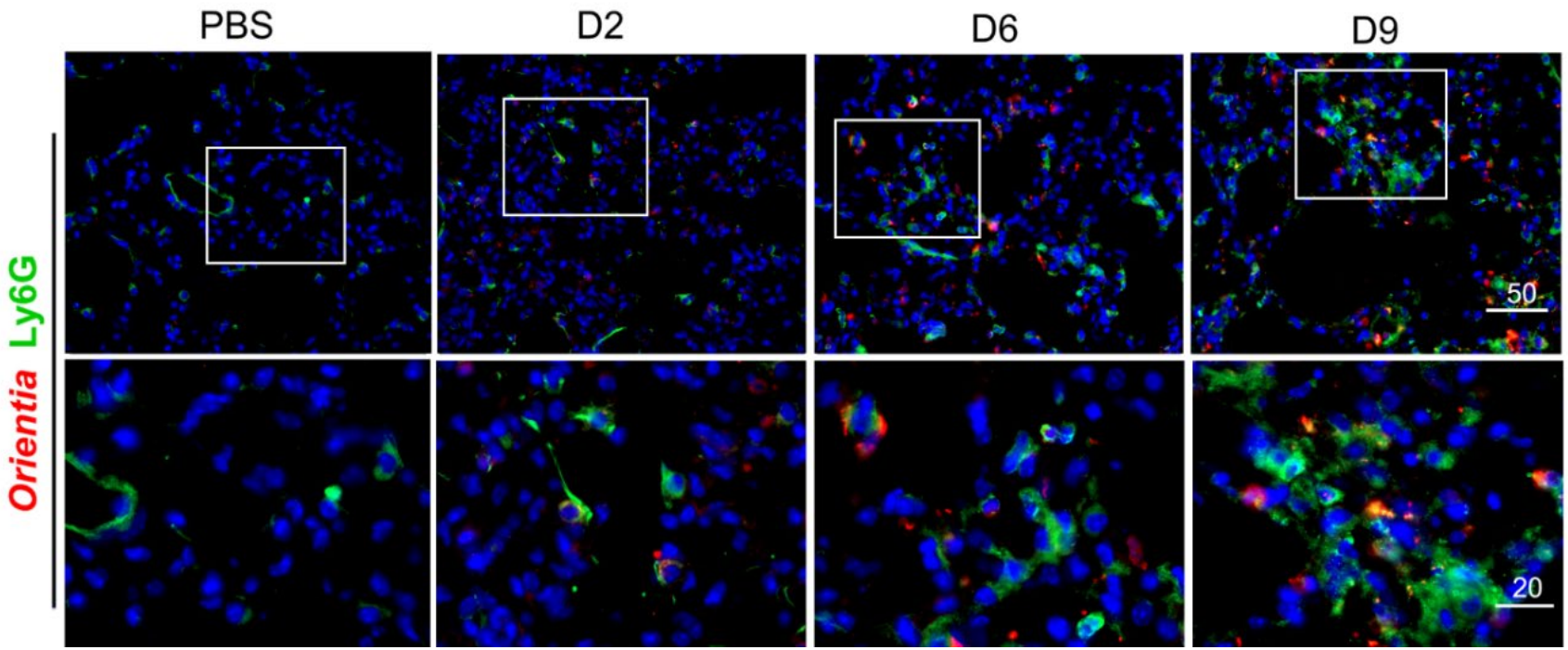

Fig. 3.13: Neutrophil recruitment in the lungs of lethally-infected mice. Lung frozen sections were co-stained for *Orientia* (red) and Ly6G (green). Shown images in a low-magnification (top rows, scale bar = 50 μm) and close-up views of the boxed areas (bottom rows, bar = 20 μm).

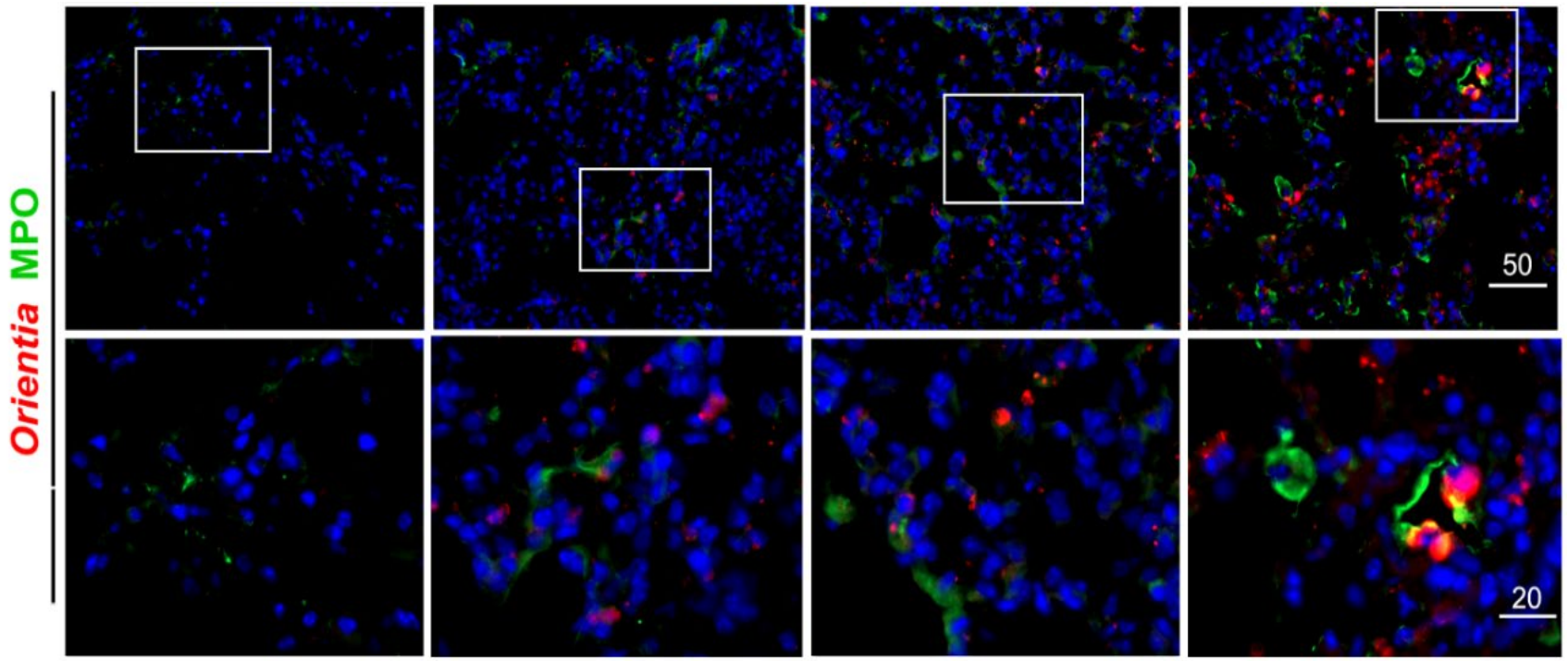

Fig. 3.14: Neutrophil recruitment and activation during infection in the lungs of lethally-infected mice. Lung frozen sections were co-stained for *Orientia* (red) and myeloperoxidase (MPO, green). Shown images in a low-magnification (top rows, scale bar = 50 μm) and close-up views of the boxed areas (bottom rows, bar = 20 μm).

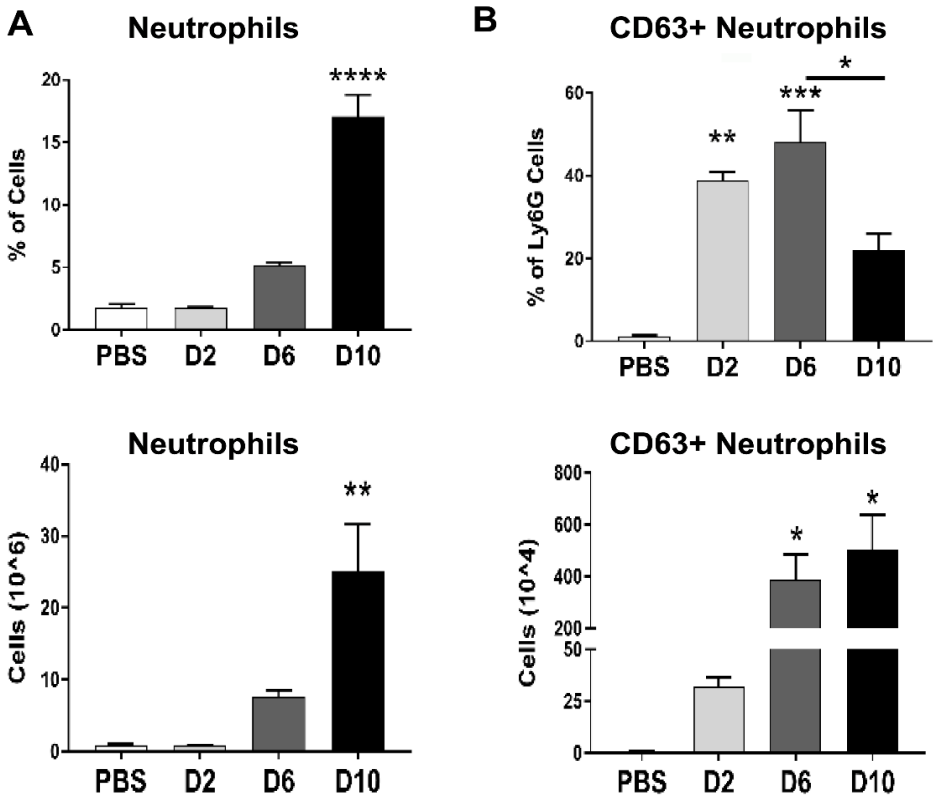

Fig. 3.15: Neutrophil recruitment and activation in the spleens during infection. Female C57BL/6J mice (3-5 mice/group) were inoculated with 1.325 x 10^6 of *O. tsutsugamushi* Karp strain. At indicated days of infection, single-cell suspensions were prepared from the spleens for flow cytometric analysis. The percentage and absolute number of $Ly6G^+$ neutrophils (A), as well as activated ($CD63^+Ly6G^+$) neutrophils (B), were quantified and compared to the PBS controls. *, $p<0.05$; **, $p<0.01$; ****, $p<0.0001$. Graphs are shown as +/- SEM and were analyzed using one-way ANOVA with Tukey's Post Hoc.

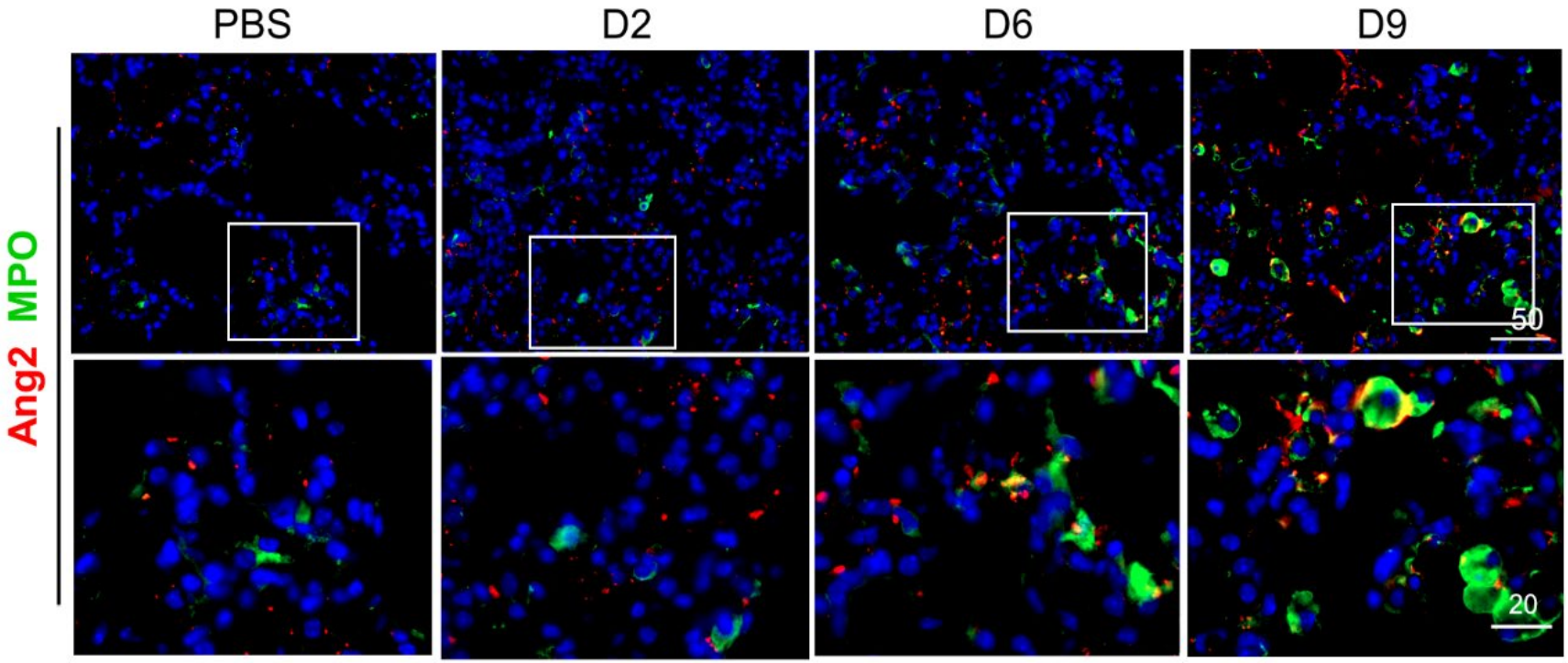

Fig. 3.16: Neutrophil activation and related EC activation in the infected lungs. Mice were infected, and lung tissues were prepared for immunofluorescent analyses. Lung frozen sections were co-stained for MPO (green) and Ang2 (red). The low-magnification images (top rows, scale bar = 50 μm) and close-up views of the boxed areas (bottom rows, bar = 20 μm) are shown.

To determine whether neutrophils played a protective or a pathogenic role during *O. tsutsugamushi* infection, we depleted neutrophils using a neutrophil-specific anti-Ly6G antibody (50μg/mouse) either before (D-1) or at (D4) infection. At D6 of infection, we collected lungs and spleens from mice and confirmed that mice that received anti-Ly6G antibody at D-1 had generally reconstituted their neutrophil populations by D6, while mice that received anti-Ly6G antibody on D4 had a significant decrease in neutrophils in the lungs at D6 (**Fig. 3.17**). Mice in neutrophil-depleted and control groups were monitored for weight loss and survival (**Fig. 3.18**). Our results showed that there was no difference in the weight loss of the infected mice treated with control IgG antibody and the mice with neutrophils depleted at D-1 (**Fig. 3.18**). D4 neutrophil-depleted mice, however, showed reduced weight loss on D5-D7 compared to IgG treated mice (**Fig. 3.18**). D-1 neutrophil-depleted mice showed a trend of decreased mortality compared to the infected IgG-treated mice, while there was no significant difference in the survival of D4 neutrophil-depleted mice compared to IgG-treated controls (**Fig. 3.18**). While there was no significant difference in lung bacterial loads at D6 of infection between infected IgG-treated mice and neutrophil-depleted mice, bacterial loads tended to be slightly decreased in both neutrophil-depleted mice (**Fig. 3.19**).

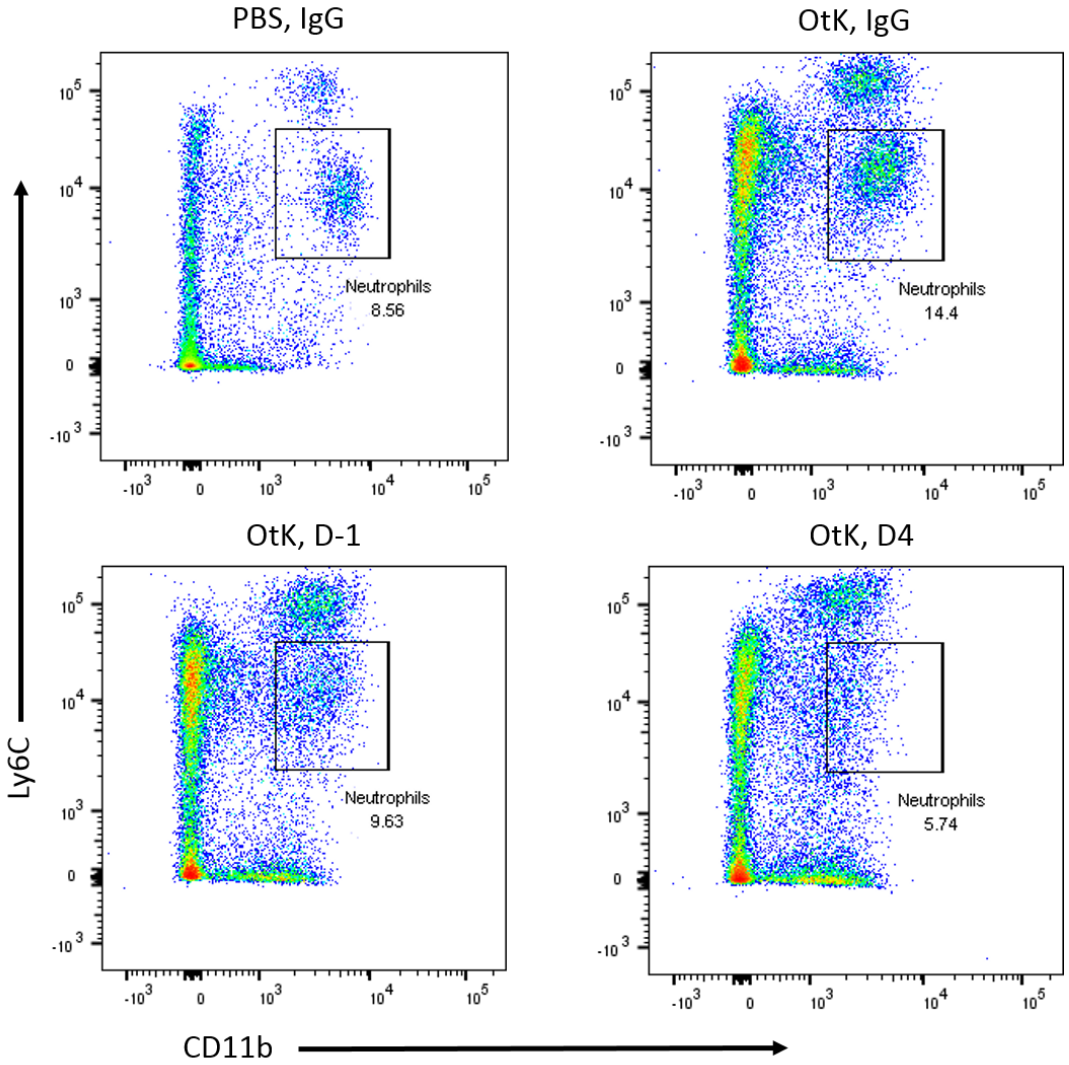

Fig. 3.17: Depleted neutrophil populations in the lungs of infected mice after anti-Ly6G antibody treatment. Female C57BL/6J mice (3-4 mice/group) were inoculated with 2.5 x 10^5 of *O. tsutsugamushi* Karp strain. PBS inoculated or infected mice were given anti-Ly6G (50 µg) antibody at D-1 or at D4 of infection, or rat IgG antibody (50 µg). At D6 of infection, single-cell suspensions were prepared from the lungs. Neutrophil populations from (A) PBS, (B) infected/IgG-treated, (C) infected/anti-Ly6G at D-1, and (D) infected/anti-Ly6G at D4 were determined after depletion as $CD11b^{+}Ly6C^{int}$.

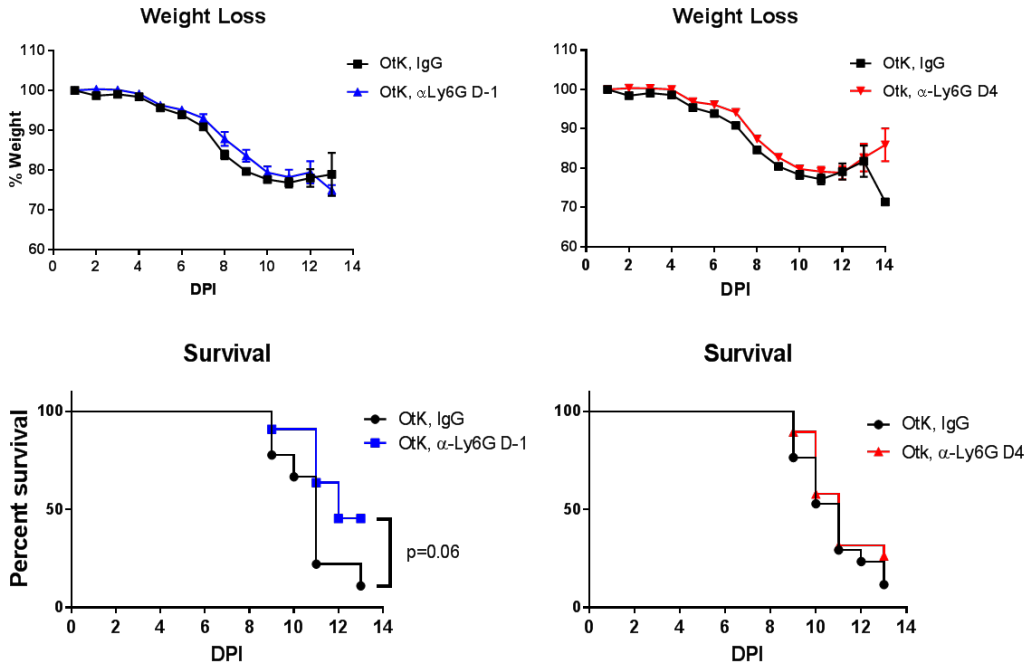

Fig. 3.18: Weight loss and survival of neutrophil depleted mice during severe *O. tsutsugamushi* infection. Female C57BL/6J mice (11-19 mice/group) were inoculated with 2.5 x 10^5 of *O. tsutsugamushi* Karp strain. Infected (OtK) mice were given anti-Ly6G antibody (50 µg) at D-1 (blue lines) or at D4 (red lines) of infection, or normal rat IgG (black lines). (A) Mice were monitored for changes in weight and (B) survival. Treatment groups are compared to rat IgG treated mice. *, $p<0.05$; **, $p<0.01$; ****, $p<0.0001$. Graphs are shown as +/- SEM and were analyzed using log rank (Mantel-Cox) test for survival and a Mann-Whitney t test for weight loss.

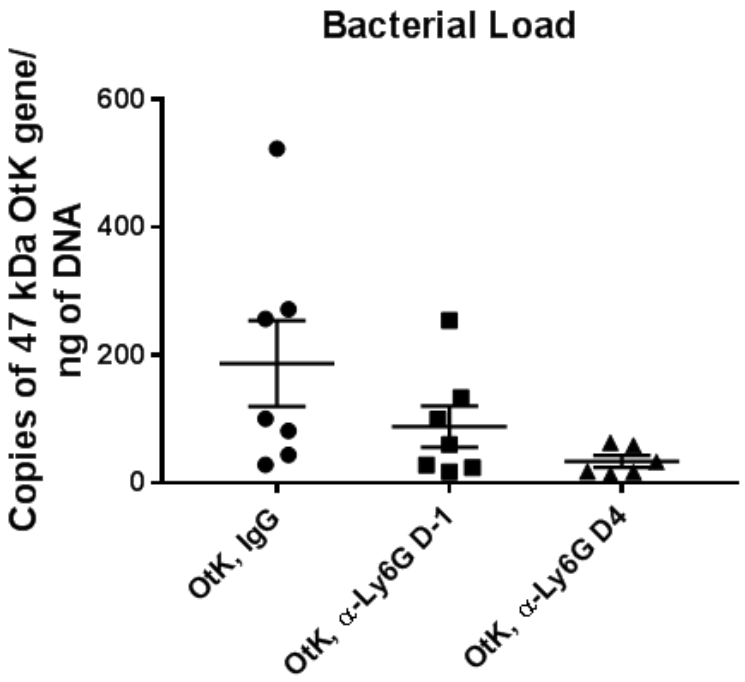

Fig. 3.19: *O. tsutsugamushi* bacterial load in the lungs of mice after neutrophil depletion. Female C57BL/6J mice (6-7 mice/group) were inoculated with 2.5 x 10^5 of *O. tsutsugamushi* Karp strain. Infected (OtK) mice were given anti-Ly6G (50ug) antibody at D-1 or at D4 of infection, or normal rat IgG (50ug). Copies of 47 kDa *O. tsutsugamushi* membrane gene were determined using a standard curve with a known concentration of plasmid as described previously [4].

In addition to monitoring weight loss and survival, we also collected lung and spleen tissue from mice to determine what effect neutrophil depletion had on the immune response during *O. tsutsugamushi* infection. Our first observation was that neutrophil depletion at either D-1 or D4 resulted in an increase in the total number of naïve CD4 and CD8 T cells in the lungs of infected mice compared to IgG-treated control mice (**Fig. 3.20**). The naïve T cell population in the spleen increased slightly in our neutrophil-depleted mice, but did not reach significance (**Fig. 3.21**).

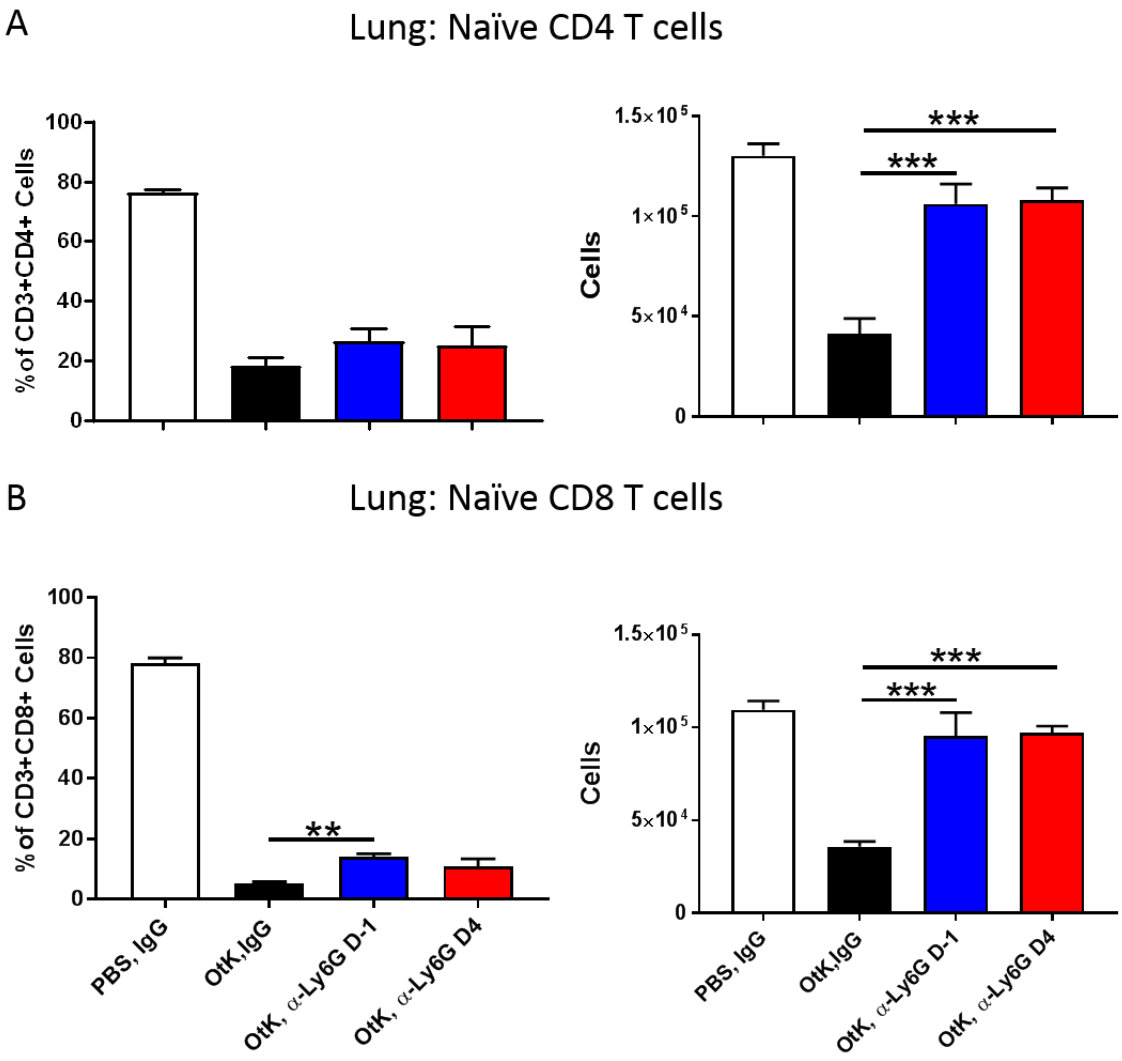

Fig. 3.20: Naïve CD4 and CD8 T cell populations in the lungs of infected mice after neutrophil depletion. Female C57BL/6J mice (3-4 mice/group) were inoculated with 2.5 x 10^5 of *O. tsutsugamushi* Karp strain. Uninfected (PBS) or infected (OtK) were given anti-Ly6G (50ug) antibody at D-1 or at D4 of infection, or normal rat IgG (50ug). At D6 of infection, single-cell suspensions were prepared from the lungs for flow cytometric analysis. (A) The percentage and absolute numbers of naïve CD4 T cells in the lung. (B) The percentage and absolute numbers of naïve CD8 T cells in the lung. Neutrophil depletion groups were compared to the IgG infected controls. **, $p<0.01$; ****, $p<0.0001$. Graphs are shown as +/- SEM and were analyzed using one-way ANOVA with Tukey's Post Hoc.

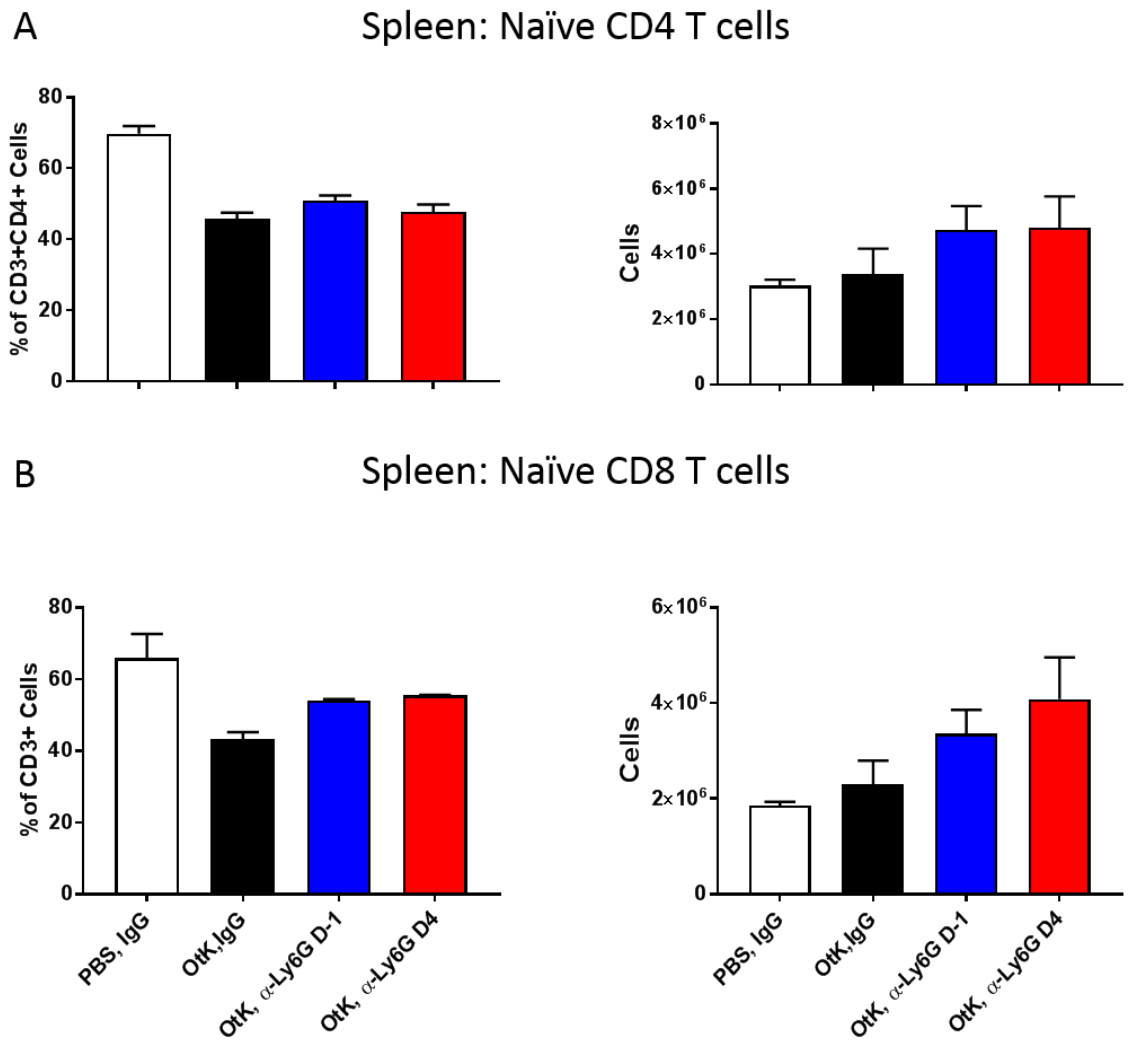

Fig. 3.21: Naïve CD4 and CD8 T cell populations in the spleens of infected mice after neutrophil depletion. Female C57BL/6J mice (3-4 mice/group) were inoculated with 2.5 x 10^5 of *O. tsutsugamushi* Karp strain. Uninfected (PBS) or infected (OtK) mice were given anti-Ly6G (50ug) antibody at D-1 or at D4 of infection, or rat IgG antibody (50ug). At D6 of infection, single-cell suspensions were prepared from the spleens for flow cytometric analysis. (A) The percentage and absolute numbers of naïve CD4 T cells ($CD62L^+CD44^-CD3^+CD4^+$) . (B) The percentage and absolute numbers of naïve CD8 T cells ($CD62L^+CD44^-CD3^+CD8^+$). Neutrophil depletion groups were compared to the IgG infected controls. Graphs are shown as +/- SEM and were analyzed using one-way ANOVA with Tukey's Post Hoc.

We also found that there were shifts in the macrophage populations in the D-1 neutrophil depletion group during infection. Specifically, there were significant increases in both percentage and absolute macrophage cell concentrations in the D-1 mice (**Fig.**

3.22). This increase in macrophages correlated with a significant increase in the total number of M1 activated macrophages, despite overall percentages of M1 macrophages being similar between control and neutrophil-depletion groups (**Fig. 3.23**)

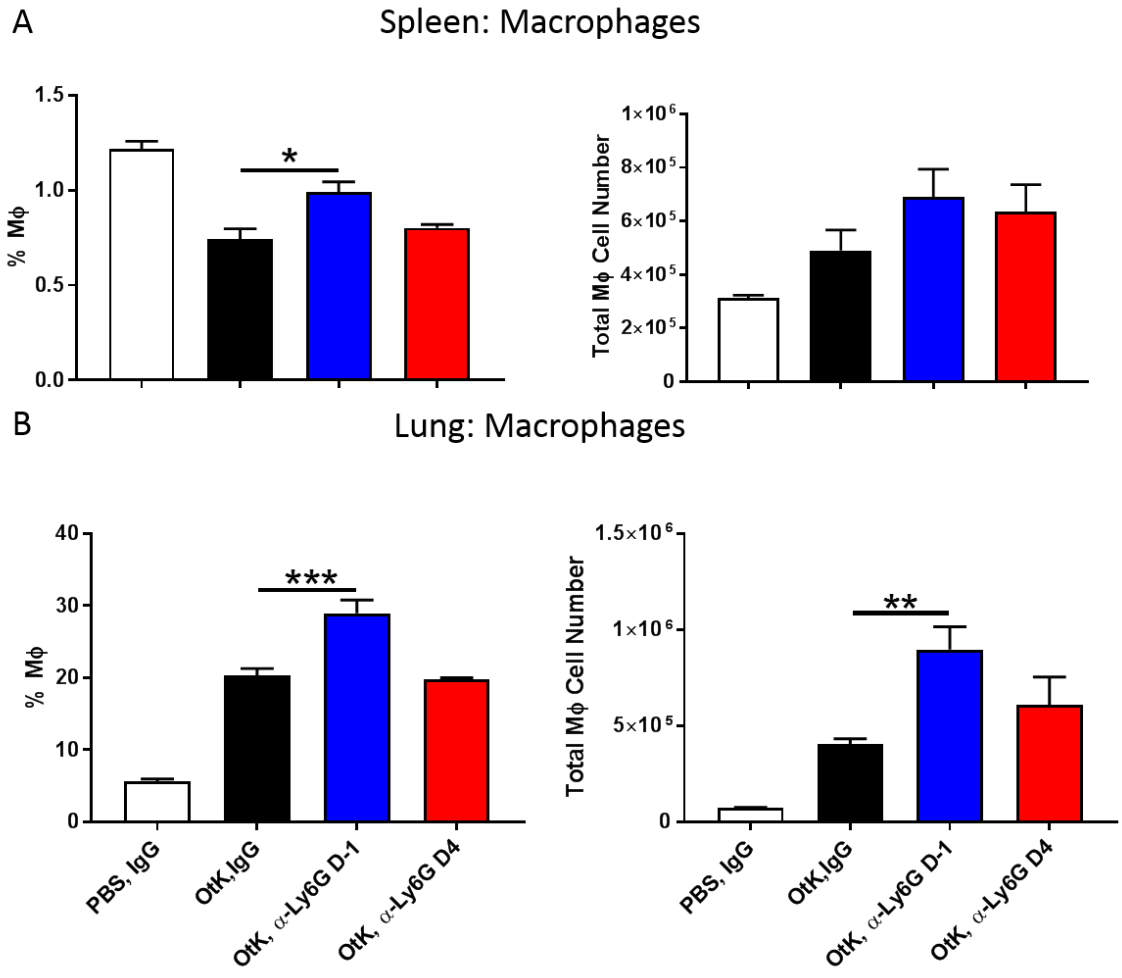

Fig. 3.22: Total macrophage populations in the spleens and lungs of infected mice after neutrophil depletion. Female C57BL/6J mice (3-4 mice/group) were inoculated with 2.5 x 10^5 of *O. tsutsugamushi* Karp strain. Uninfected (PBS) or infected (OtK) were given anti-Ly6G (50ug) antibody at D-1 or at D4 of infection, or rat IgG antibody (50ug). At D6 of infection, single-cell suspensions were prepared from the spleens and lungs for flow cytometric analysis. (A) The percentage and absolute numbers of splenic macrophages ($F4/80^+CD64^+CD11b^+$). (B) The percentage and absolute numbers of macrophages in the lung. Neutrophil depletion groups were compared to the IgG infected controls. Graphs are shown as +/- SEM and were analyzed using one-way ANOVA with Tukey's Post Hoc. *, $p<0.05$; **, $p<0.01$, ***, $p<0.001$

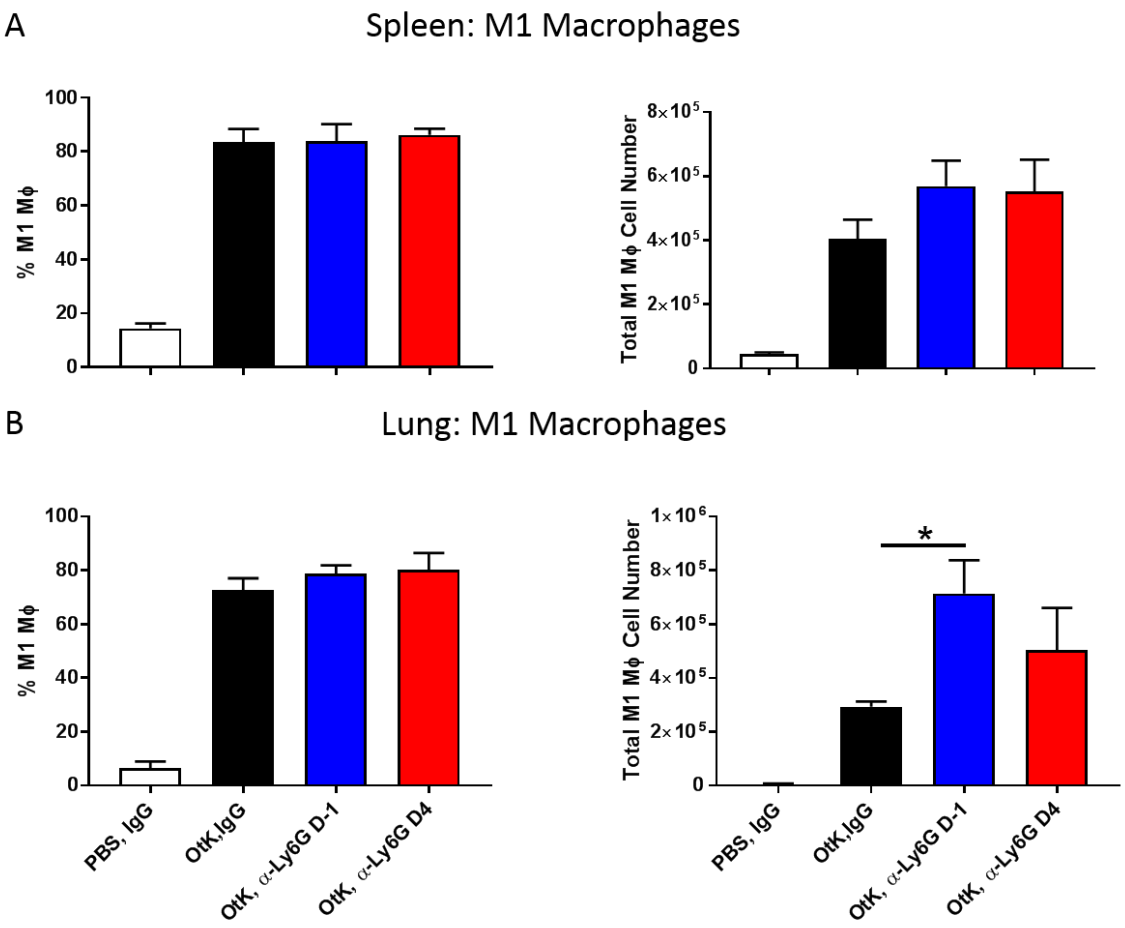

Fig. 3.23: Total M1 macrophage populations in the spleens of infected mice after neutrophil depletion. Female C57BL/6J mice (3-4 mice/group) were inoculated with 2.5 x 10^5 of *O. tsutsugamushi* Karp strain. Uninfected (PBS) or infected (OtK) were given anti-Ly6G (50ug) antibody at D-1 or at D4 of infection, or rat IgG antibody (50ug). At D6 of infection, single-cell suspensions were prepared from the spleens and lungs for flow cytometric analysis. (A) The percentage and absolute numbers of splenic M1 macrophages ($CD80^+F4/80^+CD64^+CD11b^+$) in the lung. (B) The percentage and absolute numbers of M1 macrophages in the lung. Neutrophil depletion groups were compared to the IgG infected controls. Graphs are shown as +/- SEM and were analyzed using one-way ANOVA with Tukey's Post Hoc. *, $p<0.05$

This flow cytometry data indicates that depletion of neutrophils at an early time point significantly effects T cell activation states and total macrophage populations, especially in the lungs of mice infected with *O. tsutsugamushi*.

DISCUSSION

Despite being an important emerging infectious disease, detailed immunological studies of *O. tsutsugamushi* infection *in vivo* are scarce. In this study, we used an intravenous inoculation mouse model in which the bacteria infect the endothelium, paralleling important aspects of severe scrub typhus in humans, to examine how innate immune cells respond to *O. tsutsugamushi* infections. These findings revealed important parameters and cell-specific alterations associated with acute lung injury and pathogenesis. The endothelium in infected lungs presented progressive Tie2 malfunction, increased Ang2 and ICAM-1 expression and sustained activation of neutrophils at the onset of disease and during the severe stages of infection. Since lung damage and vascular function play a prominent role in the severity of scrub typhus in patients [2], a better understanding of pathogenesis associated with acute lung injury is important for disease control and management.

The molecular characteristics of endothelial alterations during *O. tsutsugamushi* infection *in vivo* have not been explored. This study provided solid evidence for the mechanisms underlying pulmonary injury and vascular dysfunction during *O. tsutsugamushi* infection. First, the timing of ICAM-1 and VEGFR2 expression on the surface of lung-derived $CD31^{+}CD45^{-}$ endothelial cells was concurrent with the appearance of signs of vascular injury and decrease in cell junction proteins (**Figs. 3.1-3.4**). Since ICAM-1 promotes circulating immune cells to bind to the endothelium and extravasate into inflamed tissues [103], increased ICAM-1 surface expression likely contributed to immune cell influx into the infected mouse lungs (**Figs 3.1-3.4**). Our observed *ICAM1* and *IL-8/CXLC8* up-regulation in infected human EC cultures (**Fig. 3.4**) were consistent with other

reported studies of scrub typhus patients [104]. VEGFR2 is the primary receptor for vascular endothelial growth factor (VEGF) in the endothelium, and the VEGF/VEGFR2 axis regulates microvascular permeability via interacting with VE-cadherin and tight junction proteins [105, 106]. In our hands, we consistently detected a marked increase in VEGFR2 on the surface of infected ECs, but a significant reduction of VE-cadherin (adhesion junctions) in the lungs at D6 and D9. While it is unclear whether increased VEGFR2 expression is directly linked to diminished VE-cadherin expression in infected lungs, our data suggest compromised endothelial barrier integrity during severe *O. tsutsugamushi* infection in the lungs.

Second, a notable reduction of Tie2 proteins was concurrent with significant Ang2 production and/or release at the severe stages of infection (**Fig. 3.7-8**). To date, there are no reports for Tie2 expression levels in scrub typhus patients or animal models, although our group previously showed increased *ANG2/ANG1* ratios in *O. tsutsugamushi*-infected human endothelial cell cultures and mouse tissues [3]. Given the critical function of Tie2 receptor in vascular physiology and integrity, it will be important to further examine whether our observed Tie2 decrease is due to direct endothelial damage or signaling from nearby pericytes and recruited immune cells. Research in these areas would be of great value, as angiopoietin- or Tie2-targeted therapies have been evaluated as alternative treatment strategies for severe sepsis [56, 57], severe dengue [107], and in cerebral malaria [54] infection models to restore endothelial quiescence during infection. Our clinical observation that increased serum Ang2 in human scrub typhus patients correlates with *O. tsutsugamushi*-specific antibody titers demonstrates the utility of Ang2 as a pathogenic

biomarker, and highlights the potential of use Ang2- or Tie2-targeted therapies for severe scrub typhus, as in patients with severe sepsis [108, 109] and malaria [55].

Innate immune cell responses during *O. tsutsugamushi* infection in the lungs have not been explored, although the lungs carry the highest bacterial loads in different animal models following diverse routes of inoculation [31, 43]. Neutrophils play a central role in the control of acute bacterial infections, via the release of antimicrobial factors (elastase, MPO, etc.), which can kill pathogens and damage host cells [110]. While neutrophils respond rapidly (in minutes or hours) to other bacterial infections [111-113], we found no signs of neutrophil recruitment and activation in *O. tsutsugamushi*-infected lungs at D2, nor detectable levels of *CXCL1* and *CXCL2* at D2 [3]. The total numbers of lung-infiltrating $Ly6G^+$ neutrophils and activated $CD63^+Ly6G^+$ neutrophils were most remarkable at D9, suggesting the peak time of in-tissue release of neutrophil elastase and azurophilic granules [114]. While the precise roles of neutrophils *in vivo* remain unclear, our data suggested several possibilities. First, direct neutrophil-*Orientia* interactions can trigger PADI4, a contributing factor for NET formation and vascular damage [61, 115]. Although NET formation was not examined in this study, it is possible that $Ly6G^+$ and MPO^+ neutrophils engulfed bacteria *in vivo* (**Fig. 3.13-14)**. Second, MPO, a heme-containing peroxidase, that is most abundant in the primary granules of neutrophils, can damage pathogens or host tissues through the generation of reactive halogenating and nitrating agents and amplify endothelial dysfunction [116, 117]. Since neutrophils are short-lived, it is conceivable that high levels of local elastase and MPO, and other neutrophil-derived mediators promote lung tissue damage and vascular malfunction. Finally, proinflammatory cytokines expressed by *O. tsutsugamushi*-infected endothelial cells (*IL-8/CXCL8*) and infected

mouse lungs (*IL-6*, *TNF-α*, *IFN-γ*, *CXCL1*, *CXCL2*, etc.) [100], or $CD4^+$ and $CD8^+$ T cells in the lungs (**Figs. 3.10-11**) can promote neutrophil responses.

To determine the pathogenic or protective role of neutrophils during infection, we depleted neutrophils prior to infection and also during infection in infected mice. Our findings indicate that depletion of neutrophils at D-1 results in decreased mortality, but depletion of neutrophils at D4 did not affect survival of infected mice compared to infected IgG-treated mice. Furthermore, neutrophils appear to play a regulatory role for other immune subsets during *O. tsutsugamushi* infection, as depletion of neutrophils affected both T cell and macrophage populations the lungs of infected mice (**Figs. 3.20-3.23**). Similar findings have been noted by work in intracellular pathogens related to *Orientia*. Neutrophil depletion during *Ehrlichia chaffeensis* delayed time of death and modulated immune cell populations and their functions [118]. Furthermore, depletion of neutrophils during infection with *Rickettsia typhi*, another closely related pathogen to *Orientia*, resulted in decreased tissue pathology and slightly increased number of macrophages in the spleens of infected mice [119]. The cross-talk between neutrophils and macrophages influences polarization, activation, and the cellular survival of both these cell types during inflammation and infection [120]. How these cells interact during *O. tsutsugamushi* infection has not been studied previously, and future studies are needed to determine if the increased number of macrophages we observed after neutrophil depletion contributes to control of bacterial growth. In our experiments here, pulmonary bacterial loads from neutrophil depleted mice were not significantly different from infected control IgG-treated mice, but there was somewhat of a trend of decreased bacterial loads in the lungs of neutrophil depleted mice. Experiments to determine the functionality of immune cells

during neutrophil depletion will also be useful, as experiments with *E. chaffeensis* have shown that depletion of neutrophils may not directly influence numbers of cells, but may have a profound impact on the activation and cytokine secretion of various immune cell subsets [118].

Chapter 4: Macrophage Recruitment to the Lungs and Polarization during *O. tsutsugamushi* Infection

M1-LIKE RESPONSES IN THE LUNGS OF INFECTED MICE

Monocytes and MΦs are particularly noteworthy leukocytes during *O. tsutsugamushi* infection, as they can act as a target for bacterial replication and a propagator of the inflammatory response [6, 84], possibly playing a role in *O. tsutsugamushi* dissemination from skin lesions [5, 90]. While *in vitro* infection predominantly drives human monocytes/MΦs to M1-like transcription programs [5, 90], our current knowledge on *O. tsutsugamushi*-MΦ interactions in the lungs is still limited. Using IFA staining, we observed co-localization of bacteria (green) with IBA-1$^+$ MΦs (red) in mouse lungs (**Fig. 4.3**). To define monocyte/MΦ responses, we applied reported protocols and gating strategies for flow cytometric analysis of mouse lung monocyte/MΦ subsets [121] (**Fig. 4.1**). Compared with the mock controls, D6 and D9 samples had 4- to 5-fold increases in the frequency of CD64$^+$CD11b$^+$Ly6G$^-$ alveolar/interstitial monocytes/MΦs, as well as 6- and 14-fold increases in total cell numbers, respectively ($p < 0.01$ and $p < 0.001$, **Fig. 4.1**). Of note, nearly all (~97%) pulmonary MΦs were skewed toward an M1-like phenotype (CD80$^+$CD64$^+$CD11b$^+$Ly6G$^-$, **Fig. 4.1**) at D9. In contrast, while the mock and D2 lung samples contained ~3.2% of M2-like (CD206$^+$CD64$^+$CD11b$^+$Ly6G$^-$) cells, these cells were barely detectable at D6 or D9 (**Fig. 4.1**). These data suggest extensive recruitment and activation of M1-like cells, but severe loss and suppression of M2-like cells. Lung qRT-PCR assays confirmed a significant up-regulation of M1 markers (*IFNγ, FPR2, CD38*, and *NOS2*), but not M2 markers (*CD206*, *EGR2*), at D9 (**Fig. 4.2**). While the *IL10* up-expression was previously reported by our lab and other groups [122], we also detected an

increased expression of *ARG1* (**Fig. 4.2**), a marker of M2 polarization that promotes the growth of other intracellular pathogens [123]. Together with data shown in **Figs. 4.1-2**, we concluded that at the onset of disease and beyond, *O. tsutsugamushi* infection preferentially stimulated pro-inflammatory innate responses in neutrophils and M1-like monocytes/MΦs.

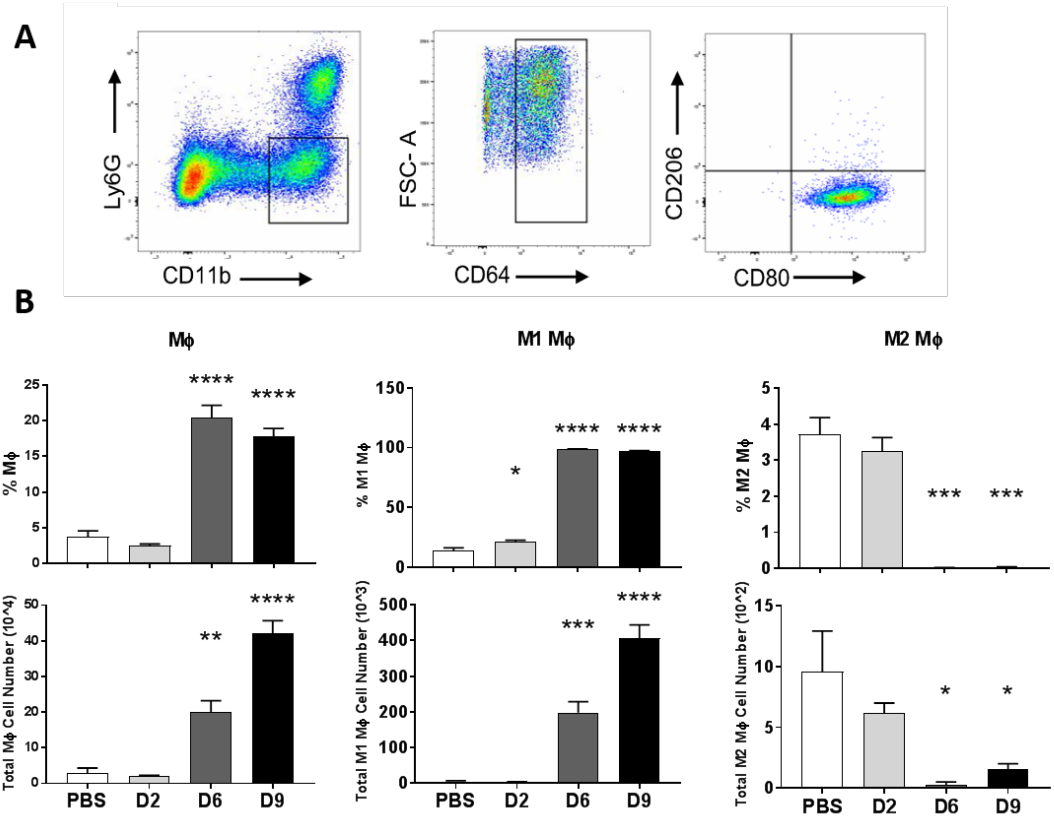

Fig. 4.1: Polarized macrophage activation in infected mouse lungs. Mice were infected with *O. tsutsugamushi* (4-5 mice/group) or innoculated with PBS (3-4 mice/group) for lung tissues collection at indicated days of infection. (A) Flow cytometric analyses of lung-derived cells, gated on $CD11b^{+}Ly6G^{-}$ MΦs and MΦ subsets, are shown for D9 samples. The percentages and total numbers of (B) MΦs ($CD64^{+}CD11b^{+}Ly6G^{-}$), (C) M1-type MΦs, and (D) M2-type MΦs. ($CD80^{+}CD64^{+}CD11b^{+}Ly6G^{-}$). Data are presented as relative to β-actin values. *, $p<0.05$; **, $p<0.01$; ***, $p<0.001$; and ****, $p<0.0001$ compared to the PBS controls. Graphs are shown as mean +/- SEM. One-way ANOVA with Tukey's Post Hoc was used for statistical analysis. Two independent mouse infection experiments were performed with similar trends and shown are representative data.

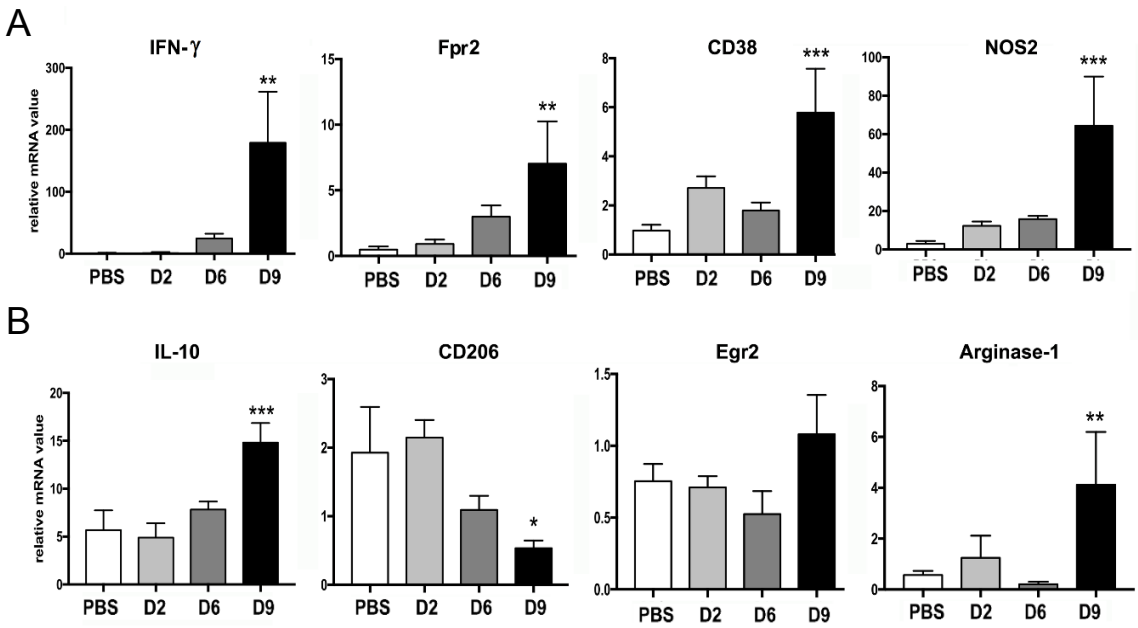

Fig. 4.2: Lung transcripts demonstrating polarized MΦ activation during lethal *O. tsutsugamushi* infection. Mice were infected with *O. tsutsugamushi* (4-5 mice/group) or PBS (3-4 mice/group) for lung tissues collection at indicated days of infection, as in *Figs. 1* and *3*. Lung tissues were measured for the expression of M1-related genes (A) and M2-related genes (B), respectively. Data are presented as relative to β-actin values. *, $p<0.05$; **, $p<0.01$; ***, $p<0.001$; and ****, $p<0.0001$ compared to the PBS controls. Graphs are shown as mean +/- SEM. One-way ANOVA with Tukey's Post Hoc was used for statistical analysis. Two independent mouse infection experiments were performed with similar trends and shown are representative data.

MACROPHAGE POLARIZATION IN FAVOR OF *ORIENTIA* REPLICATION *IN VITRO*

Because we had demonstrated differential monocyte/MΦ responses *in vivo*, we asked how MΦ polarization might influence intracellular growth of the bacteria. We generated bone marrow-derived MΦs from naïve C57BL/6J mice, polarized cells via pretreatment with LPS (100 ng/ml) or recombinant IL-4 (rIL-4, 10 ng/ml) for 24 h, infected cells with *O. tsutsugamushi* (MOI 5), and measured bacterial loads at different time points. Flow cytometry and gene profile analyses of primed but uninfected cells confirmed their corresponding polarization to either classically activated M1 or alternatively activated M2 phenotypes (**Fig. 4.3**), as documented by others [124]. At 48 h post-infection, IL-4-primed

M2 cells contained significantly increased loads of bacteria (determined by the copy number of *Orientia* 47-kDa gene) than LPS-primed M1 cells ($p < 0.01$, **Fig. 4.4**). At 72 h post-infection, M2 cells contained 10-fold more bacteria than M1 cells (**Fig. 4.4**), with extensive accumulation of bacteria (green) within IBA-1-positive MΦs (red, **Fig. 4.4**). To define cellular conditions relevant to bacterial growth, we compared host gene profiles in M1 versus M2 cells at 3 and 72 h post-infection. As shown in **Fig. 4.5**, a significant up-regulation of the *IL10* gene, with no measurable *NOS2* expression, was the notable phenotype of M2 cells at 72 h, which correlated with enhanced bacterial growth. Of note, we also found differential expression of two members of the suppressor of cytokine signaling (SOCS) genes, *SOCS1* and *SOCS3*. SOCS1 promotes an M2-type phenotype via inhibiting IFN-γ, IL-6, and TLR4 stimulation in MΦs, whereas SOCS3 promotes an M1 phenotype via inhibiting IL-4, IL-10, and TGF-β signaling [125].

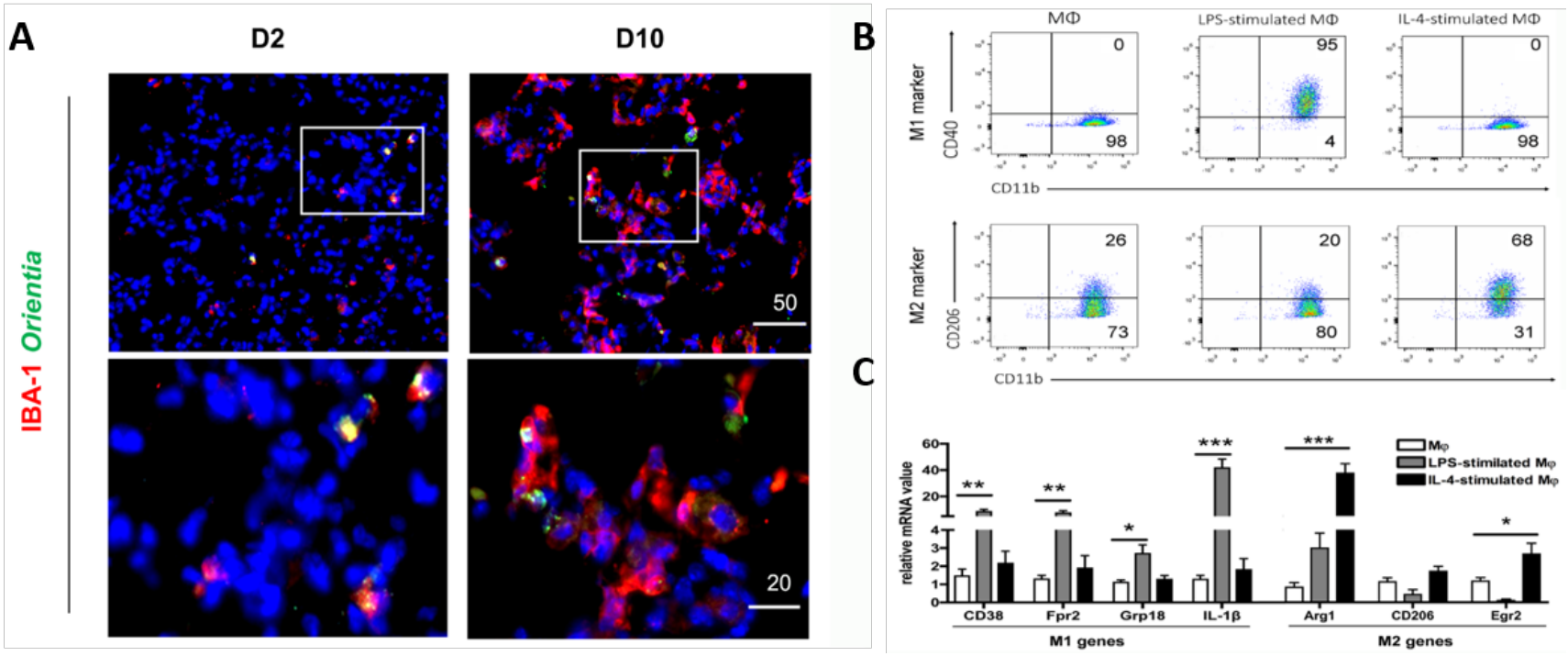

Fig. 4.3: MΦ infection in mouse lungs and differentiation *in vitro*. (A) Female C57BL/6J mice (4-6 mice per group) were inoculated with 1.325 x 10^6 of *O. tsutsugamushi* Karp strain. At days 2 and 10, equivalent lung portions were processed; frozen sections were co-stained for *Orientia* (red) and IBA-1 (green, a macrophage marker), showing images in a low-magnification (top rows, scale bar = 50 µm) and close-up views of the boxed areas (bottom rows, bar = 20 µm). (B) Bone marrow-derived MΦs were treated with LPS (100 ng/ml) or rIL-4 (10 ng/ml) for 24 h and analyzed for the expression of indicated markers via flow cytometry. The numbers represent the percentages (%) of gated cells. (C) LPS- and IL-4-primed cells were analyzed by qRT-PCR for the expression of the indicated markers, showing the polarization of MΦ subsets compared with control cells (*, $p<0.05$; **, $p<0.01$; and ****, $p<0.0001$). Data are shown as +/- SEM and were analyzed using one-way ANOVA with Tukey's Post Hoc.

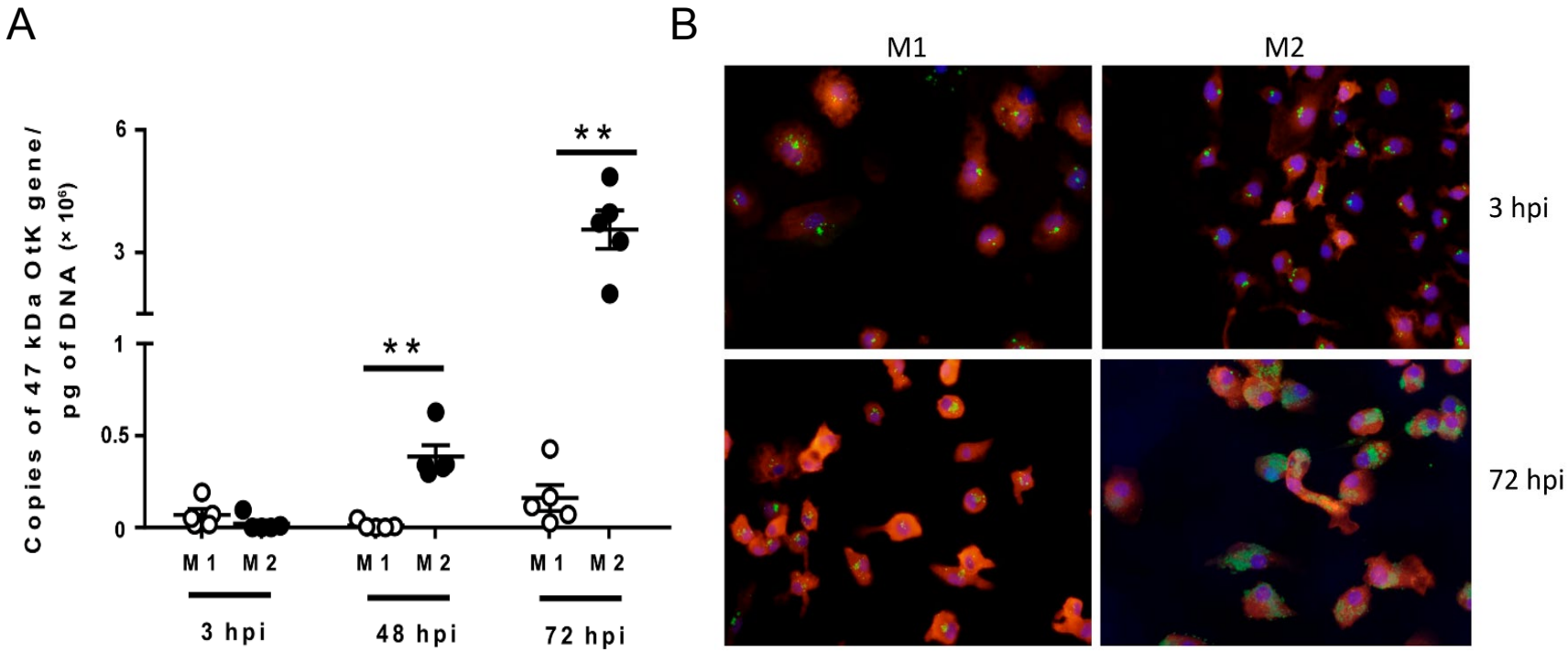

Fig. 4.4: Enhanced bacterial growth in M2-polarized MΦs. Bone marrow-derived MΦs were generated from C57BL/6J mice, polarized into M1 or M2 types by pre-treatment of cells with LPS (100 ng/ml) or rIL-4 (10 ng/ml), and infected with bacteria (5 MOI). (A) Bacterial loads at 3, 48 and 72 hpi (n=5) were determined by qPCR. Data are presented as the *Orientia* 47-kDa gene copy per pg of DNA. (B) Cells were co-stained for *Orientia* (green), IBA-1 (a MΦ marker, red), and DAPI (blue) at 3 and 72 hpi. *, $p<0.05$. Data for qRT-PCR were analyzed via a Mann-Whitney T test. Three independent experiments were performed with similar trends and shown are representative data.

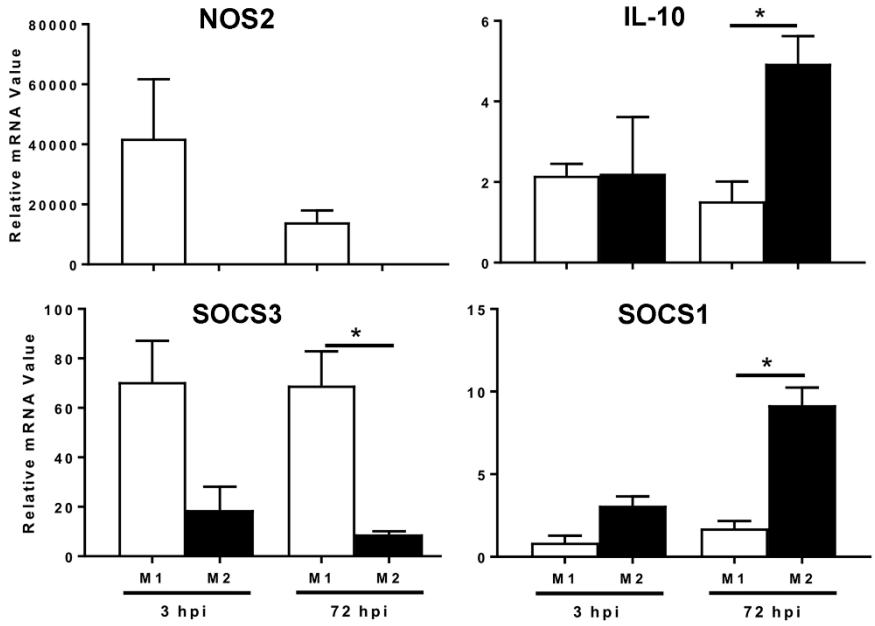

Fig 4.5: Expression of *NOS2, SOCS3, IL10,* and *SOCS1* in infected polarized MΦs. Bone marrow-derived MΦs were generated from C57BL/6J mice, polarized into M1 or M2 types by pre-treatment of cells with LPS (100 ng/ml) or rIL-4 (10 ng/ml), and infected with bacteria (5 MOI). Gene expression profiles of infected M1 and M2 MΦs (n=3) were analyzed at 3 and 72 hpi via qRT-PCR. *, $p<0.05$. Data for qRT-PCR were analyzed via a Mann-Whitney T test. Three independent experiments were performed with similar trends and shown are representative data.

DISCUSSION

Conditions that promote the killing or growth of *O. tsutsugamushi* remain unclear, in part due to difficulties in bacterial cultivation, genetic modification, or visualization for studying the host-bacterium interactions [87]. Currently, there are no available reports or data for the phenotype of *Orientia*-carrying MΦ subsets or the roles of arginase-1 *in vivo*. Our *in vitro* comparative studies suggested limited bacterial replication in LPS-primed M1-like MΦs (**Fig. 4.4**), supporting a role of NOS2-mediated mechanisms in the control of *O. tsutsugamushi* Karp strain [32]. Yet, our *in vitro* findings were contradictory to another

reported study, in which NO-enhanced the growth of *O. tsutsugamushi* Ikeda bacteria was observed in LPS-activated RAW 264.7 murine macrophages at days 6 to 8 post-infection [94]. While the use of different bacterial strains, MΦ sources, and examination times may account for these discrepancies, our study calls for careful examination of the intracellular niche for the replication of these obligate intracellular bacteria under different polarizing conditions. For bone marrow-derived MΦs, we found comparable bacterial loads in LPS- and IL-4-primed cells at 3 h, implying similar attachment and invasion of the bacteria under these two treatments. However, IL-4-primed M2 cells contained 10-fold more *O. tsutsugamushi* than LPS-primed M1 cells at 72 h. At present, our data did not exclude the possibility of bacterial growth in LPS-primed M1 cells after prolonged time *in vitro*, or in M1- vs. M2-like MΦs in mouse lungs or other organs. Given the recent report that specific MΦ responses, such as miR-155 and IL-10 production, correlate with prevention of cytokine storm in severe *O. tsutsugamushi* infection [88], it will be important to further examine whether the strong type-1 inflammatory responses *in vivo* [3] and M1-skewed responses (**Fig. 4.1**) are responsible for marked decrease in M2 MΦs in the lungs. The use of transgenic mouse strains for tracking MΦ subsets would also help reveal whether *O. tsutsugamushi* bacteria preferentially replicate within M2 MΦs *in vivo* or contribute to the impairment of type 2 immune responses.

Chapter 5: Discussion and Future Work

SUMMARY

The purpose of this work was to detail elements of vascular dysregulation and activation and the proceeding inflammatory immune response in the lungs of severely infected mice. Several recent studies have developed and characterizated of various murine models of *O. tsutsugamushi* infection, including intradermal infection [32, 43], i.v. infection [31], and even infection in a humanized mouse model [126]. All of these studies add details to the disease pathogenesis and immune response to various severities of *O. tsutsugamushi* infection that were previously unexplored. My focus for this dissertation was to investigate various aspects of pulmonary pathogenesis during lethal murine *O. tsutsugamushi* infection. Furthermore, this work characterized the contributions of two innate cell populations, neutrophils and macrophages. These cells are recruited in large numbers to the lungs in both our mouse model of infection and in human scrub typhus patients with severe pulmonary complications [2, 3].

The first specific Aim (**Chapter 3**) detailed the activation of endothelial cells in the lung (**Fig 3.1**). Increases of pulmonary endothelial markers was contrasted with the changes in endothelial expression of VE-cadherin and the receptor Tie2, both of which decreased during infection **(Figs. 3.2-3**). Decreases in Tie2 expression are often observed in disease models frequently associated with lung injury and ARDS such as sepsis and influenza [99, 127]. Previously, our lab had shown alterations in the transcript levels of the ligands of Tie2, Ang2 and Ang1 [3]. Ang1 is produced by endothelial pericytes to stimulate

Tie2 signaling, maintaining endothelial survival and quiescence [99]. We observed Ang1 production in the lungs throughout infection, although to a lesser extent when the mice are moribund at D9 (**Fig. 3.6**). Whether the decrease in Ang1 is due to actual changes in pulmonary endothelial pericytes at a transcription/translational level or whether these cells are damaged late in infection by the persistent inflammatory microenvironment of the lung is unclear. Ang2, which is stored in Weibel-Palade bodies in endothelial cells and released shortly after endothelial activation to compete with Ang1 binding and inhibit Tie2 signaling, is indeed released during *O. tsutsugamushi* infection as early as D2 and is observed readily in the lungs until the mice expire at D9-10. The ability to modulate Tie2 signaling to maintain endothelial integrity and ameliorate disease is an intriguing area of future study.

Chapter 3 also reported on the recruitment and activation of neutrophils in the lungs of severely infected mice. As expected from our previous IHC work, we observed a large increase in the number of neutrophils recruited to the lung and a clear shift in the level of activation of these neutrophils (**Fig. 3.12**). Neutrophils play important roles in combating extracellular pathogens, but *O. tsutsugamushi* is an obligate intracellular bacterium; thus this large increase in the activated neutrophils in the lungs of infected mice led us to the hypothesis that neutrophils may be playing an immunopathogenic role, as they do in a number of diseases, including ARDS [63, 64, 128]. By depleting neutrophils at both D-1 and D4 of infection we were able to determine that early depletion of neutrophils (D-1) can ameliorate disease, while depletion at D4 led to decreased weight loss compared to controls at D5-D7 of infection. Despite this decrease in loss of weight in total body weight, depletion of neutrophils at D4 did not affect survival of infected mice (**Fig. 3.18**).

Regardless of when neutrophils are depleted, mice never died at earlier time points or lost more weight compared to control infected mice. Our data demonstrate that neutrophils do not play a protective role during *O. tsutsugamushi* infection. Neutrophil depletion resulted in increased naïve T cells in the lungs of infected mice compared to infected IgG-treated control mice (**Fig. 3.20).** Additionally, D-1 neutrophil-depleted mice showed increased number of macrophages in the lungs as well compared to infected IgG mice (**Fig. 3.22**). The mechanism by which neutrophils may regulate the activation/generation of these cell subsets during *O. tsutsugamushi* infection is unknown. Investigation into the alterations in the effector functions of macrophages and T cells after neutrophil depletion during *O. tsutsugamushi* infection help elucidate the differences in survival that occur between the D-1 neutrophil depletion group and the infected IgG treated controls.

My second aim (**Chapter 4**) describes the recruitment and polarization of recruited MΦs in the lungs of mice severely infected with *O. tsutsugamushi*. We observed a large increase in the number of MΦs in the lung by D6 and D9 (**Fig. 4.1**). The recruited MΦs are almost entirely polarized to a "classical" or "M1" type profile. This was confirmed by flow cytometry and correlates quite clearly with what we observe in total lung mRNA when we measured M1 related genes (**Fig. 4.2**). When the effect of polarized MΦs *in vitro* to either M1 or M2 was investigated, I observed a striking difference in the ability of *O. tsutsugamushi* to grow in the differentially polarized MΦs (**Fig. 4.4**). *O. tsutsugamushi* was able to readily replicate in M2-polarized macrophages by 48 and 72 hpi. In comparison, M1 polarized MΦs suppressed the infection. These MΦ polarization studies are largely in agreement with what has been observed in sublethal mouse models and in circulating monocytes/MΦs in human patients [32, 90]. We hypothesize that iNOS production of nitric

oxide could be instrumental in control of the bacteria in M1 MΦs, as this enzyme is highly upregulated in M1 MΦs and has been shown to be important in *O. tsutsugamushi* bacterial replication in IFN-γ treated MΦ [32].

MΦ activation during *O. tsutsugamushi* infection appears to be an important component of the host immune response. However, current studies have not identified what, if any, bacterial antigen from *Orientia* is responsible for triggering this effect. Previous work has identified that *in vitro* infection of mouse macrophages demonstrated that *Orientia* quickly induced production of chemokines CCL2, CCL3, CCL4, and CCL5 in infected macrophages [84]. These responses were found to be controlled by NF-κB transcription and could be induced by both live and heat-killed bacteria, most likely due to recognition of *Orientia* PAMPs by pathogen recognition receptors (PRRs) such as Toll-like receptors (TLRs) or intracellular Nod-like receptors (NLRs). Identification of TLRs and NLRs that may play a role in triggering the immune response to *Orientia* infection is an ongoing and interesting area of study as *Orientia* do not produce membrane structures such as LPS or traditional peptidoglycan that are commonly recognized bacterial PAMPs [129, 130]. Studies using $TLR2^{-/-}$ bone marrow-derived macrophages (BMDMs) have demonstrated that TLR2 receptor is required to generate inflammatory cytokines IL-6 and TNF-α [131]. TLR2 deletion in mice results in ameliorated disease, but comparable bacterial growth, in infected organs after intraperitoneal infection with *O. tsutsugamushi* Karp [131]. In contrast, macrophages expressing a hyporesponsive TLR4 had only a modest reduction in the amount of TNF-α during *Orientia* infection compared to control macrophages [86]. Deletion of the TLR proximal signaling adaptor protein, MyD88, in BMDMs also caused a significant decrease in TNF-α production, further implicating TLR

signaling during *Orientia* infection of macrophages [122]. Low infectious doses of *Orientia* in macrophages also correlated with decreasing TNF-α production [86, 88]. Given that circulating TNF-α is a correlative of severity of disease in human patients [132], understanding the mechanisms of PRR and TLR signaling in infected macrophages and production of TNF-α and related inflammatory cytokines is important to understanding macrophage polarization and disease progression during scrub typhus.

Orientia infection can also initiate inflammasome activation and IL-1β secretion in infected macrophages [85]. *Orientia* is believed to be phagocytosed by macrophages where acidification of the phagosome leads so bacterial release and recognition by an intracellular NLR that promotes inflammasome formation, caspase activation and eventual secretion of IL-1β by macrophages [85]. Importantly, *Orientia* does not provide the initial priming signal of inflammasome formation via plasma membrane PRRs [85], thus these PRRs (such as TLR2) must be activated by other inflammatory mediators. Identifying what inflammatory mediators during *O. tsutsugamushi* infection lead to macrophage activation and thus a protective response will be important for identifying biomarkers of disease severity and understanding definitive correlates of immunity during scrub typhus.

My work here is the first investigate the presence (or lack thereof) of "M2" MΦs during *O. tsutsugamushi* infection. Despite the decrease in M2-type MΦs in the lungs of infected mice, we detected an increase in the transcription of *ARGINASE1*, a gene typically associated with M2 MΦs. The M2 MΦs are critical for tissue repair and resolution of the inflammatory response [133]. There is small population of M2 MΦs in the lungs of mice early in infection (**Fig. 4.1**); however, this population almost completely disappears at 6 and 9 dpi. At present it is unknown whether M2 MΦs play a role early on in infection as a

cellular niche where *O. tsutsugamushi* is able to replicate in the lungs, mirroring what we observed *in vitro* (**Fig. 4.4**). Furthermore, there have been no studies conducted in the self-resolving infection models of *O. tsutsugamushi* to investigate if MΦs are polarized to M2 MΦs during disease resolution. Despite the decrease in the M2 MΦs during infection, we detected the increase two genes associated with M2-polarization, *IL10* and *ARGINASE1* (**Fig. 4.2**). Scrub typhus patients have increased circulating IL-10 concentrations during acute infection [134] and is hypothesized to prevent cytokine storm during scrub typhus [88]. Currently we are unclear what the increase in *ARGINASE1* transcription in the lungs of infected mice contributes to disease pathogenesis. *Mycobacterium tuberculosis* infection (another intracellular bacterium), Arginase-1 production during results in greater bacterial load and exacerbated pathology in mice [135]. This study also demonstrated that arginase-1-producing cells affected local T cell proliferation in the infected mice [135]. Given the importance of macrophages as a cellular target of infection and directors of inflammation, understanding how MΦs become polarized during scrub typhus and what effect this polarization has on bacterial growth and inflammatory damage of host tissues are important topics for future study.

FUTURE STUDIES BASED ON INITIAL PILOT EXPERIMENTS

Angiopoietin 1 and 2 – Targeted Treatment

After documenting decreases in the lung in Ang1 and Tie2 as well as increases in Ang2, we hypothesized that this imbalance could be contributing to disease pathogenesis (**Fig. 3.6-8**). Ang2 release and subsequent blocking of Ang1/Tie2 signaling, contribute to endothelial barrier break down, increases in leukocyte adhesion molecules, and even endothelial death [136]. Furthermore, increases in released Ang2 correlates with mortality

of patients with ARDS and patients with hyper-inflammatory diseases, such as sepsis [53, 109]. To contrast Ang2 release predicting an unfavorable outcome in patients, the administration of Ang1 has been shown to decrease plasma leakage in adult vasculature via inhibition of VEGF signaling [137, 138]. Administration of an Ang2 inhibitor has been shown to improve the survival of mice with cecal ligation puncture (CLP)-induced sepsis [139]. Additionally, siRNA against Ang2 has also been shown to ameliorate disease and mortality in another CLP sepsis mouse model [57]. To complement these studies, recent translational research has shown that activation of Tie2 via Ang2-antibody or administration of recombinant Ang1 are able to ameliorate disease in sepsis [56, 140].

To test whether blocking Ang2/Tie2 interaction would result in an attenuated disease course in *O. tsutsugamushi* infection, we first treated infected mice with Simvastatin, a 3-hydroxy-3-methyl-glutaryl-CoA reductase inhibitor. The Simvastatin compound is generally used as an inhibitor of cholesterol biosynthesis to control the cholesterol level [141]. Simvastatin has been shown to reduce Ang2 inhibition of Tie2 signaling *in vitro* in HUVECs and to ameliorate disease *in vivo* in LPS and CLP-induced sepsis model in mice [142, 143]. Although the exact mechanism of action by which Simvastatin works to do this is unknown, it is clear that treatment of HUVECs with Simvastatin inhibits the translocation of the transcription factor Foxo1 into the nucleus [142]. This nuclear translocation of Foxo1 occurs when Ang2 binds to Tie2 and induces several endothelial activation processes as well as upregulates the transcription of *ANG2*. Additionally, Simvastatin has already been studied in human patients who developed pulmonary sepsis [142]. These patients had significantly less circulating Ang2 upon use of Simvastatin. Given these *in vitro* and *in vivo* findings we wondered whether treatment with

Simvastatin during severe *O. tsutsugamushi* infection would attenuate disease. To test this hypothesis, we treated mice with Simvastatin (1 µg/g) during a lethal infection of *O. tsutsugamushi* (**Fig. 5.1**).

I observed that there was no significant change in either weight loss or survival in the Simvastatin-treated infected mice (blue, solid line, **Fig. 5.1**) compared to infected mice treated with vehicle (red, dotted line, **Fig. 5.1**). This was surprising to us as we had expected

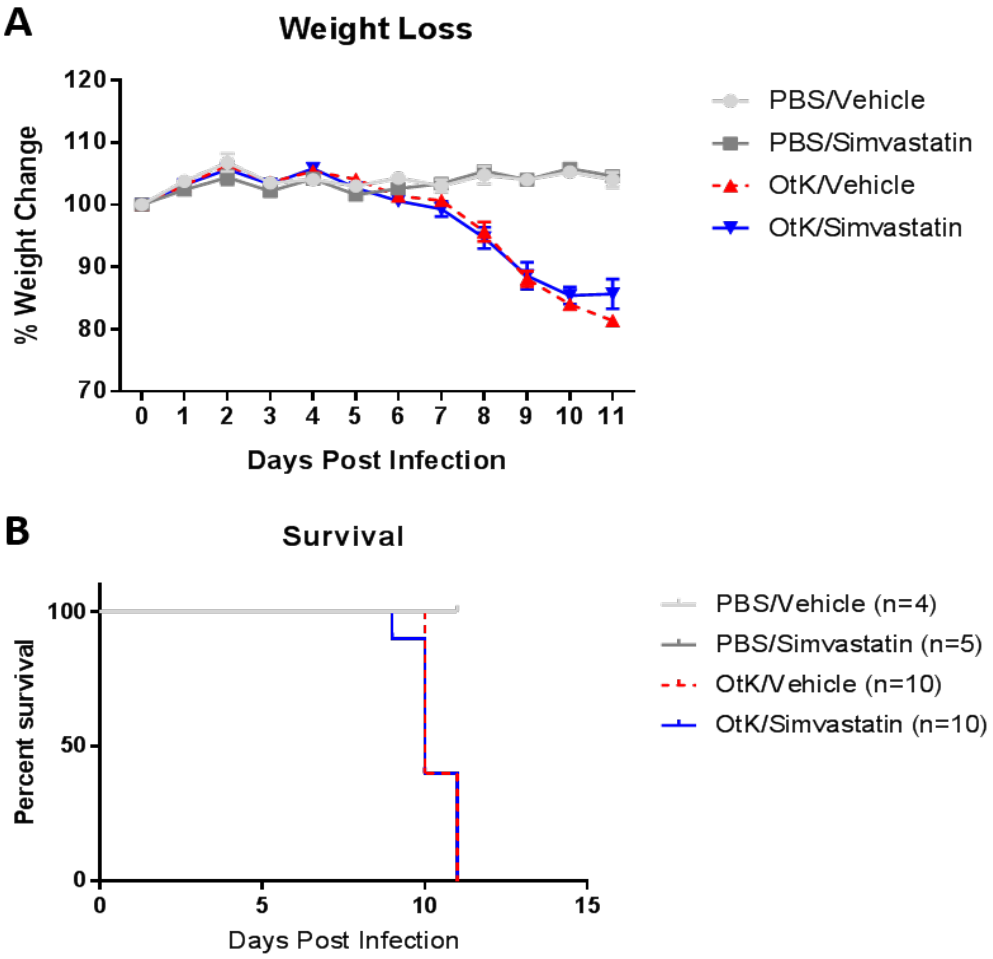

Fig. 5.1: Survival and weight loss of Simvastatin treated mice during lethal infection with *O. tsutsugamushi*. Female C57Bl/6 mice were infected with ~1.0x10^6 of *O. tsutsugamushi* Karp strain and treated with Simvastatin intraperitoneally (1µg/g) at -1, 3, 6, and 9 dpi. (A-B) Mice were monitored for weight loss and survival.

to see an amelioration of disease given the imbalance in Ang2/1 production during late infection in our lethally challenged mice (**Fig. 3.6**). Future studies of Simvastatin treatment in our murine model will use lower infectious doses of bacteria as well as different concentrations of Simvastatin to determine if treatment with the compound improves host recovery during sublethal scrub typhus.

To modulate Ang2/Ang1 levels in a more direct manner during *O. tsutsugamushi* infection, we procured anti-Ang2 blocking antibodies (anti-Ang2, REGN 910) and recombinant Ang1 protein (rAng1, REGN108). It has been reported by other in a murine model of *Mycoplasma pulmonis* that administration of REGN910 blocks Ang2 signaling and REGN108 was shown to stimulate Tie2 signaling as recombinant Ang1, leading to decreased endothelial activation [144]. Additionally, these compounds have demonstrated the ability to decrease leukocyte trafficking in the lungs of mice during *M. pulmonis* infection [145].

Given the observed changes in Tie2 expression and activation during *O. tsutsugamushi* infection (**Fig. 3.8**), we conducted a pilot study to determine if administration of anti-Ang2 or combination of anti-Ang2/rAng1 could ameliorate disease during *O. tsutsugamushi* infection. Mice were dosed with anti-Ang2 antibody (REGN910 5 μg/g every 4 days), rAng1+anti-Ang2 antibody (REGN108 25 μg/g every 3 days, REGN 910 5ug/g every 4 days, respectively), or human IgG control antibody (10 μg/g) and

infected with a subtlethal i.v. infection of $1x10^5$ *O. tsutsugamushi*. Mice were then monitored for weight loss, survival, and disease score (**Figs. 5.2-5.3**).

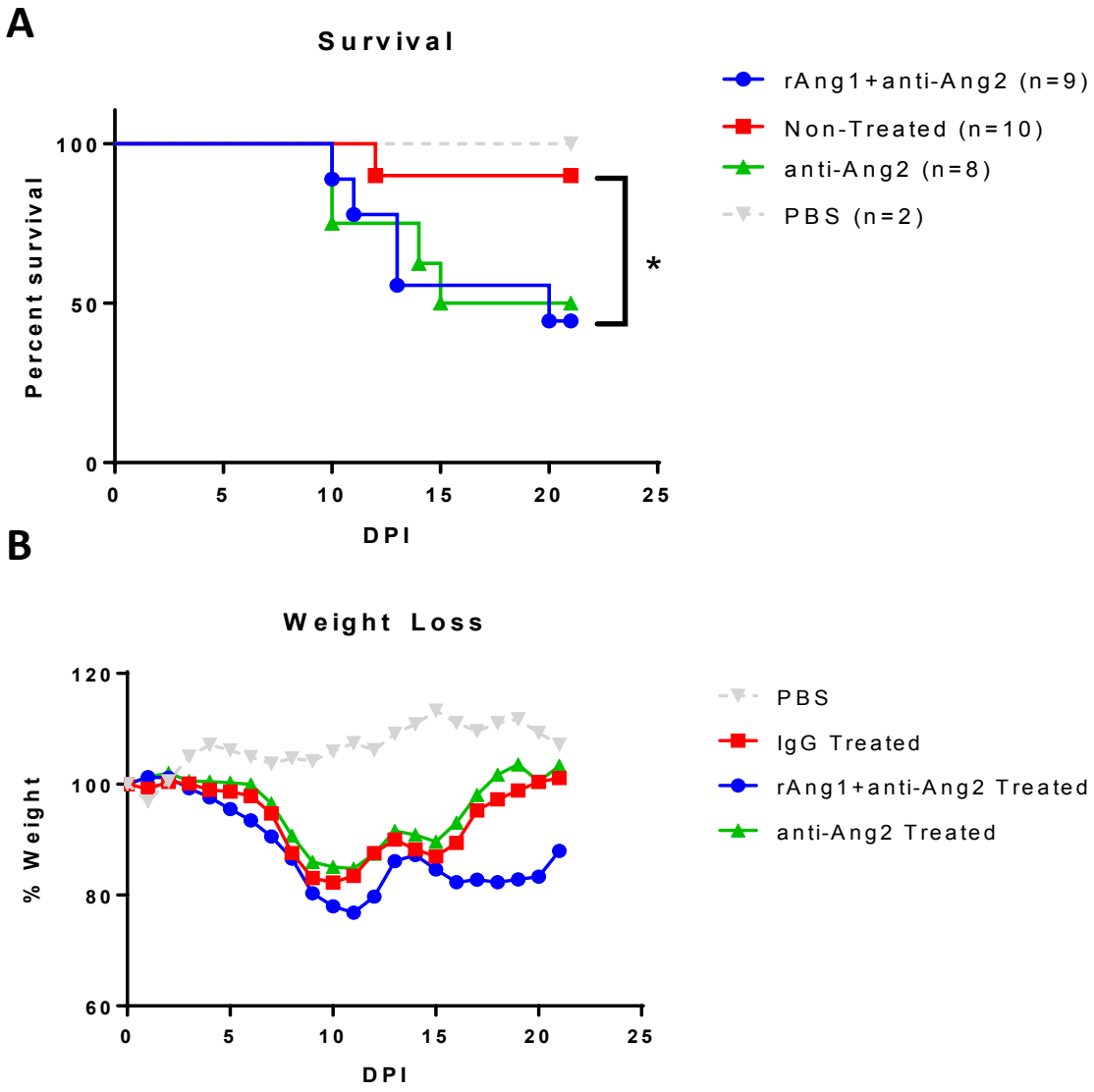

Fig. 5.2: Weight loss and survival of mice treated with anti-Ang2 blocking antibodies or rAng1+anti-Ang2 antibodies. Female C57BL/6J mice were inoculated with 1.0 x 10^5 of *O. tsutsugamushi* Karp strain (8-10 mice/group) or PBS (2 mice/group). Mice were dosed with anti-Ang2 antibody (REGN910 5 µg/g every 4 days), rAng1+anti-Ang2 antibody (REGN108 25 ug/g every 3 days, REGN 910 5 µg/g every 4 days, respectively), or human IgG control antibody (10µg/g) till D8 of infection. (A-B) Survival and weight loss curves of PBS infected mice (n = 2, gray dotted line), *O. tsutsugamushi* infected/IgG treated (n = 10, red line), *O. tsutsugamushi* infected/anti-Ang2 treated (n = 9, blue line), *O. tsutsugamushi* infected/rAng1+anti-Ang2 treated (n=8, green line). *, $p<0.05$

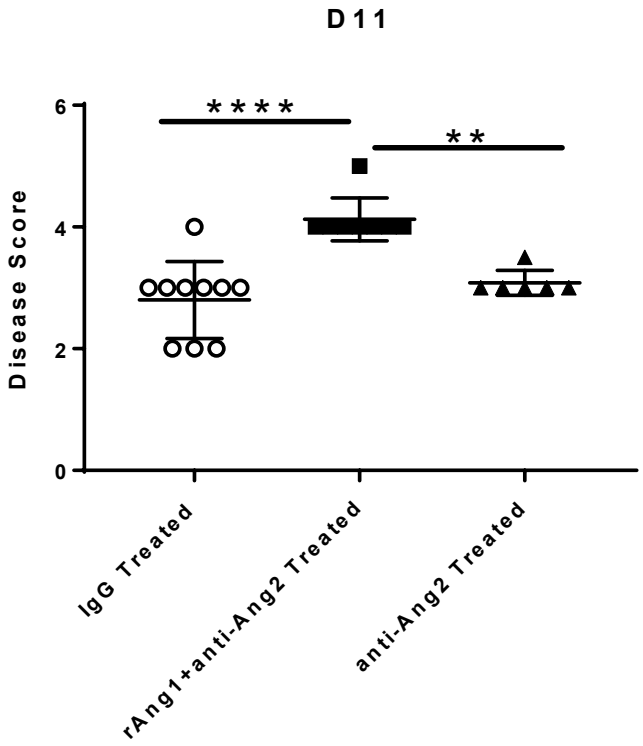

Fig. 5.3: Day 11 disease score for infected mice groups during rAng1 and anti-Ang2 treatment. Disease scores from sublethally infected mice at the peak of weight loss (D11) during infection. Graphs are shown as mean +/- SEM. One-way Anova with a Tukey's post-hoc analysis was used for statistical analysis. **, $p < 0.01$; and ***, $p<0.001$ compared to indicated groups.

Surprisingly, we observed that a greater number of mice died in both groups treated with either anti-Ang2 antibody or combination rAng+anti-Ang2 therapy (**Fig. 5.2**). Only one mouse died from infected control mice given $1x10^5$ dose of *O. tsutsugamushi*, which resulted in a significant difference compared to the mice dosed with rAng1+anti-Ang2. Furthermore, rAng1+anti-Ang2 treatment resulted in a more severe disease score, as demonstrated at the peak of weight loss during infection, D11 (**Fig. 5.3, Table 2.2**).

Further experiments with anti-Ang2 and rAng1 treatment during *O. tsutsugamushi* infection are needed to optimize this initial pilot study. Mice were dosed frequently (REGN108 every 3 days, REGN 910 every 4 days) from D-1of the infection until D8. It may be that Ang2 production is important during *O. tsutsugamushi* infection at early time points to initiate the early immune response and thus provide protection [146]. Additionally, we have only utilized one dosing concentration thus far for both REGN108 (25 μg/g) and REGN910 (5 μg/g) and additional studies to determine the range of effective doses during infection is necessary. In a number of models such as murine endotoxemia, murine and rabbit gram-negative sepsis, polymicrobial sepsis, and influenza infection Ang2 abrogation and/or treatment with Ang1 has been shown to ameliorate disease [147]. Ang2 blockade or Ang1 treatment has never been investigated in the context of infection with an endotheliotropic agent such as *O. tsutsugamushi*, thus unexpected outcomes may occur. Lastly, I have yet to investigate the effect of rAng1 treatment alone during infection, as this is an important condition to study whether Ang1 alone has the capacity to dampen endothelial activation in a less extreme fashion than completely blocking Ang2 signaling. Ang1 treatment has been studied in murine models of endotoxemia, malaria, and sepsis and shown to improve survival [147]. Studies to elucidate the pathogenic/protective roles of Tie2/Angiopoietin signaling in scrub typhus will allow us to not only understand better the vascular dysregulation in this endotheliotropic pathogen, but also explore alternate therapeutics, as is being researched in other strong inflammatory diseases [147].

T Cell Immune Memory in the Lungs and Spleen

Studies in non-human primates and humans have shown that immune memory to *O.tsutsugamushi* challenge is long lasting to homologous strains of bacteria [148, 149].

This protection, however, quickly wanes for heterologous strain challenge, which has been investigated in mice and humans [148, 150]. It is believed that the variability in the "immunodominant" proteins such as the 56 kDa outer-membrane protein between strains accounts for the lack of heterologous strain protection [151].

Immunity to *O. tsutsugamushi* re-infection with a heterologous strain is believed to be mediated mostly by cellular immunity. In 1976, Shirai *et. al* reported that mice could be protected from lethal challenge by transfer of splenocytes from previously infected mice, and that this protection was ablated with the depletion of T cells [152]. Later studies demonstrated that use of the 56 kDa antigen to immunize mice induced a strong IL-2 and IFN-γ response, indicative of a Th1 response [153]. The importance of cellular immunity during scrub typhus has been investigated in two recent reports, especially the necessity of CD8 T cells during infection, as depletion of CD8 T cells resulted in a lethal outcome during a normally sublethal challenge of mice with *O. tsutsugamushi* [1, 101].

Only a few studies have investigated specific characteristics of memory T cells from scrub typhus patients or in animal models. After infection, several memory T cell populations arise: A central memory (CM) population trafficked through lymphoid tissue, effector memory (EM) cells circulating in both lymphoid and non-lymphoid tissue, and tissue resident memory cells (Trm) maintained in non-lymphoid tissues [154]. These subsets act in various tissues to establish a robust and rapid response to a previously encountered pathogen. Cho *et al.* reported that scrub typhus patients in both the acute and convalescent phases of infection had significantly increased circulating CD8 effector memory populations compared to healthy controls [155]. This increase was not observed, however, in the central memory CD8 cell populations or in the CD4 central or effector T

cells of patients in the convalescent phase [155]. Ha *et al*. reported both circulating CD4 and CD8 T cells from individuals that had scrub typhus previously and were rechallenged with *O. tsutsugamushi* membrane antigen (TSA 56 or ScaA protein) showed increased IFN-γ and TNF-α production within a year of the original infection, but this antigen-stimulated cytokine production decreased after a year [156]. In a murine model, Min *et al.* recently of infection demonstrated that CD4 T cells from mice previously infected with *O. tsutsugamushi* were able to produce IFN-γ and TNF-α (to a lesser extent) upon restimulation with *O. tsutsugamushi* antigen [122]. This report also discovered that this CD4 memory response is, in part, dependent on type-1 IFN and IL-10 signaling, previously unknown in scrub typhus [122].

While much of this dissertation work focused on early endothelial and innate immune responses to scrub typhus and their implications throughout infection, I also used lung and spleen tissues and analyzed several aspects of the adaptive immune response during *O. tsutsugamushi* infection. As shown in **Figs. 3.9-10**, flow cytometry and IFA analyses were conducted to assess the T cell response in the lungs of mice lethally infected with *O. tsutsugamushi*. We observed that by D10 of infection, total lung-recruited T cells were predominantly CD8 compared to CD4 by a ratio of ~3:1 (**Fig. 3.11**). This finding highlights the importance of $CD8^+$ T cell immunity, echoing previous reports [1, 101]. To complement our lethal T cell responses, I also performed a sublethal infection and determined the presence of CD4 and CD8 T cells at D31 in both the spleens and lungs of mice that had recovered weight from infection (**Fig. 5.4**).

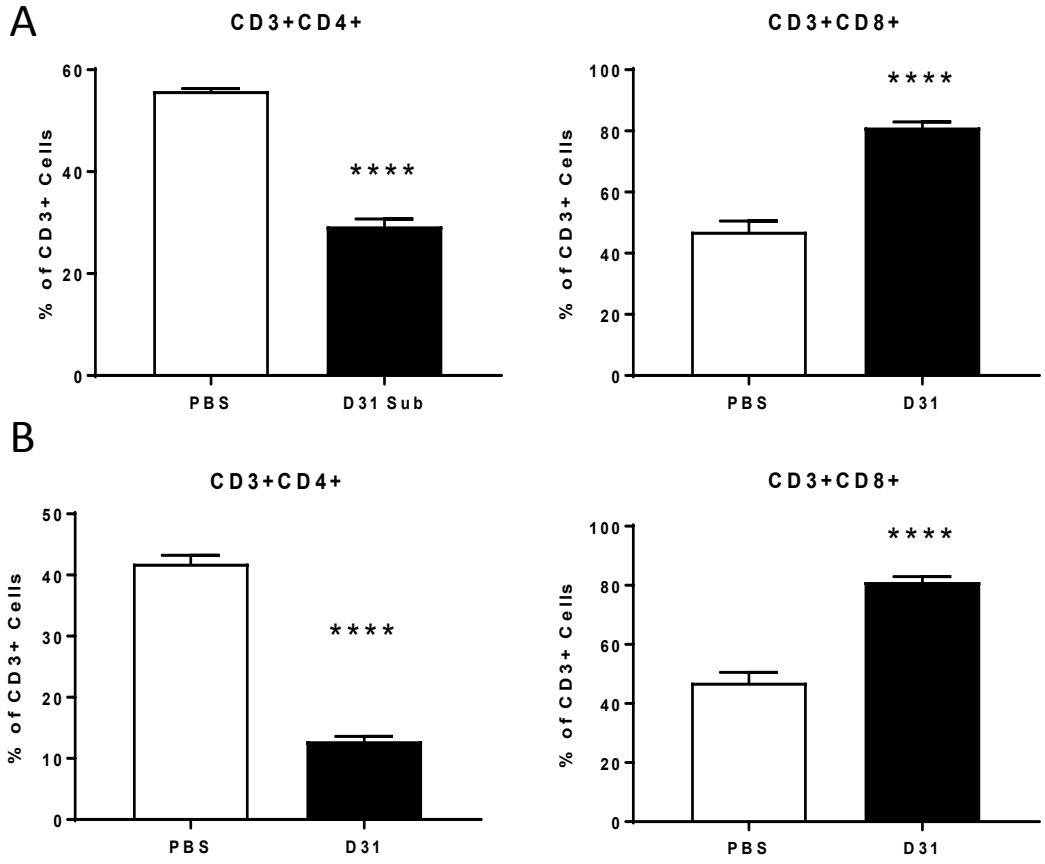

Fig. 5.4: Percentages of CD4 and CD8 T cells in the spleens and lungs of sublethally infected mice. Female C57BL/6J mice (4-5 mice/group) were inoculated with 1.0 x 10^5 of *O. tsutsugamushi* Karp strain. At 31 days post infection, single-cell suspensions were prepared from the spleens for flow cytometric analysis. Data here show the percentage of CD4 and CD8 T cells in the (A) spleens and (B) lungs of mice recovered from infection. Graphs are shown as mean +/- SEM. T-test with Welch's correction was used for statistical analysis. ****, $p < 0.0001$ compared to PBS controls.

In both the spleen and lungs, we observed significant decreases in the CD4 T cell percentages ($p < 0.0001$) compared to PBS inoculated controls at D31 of infection (**Fig. 5.4**). In contrast, percentages of CD8 T cells were significantly increased in both organs at D31 ($p < 0.0001$, **Fig. 5.4**). To further characterize the T cell populations in the spleen and lungs, flow cytometry was performed to detect markers of T memory cells. For T cells in the spleen I determined the presence of EM (IL-$7R^+CD44^+CD62L^-$) and CM (IL-

7R$^+$CD44$^+$CD62L$^+$) CD4 and CD8 T cells at D31 of sublethal infection in both percentages (**Fig. 5.5**) and total cell numbers (**Fig. 5.6**).

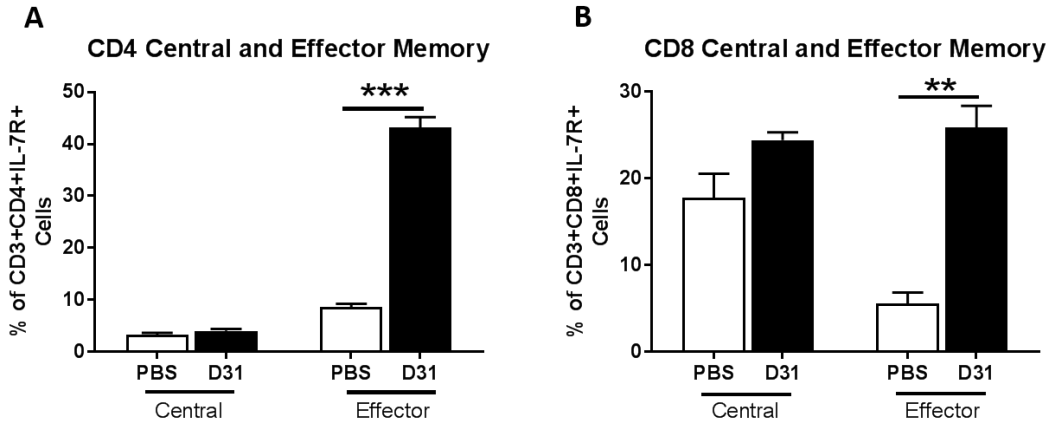

Fig. 5.5: Changes in EM and CM T cell populations in the spleen of sublethally infected mice. Female C57BL/6J mice (4-5 mice/group) were inoculated with 1.0 x 10^5 of *O. tsutsugamushi* Karp strain. At 31 days post infection, single-cell suspensions were prepared from the spleens for flow cytometric analysis. (A) Total CM (IL-7R$^+$CD44$^+$CD62L$^+$) T cells in the CD4 (blue) and CD8 (green) T cell populations. (B) Total EM (IL-7R$^+$CD44$^+$CD62L$^-$) T cells in the CD4 (red) and CD8 (purple) T cell populations. Graphs are shown as mean +/- SEM. T-test with Welch's correction was used for statistical analysis. **, $p < 0.01$; and ***, $p<0.001$ compared to PBS controls.

As shown in **Fig. 5.5**, we found there is no growth in total number of our CD4 central memory cell population in the spleens of mice at D31 compared to PBS inoculated controls. There a slight, not significant, increase in the total number of our CD8 central memory cells in our recovered mice (**Fig. 5.6**). Both total CD4 and CD8 effector memory populations in the spleen had a significant increase compared to PBS controls (**Fig. 5.5**). Our data is consistent with previous studies from Cho *et al.* that revealed increased numbers of effector CD8 T cells in the circulation from convalescent scrub typhus patients [155]. Cho *et al.* did not observe any significant increase in the circulating CD4 effector memory population from human patients, as we have in the spleens of mice at D31 [155]. Our

observations of memory T cells in the spleens of mice at D31 of sublethal infection, coupled with the data from recovering scrub typhus patients highlights the maintenance of the effector memory population after infection. The central memory population, however, does not undergo the same level of expansion. Min *et al*. have recently shown that there is a population of active CD4 T cells in the spleen of previously infected mice that can responds to stimulation with *Orientia* peptide, but whether this is mirrored in the central memory CD8 T cell population has not been explored [122]. The expansion of the splenic memory CD4 T cell population was shown to be controlled by type I IFN/IL-10 signaling during *O. tsutsugamushi* infection, but investigations into how this signaling is controlling the central memory expansion particularly have not been conducted [157].

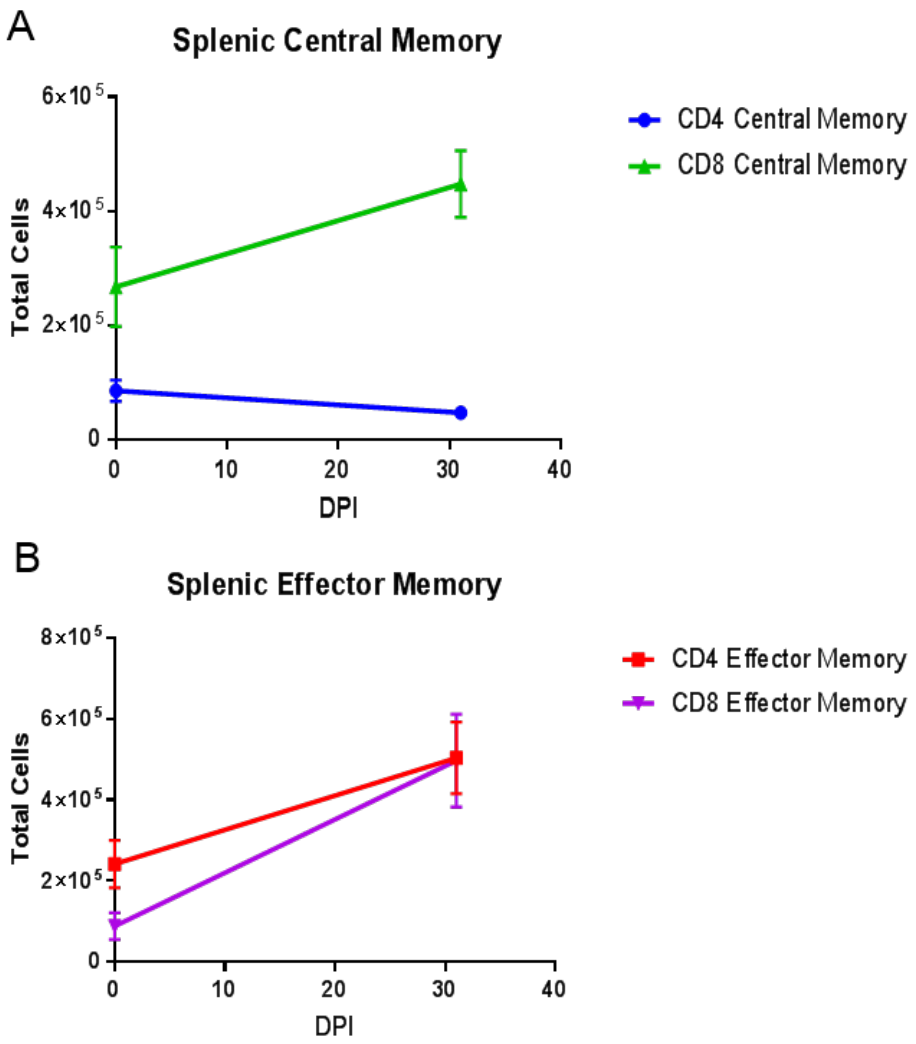

Fig. 5.6: Total cell populations of EM and CM T cells in the spleen of sublethally infected mice. Female C57BL/6J mice (4-5 mice/group) were inoculated with 1.0 x 10^5 of *O. tsutsugamushi* Karp strain. At 31 days post infection, single-cell suspensions were prepared from the spleens for flow cytometric analysis. (A) Total CM (IL-$7R^+CD44^+CD62L^+$) T cells in the CD4 (blue) and CD8 (green) T cell populations. (B) Total EM (IL-$7R^+CD44^+CD62L^-$) T cells in the CD4 (red) and CD8 (purple) T cell populations. Graphs are shown as mean +/- SEM.

In addition to characterizing the T cell memory subsets in the spleen of sublethally infected mice, I also investigated tissue resident memory (Trm) cells in the lungs of mice recovered from *O. tsutsugamushi* infection (**Fig. 5.7**). Trm are believed to be long lived cells stationed in tissues to act as a first line of defense to pathogens in non-lymphoid tissues [154]. Trms are phenotypically different from EM and CM cells, and upregulate

specific cell surface markers [154]. Two markers in particular are used to delineate Trms from other T cell populations, CD103 and CD69 [158, 159]. CD69 is an inhibitor of sphigosine-1-phosphate receptor 1 (S1PR1) function, and CD103 is an $\alpha_E\beta_7$ integrin. The function of both of these markers is to prevent cellular egress from tissues [159]. Given that Trms in scrub typhus has not been explored previously, we performed a pilot study using flow cytometry analysis of lung tissues from sublethally infected mice on D31 of infection described in our lethal infection studies (**Fig. 5.7**). Our results showed a clear $CD69^+CD103^+$ population in the CD8 T cells at D31 post infection in the lung (**Fig. 5.7**). However, $CD69^+CD103^+$ population is not present in the CD4 T cell population (**Fig. 5.7**). $CD69^+CD103^+$ Trms express several important molecules for tissue homing and cellular retention [159]. I determined the expression of two surface markers $CD69^+CD103^+$ Trms, VLA-1 and CXCR6, as reported by Oja *et al.* [159]. VLA-1 is an integrin molecule important for tissue retention and has been shown to be on lung CD8 Trms after influenza infection and adenoviral-vectored tuberculosis vaccine innoculation [158, 160]. CXCR6 is a chemokine receptor that is involved in T cell homing to inflamed tissues [161, 162]. My flow cytometry analysis of the $CD8^+CD69^+CD103^+$ Trm population showed that the vast majority (~90%) of these cells were VLA-1^+CXCR6^+ (**Fig. 5.8**). Collectively, these pilot data suggest that a CD8 Trm population arises after *O. tsutsugamushi* infection in the lungs of infected mice.

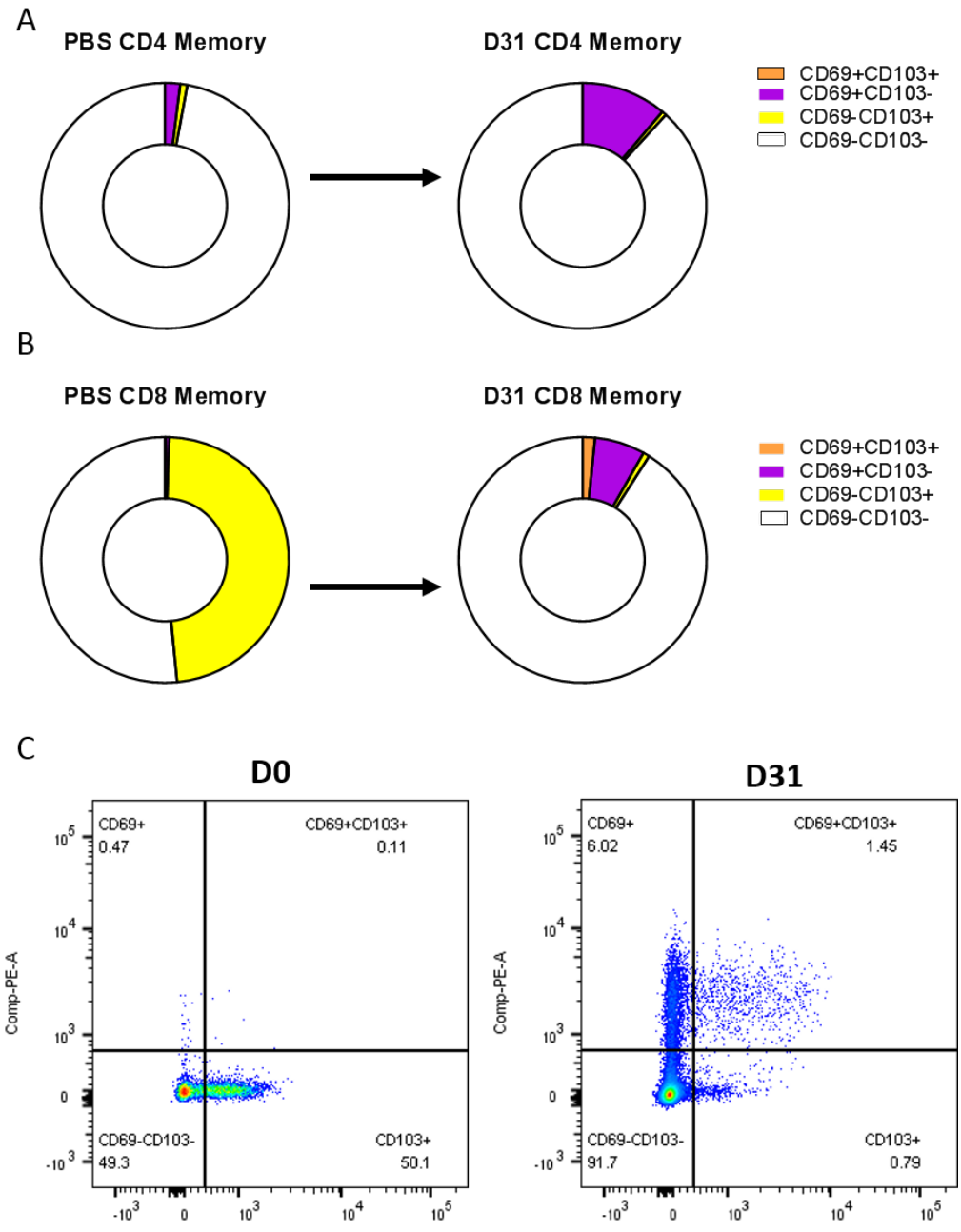

Fig. 5.7: Trm T cells in the lungs of mice sublethally infected with *O. tsutsugamushi*. C57BL/6J mice (4-5 mice/group) were inoculated with 1.0 x 10^5 of *O. tsutsugamushi* Karp strain. At 31 days post infection, single-cell suspensions were prepared from the lungs for flow cytometric analysis. Proportions of (A) CD4 and (B) CD8 T cells expressing Trm markers. Cells expressing $CD69^+CD103^+$ (orange), $CD69^+CD103^-$ (purple), $CD69^-CD103^+$ (yellow), and $CD69^-CD103^-$ (white) are shown as parts of the total T cell populations. (C) Gating strategy employed to analyze lung T cells displayed in (A-B, cells shown here are the CD8 T cells).

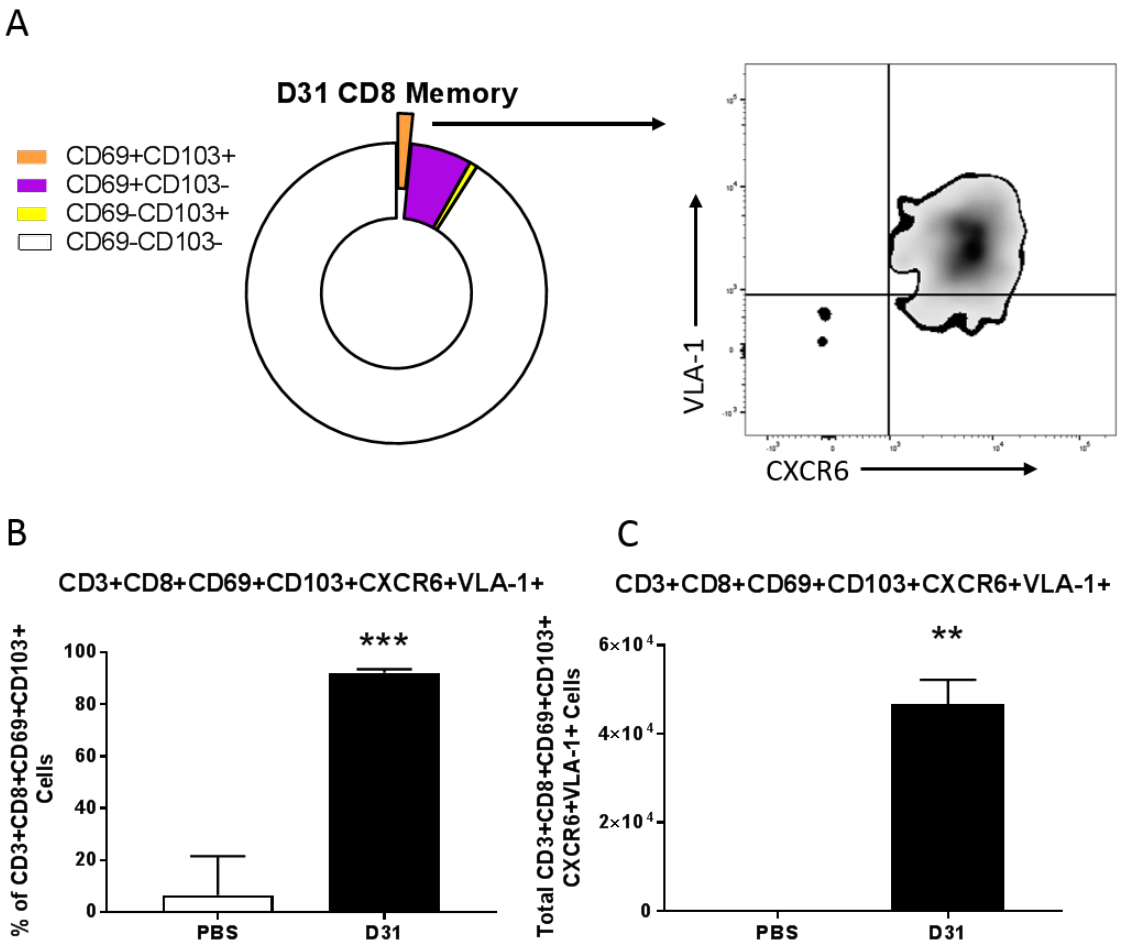

Fig. 5.8: Phenotype of CD69$^+$CD103$^+$ CD8 Trms in the lung of sublehthally infected mice. C57BL/6J mice (4-5 mice/group) were inoculated with 1.0 x 10^5 of *O. tsutsugamushi* Karp strain. At 31 days post infection, single-cell suspensions were prepared from the lungs for flow cytometric analysis. (A) Flow cytometry analysis from the CD8$^+$CD69$^+$CD103$^+$ (orange) population. This population was analyzed for VLA-1/CXCR6 expression (A, right panel). (B) Percentage and total cells (C) of VLA-1$^+$CXCR6$^+$ within the CD8$^+$CD69$^+$CD103$^+$ cells. Graphs are shown as mean +/- SEM. T-test with Welch's correction was used for statistical analysis. **, $p < 0.01$; and ***, $p<0.001$ compared to PBS controls.

To our knowledge this is the first work to identify pulmonary Trms after *O. tsutsugamushi* infection. Our results demonstrate the presence of a CD69$^+$CD103$^+$ CD8 T cell population after infection that express markers typical to Trms evaluated in other models [158, 159, 162]. Further experiments are needed to assess the protective capabilities

of these CD8 cells and to determine the ability of these cells to recognize and respond to various *O. tsutsugamushi* antigens. Previous work in *Bordetella pertussis* has demonstrated that adoptive transfer of lung CD4 Trms to naïve mice provided protection upon *B. pertussis* challenge [163]. Similar work to transfer the CD8 Trms we observe in the lung may allow us to understand what role this $CD69^{+}CD103^{+}$ population plays upon reinfection with *O. tsutsugamushi*. It is interesting that the $CD69^{+}CD103^{+}$ T cell population only emerged in the CD8 T cells; however, this finding may be expected as our own flow cytometry analysis and others have shown that the T cell population in the lung skews to a predominately CD8 T cell response late in *O. tsutsugamushi* infection (**Fig. 3.10**; [101]). Understanding what cells generated after infection provide long term, effective protection is critical to understand how immunity is generated in scrub typhus and for the development of an optimal vaccine candidate.

Concluding Remarks

Work in this dissertation has been to characterize specific immune responses in the lungs of mice infected with *O. tsutsugamushi*. Understanding the strong inflammatory response generated during scrub typhus and what is protective vs. pathogenic is an important area of study not only in *Orientia* but in many related pathogens. Research regarding specific alterations in the innate and adaptive immune response that occur during severe scrub typhus are sparse. Basic questions regarding endothelial dysfunction, immunopathogenic roles of innate inflammatory cells, and establishment of an adaptive memory response remain largely unanswered in scrub typhus. The utilization of new technologies (e.g, single-cell RNA sequencing, cell fate mapping, and cell-specific *cre-flox* deletions in mice) would help address some of the unanswered questions an unexpected findings from this dissertation. Such new approaches will bring much needed answers

regarding the specific interactions of host cells during infection with this deadly pathogen. As scrub typhus outbreaks continue to happen at an increasing rate, this research is timely and important.

References

1. Xu G, Mendell NL, Liang Y, Shelite TR, Goez-Rivillas Y, Soong L, et al. Correction: CD8+ T cells provide immune protection against murine disseminated endotheliotropic *Orientia tsutsugamushi* infection. PLoS Negl Trop Dis. 2017;11(12):e0006127. Epub 2017/12/06. doi: 10.1371/journal.pntd.0006127. PubMed PMID: 29211737; PubMed Central PMCID: PMCPMC5718426.

2. Hsu YH, Chen HI. Pulmonary pathology in patients associated with scrub typhus. Pathology. 2008;40(3):268-71. doi: 10.1080/00313020801911488. PubMed PMID: 18428046.

3. Soong L, Wang H, Shelite TR, Liang Y, Mendell NL, Sun J, et al. Strong type 1, but impaired type 2, immune responses contribute to *Orientia tsutsugamushi*-induced pathology in mice. PLoS Negl Trop Dis. 2014;8(9):e3191. doi: 10.1371/journal.pntd.0003191. PubMed PMID: 25254971; PubMed Central PMCID: PMCPMC4177881.

4. Mendell NL, Bouyer DH, Walker DH. Murine models of scrub typhus associated with host control of *Orientia tsutsugamushi* infection. PLoS Negl Trop Dis. 2017;11(3):e0005453. Epub 2017/03/10. doi: 10.1371/journal.pntd.0005453. PubMed PMID: 28282373; PubMed Central PMCID: PMCPMC5362142.

5. Paris DH, Phetsouvanh R, Tanganuchitcharnchai A, Jones M, Jenjaroen K, Vongsouvath M, et al. *Orientia tsutsugamushi* in human scrub typhus eschars shows tropism for dendritic cells and monocytes rather than endothelium. PLoS Negl Trop Dis. 2012;6(1):e1466. Epub 2012/01/10. doi: 10.1371/journal.pntd.0001466. PubMed PMID: 22253938; PubMed Central PMCID: PMCPMC3254662.

6. Moron CG, Popov VL, Feng HM, Wear D, Walker DH. Identification of the target cells of *Orientia tsutsugamushi* in human cases of scrub typhus. Mod Pathol. 2001;14(8):752-9. doi: 10.1038/modpathol.3880385. PubMed PMID: 11504834.

7. Varghese GM, Janardhanan J, Trowbridge P, Peter JV, Prakash JA, Sathyendra S, et al. Scrub typhus in South India: clinical and laboratory manifestations, genetic variability, and outcome. Int J Infect Dis. 2013;17(11):e981-7. Epub 2013/07/26. doi: 10.1016/j.ijid.2013.05.017. PubMed PMID: 23891643.

8. Wang CC, Liu SF, Liu JW, Chung YH, Su MC, Lin MC. Acute respiratory distress syndrome in scrub typhus. Am J Trop Med Hyg. 2007;76(6):1148-52. PubMed PMID: 17556627.

9. Zhao D, Zhang Y, Yin Z, Zhao J, Yang D, Zhou Q. Clinical Predictors of Multiple Organ Dysfunction Syndromes in Pediatric patients with Scrub Typhus. J Trop Pediatr. 2017;63(3):167-73. doi: 10.1093/tropej/fmw066. PubMed PMID: 27697827.

10. Taylor AJ, Paris DH, Newton PN. A Systematic Review of Mortality from Untreated Scrub Typhus (*Orientia tsutsugamushi*). PLoS Negl Trop Dis. 2015;9(8):e0003971. doi: 10.1371/journal.pntd.0003971. PubMed PMID: 26274584; PubMed Central PMCID: PMCPMC4537241.

11. Jayasimha K, Varma M, Kamath A, Bairy I, Singh R, Mounika S, et al. Risk factors of acute respiratory distress syndrome in Scrub typhus. International Journal of Research in Medical Sciences. 2017;5(9):3912-5. Epub September 2017.

12. Brown GW, Robinson DM, Huxsoll DL, Ng TS, Lim KJ. Scrub typhus: a common cause of illness in indigenous populations. Trans R Soc Trop Med Hyg. 1976;70(5-6):444-8. PubMed PMID: 402722.

13. Phongmany S, Rolain JM, Phetsouvanh R, Blacksell SD, Soukkhaseum V, Rasachack B, et al. Rickettsial infections and fever, Vientiane, Laos. Emerg Infect Dis. 2006;12(2):256-62. doi: 10.3201/eid1202.050900. PubMed PMID: 16494751; PubMed Central PMCID: PMCPMC3373100.

14. Chakraborty S, Sarma N. Scrub Typhus: An Emerging Threat. Indian J Dermatol. 2017;62(5):478-85. doi: 10.4103/ijd.IJD_388_17. PubMed PMID: 28979009; PubMed Central PMCID: PMCPMC5618834.

15. Min KD, Cho SI. Mathematical Modeling for Scrub Typhus and Its Implications for Disease Control. J Korean Med Sci. 2018;33(12):e98. Epub 2018/03/19. doi: 10.3346/jkms.2018.33.e98. PubMed PMID: 29542303; PubMed Central PMCID: PMCPMC5852423.

16. Weitzel T, Dittrich S, López J, Phuklia W, Martinez-Valdebenito C, Velásquez K, et al. Endemic Scrub Typhus in South America. N Engl J Med. 2016;375(10):954-61. doi: 10.1056/NEJMoa1603657. PubMed PMID: 27602667.

17. Kawamura R. Studies on tsutsugamushi disease (Japanese blood fever): Spokesman printing company; 1926.

18. Philip CB. Tsutsugamushi disease in World War II. J Parasitol. 1948;34(3):169-91. PubMed PMID: 18867393.

19. Luce-Fedrow A, Lehman ML, Kelly DJ, Mullins K, Maina AN, Stewart RL, et al. A Review of Scrub Typhus (*Orientia tsutsugamushi* and Related Organisms): Then, Now, and Tomorrow. Trop Med Infect Dis. 2018;3(1). doi: 10.3390/tropicalmed3010008. PubMed PMID: 30274407; PubMed Central PMCID: PMCPMC6136631.

20. Theodore W. NTRODUCTION TO THE HISTORY OF THE ARMED FORCES MEDICAL UNIT IN KUALA LUMPUR MALAYA AND THE ARMED FORCES RESEARCH INSTITUTE OF MEDICAL SCIENCES (AFRIMS) IN BANGKOK, THAILAND. Walter Army Research Institute, 1987.

21. Berman SJ, Irving GS, Kundin WD, Gunning JJ, Watten RH. Epidemiology of the acute fevers of unknown origin in South Vietnam: effect of laboratory support upon clinical diagnosis. Am J Trop Med Hyg. 1973;22(6):796-801. PubMed PMID: 4355456.

22. Kelly DJ, Richards AL, Temenak J, Strickman D, Dasch GA. The past and present threat of rickettsial diseases to military medicine and international public health. Clin Infect Dis. 2002;34(Suppl 4):S145-69. doi: 10.1086/339908. PubMed PMID: 12016590.

23. Dangerfield HG. Some clinical and epidemiological observations on scrub typhus in the Republic of Vietnam. Vietnam report: US Army Medical Research Team (WRAIR), Army Dot; 1967.

24. Song SW, Kim KT, Ku YM, Park SH, Kim YS, Lee DG, et al. Clinical role of interstitial pneumonia in patients with scrub typhus: a possible marker of disease severity. J Korean Med Sci. 2004;19(5):668-73. doi: 10.3346/jkms.2004.19.5.668. PubMed PMID: 15483341; PubMed Central PMCID: PMCPMC2816328.

25. Jeong YJ, Kim S, Wook YD, Lee JW, Kim KI, Lee SH. Scrub typhus: clinical, pathologic, and imaging findings. Radiographics. 2007;27(1):161-72. doi: 10.1148/rg.271065074. PubMed PMID: 17235005.

26. Longo DL, Harrison TR. Harrison's principles of internal medicine. 18th ed. New York: McGraw-Hill; 2012.

27. Varghese GM, Trowbridge P, Janardhanan J, Thomas K, Peter JV, Mathews P, et al. Clinical profile and improving mortality trend of scrub typhus in South India. Int J Infect Dis. 2014;23:39-43. Epub 2014/03/21. doi: 10.1016/j.ijid.2014.02.009. PubMed PMID: 24661931.

28. Tsay RW, Chang FY. Acute respiratory distress syndrome in scrub typhus. QJM. 2002;95(2):126-8. PubMed PMID: 11861962.

29. Abhilash K, Mannam PR, Rajendran K, John RA, Ramasami P. Chest radiographic manifestations of scrub typhus. J Postgrad Med. 2016;62(4):235-8. doi: 10.4103/0022-3859.184662. PubMed PMID: 27763480; PubMed Central PMCID: PMCPMC5105208.

30. Sahoo JN, Gurjar M, Harde Y. Acute respiratory failure in scrub typhus patients. Indian J Crit Care Med. 2016;20(8):480-4. doi: 10.4103/0972-5229.188206. PubMed PMID: 27630462; PubMed Central PMCID: PMCPMC4994130.

31. Shelite TR, Saito TB, Mendell NL, Gong B, Xu G, Soong L, et al. Hematogenously disseminated *Orientia tsutsugamushi*-infected murine model of scrub typhus [corrected]. PLoS Negl Trop Dis. 2014;8(7):e2966. doi: 10.1371/journal.pntd.0002966. PubMed PMID: 25010338; PubMed Central PMCID: PMCPMC4091938.

32. Keller CA, Hauptmann M, Kolbaum J, Gharaibeh M, Neumann M, Glatzel M, et al. Dissemination of *Orientia tsutsugamushi* and inflammatory responses in a murine model of scrub typhus. PLoS Negl Trop Dis. 2014;8(8):e3064. Epub 2014/08/14. doi: 10.1371/journal.pntd.0003064. PubMed PMID: 25122501; PubMed Central PMCID: PMCPMC4133189.

33. Kim MK, Kee SH, Cho KA, Chung MH, Lim BU, Chang WH, et al. Apoptosis of endothelial cell line ECV304 persistently infected with *Orientia tsutsugamushi*. Microbiol Immunol. 1999;43(8):751-7. PubMed PMID: 10524792.

34. Cho NH, Seong SY, Choi MS, Kim IS. Expression of chemokine genes in human dermal microvascular endothelial cell lines infected with *Orientia tsutsugamushi*. Infect Immun. 2001;69(3):1265-72. doi: 10.1128/IAI.69.3.1265-1272.2001. PubMed PMID: 11179287; PubMed Central PMCID: PMCPMC98016.

35. Cho KA, Jun YH, Suh JW, Kang JS, Choi HJ, Woo SY. *Orientia tsutsugamushi* induced endothelial cell activation via the NOD1-IL-32 pathway. Microb Pathog. 2010;49(3):95-104. Epub 2010/05/12. doi: 10.1016/j.micpath.2010.05.001. PubMed PMID: 20470879.

36. Matthay MA, Zemans RL. The acute respiratory distress syndrome: pathogenesis and treatment. Annu Rev Pathol. 2011;6:147-63. doi: 10.1146/annurev-pathol-011110-130158. PubMed PMID: 20936936; PubMed Central PMCID: PMCPMC3108259.

37. Gonzales JN, Lucas R, Verin AD. The Acute Respiratory Distress Syndrome: Mechanisms and Perspective Therapeutic Approaches. Austin J Vasc Med. 2015;2(1). PubMed PMID: 26973981; PubMed Central PMCID: PMCPMC4786180.

38. Orfanos SE, Mavrommati I, Korovesi I, Roussos C. Pulmonary endothelium in acute lung injury: from basic science to the critically ill. Intensive Care Med. 2004;30(9):1702-14. Epub 2004/07/16. doi: 10.1007/s00134-004-2370-x. PubMed PMID: 15258728.

39. Mai J, Virtue A, Shen J, Wang H, Yang XF. An evolving new paradigm: endothelial cells--conditional innate immune cells. J Hematol Oncol. 2013;6:61. Epub 2013/08/22. doi: 10.1186/1756-8722-6-61. PubMed PMID: 23965413; PubMed Central PMCID: PMCPMC3765446.

40. Moussa MD, Santonocito C, Fagnoul D, Donadello K, Pradier O, Gaussem P, et al. Evaluation of endothelial damage in sepsis-related ARDS using circulating endothelial cells. Intensive Care Med. 2015;41(2):231-8. Epub 2014/12/16. doi: 10.1007/s00134-014-3589-9. PubMed PMID: 25510299.

41. Silliman CC, Curtis BR, Kopko PM, Khan SY, Kelher MR, Schuller RM, et al. Donor antibodies to HNA-3a implicated in TRALI reactions prime neutrophils and cause PMN-mediated damage to human pulmonary microvascular endothelial cells in a two-event in vitro model. Blood. 2007;109(4):1752-5. Epub 2006/10/12. doi: 10.1182/blood-

2006-05-025106. PubMed PMID: 17038531; PubMed Central PMCID: PMCPMC1794055.

42. Gill SE, Rohan M, Mehta S. Role of pulmonary microvascular endothelial cell apoptosis in murine sepsis-induced lung injury in vivo. Respir Res. 2015;16:109. Epub 2015/09/16. doi: 10.1186/s12931-015-0266-7. PubMed PMID: 26376777; PubMed Central PMCID: PMCPMC4574190.

43. Soong L, Mendell NL, Olano JP, Rockx-Brouwer D, Xu G, Goez-Rivillas Y, et al. An Intradermal Inoculation Mouse Model for Immunological Investigations of Acute Scrub Typhus and Persistent Infection. PLoS Negl Trop Dis. 2016;10(8):e0004884. Epub 2016/08/01. doi: 10.1371/journal.pntd.0004884. PubMed PMID: 27479584; PubMed Central PMCID: PMCPMC4968841.

44. Sunyakumthorn P, Paris DH, Chan TC, Jones M, Luce-Fedrow A, Chattopadhyay S, et al. An intradermal inoculation model of scrub typhus in Swiss CD-1 mice demonstrates more rapid dissemination of virulent strains of *Orientia tsutsugamushi*. PLoS One. 2013;8(1):e54570. Epub 2013/01/16. doi: 10.1371/journal.pone.0054570. PubMed PMID: 23342173; PubMed Central PMCID: PMCPMC3546997.

45. Sunyakumthorn P, Somponpun SJ, Im-Erbsin R, Anantatat T, Jenjaroen K, Dunachie SJ, et al. Characterization of the rhesus macaque (Macaca mulatta) scrub typhus model: Susceptibility to intradermal challenge with the human pathogen *Orientia tsutsugamushi* Karp. PLoS Negl Trop Dis. 2018;12(3):e0006305. Epub 2018/03/09. doi: 10.1371/journal.pntd.0006305. PubMed PMID: 29522521; PubMed Central PMCID: PMCPMC5862536.

46. Otterdal K, Janardhanan J, Astrup E, Ueland T, Prakash JA, Lekva T, et al. Increased endothelial and macrophage markers are associated with disease severity and mortality in scrub typhus. J Infect. 2014;69(5):462-9. Epub 2014/07/01. doi: 10.1016/j.jinf.2014.06.018. PubMed PMID: 24995849.

47. Shelite TR, Liang Y, Wang H, Mendell NL, Trent BJ, Sun J, et al. IL-33-Dependent Endothelial Activation Contributes to Apoptosis and Renal Injury in *Orientia tsutsugamushi*-Infected Mice. PLoS Negl Trop Dis. 2016;10(3):e0004467. doi: 10.1371/journal.pntd.0004467. PubMed PMID: 26943125; PubMed Central PMCID: PMCPMC4778942.

48. Cayrol C, Girard JP. The IL-1-like cytokine IL-33 is inactivated after maturation by caspase-1. Proc Natl Acad Sci U S A. 2009;106(22):9021-6. Epub 2009/05/13. doi: 10.1073/pnas.0812690106. PubMed PMID: 19439663; PubMed Central PMCID: PMCPMC2690027.

49. Gautier V, Cayrol C, Farache D, Roga S, Monsarrat B, Burlet-Schiltz O, et al. Extracellular IL-33 cytokine, but not endogenous nuclear IL-33, regulates protein expression in endothelial cells. Sci Rep. 2016;6:34255. Epub 2016/10/03. doi: 10.1038/srep34255. PubMed PMID: 27694941; PubMed Central PMCID: PMCPMC5046127.

50. Thurston G, Daly C. The complex role of angiopoietin-2 in the angiopoietin-tie signaling pathway. Cold Spring Harb Perspect Med. 2012;2(9):a006550. Epub 2012/09/01. doi: 10.1101/cshperspect.a006650. PubMed PMID: 22951441; PubMed Central PMCID: PMCPMC3426817.

51. van Meurs M, Kümpers P, Ligtenberg JJ, Meertens JH, Molema G, Zijlstra JG. Bench-to-bedside review: Angiopoietin signalling in critical illness - a future target? Crit Care. 2009;13(2):207. Epub 2009/03/09. doi: 10.1186/cc7153. PubMed PMID: 19435476; PubMed Central PMCID: PMCPMC2689450.

52. Wada T, Jesmin S, Gando S, Yanagida Y, Mizugaki A, Sultana SN, et al. The role of angiogenic factors and their soluble receptors in acute lung injury (ALI)/ acute respiratory distress syndrome (ARDS) associated with critical illness. J Inflamm (Lond). 2013;10(1):6. Epub 2013/02/11. doi: 10.1186/1476-9255-10-6. PubMed PMID: 23394254; PubMed Central PMCID: PMCPMC3574858.

53. Tsangaris I, Tsantes A, Vrigkou E, Kopterides P, Pelekanou A, Zerva K, et al. Angiopoietin-2 Levels as Predictors of Outcome in Mechanically Ventilated Patients with Acute Respiratory Distress Syndrome. Dis Markers. 2017;2017:6758721. Epub 2017/08/29. doi: 10.1155/2017/6758721. PubMed PMID: 28947844; PubMed Central PMCID: PMCPMC5602490.

54. Ghosh CC, David S, Zhang R, Berghelli A, Milam K, Higgins SJ, et al. Gene control of tyrosine kinase TIE2 and vascular manifestations of infections. Proc Natl Acad Sci U S A. 2016;113(9):2472-7. Epub 2016/02/16. doi: 10.1073/pnas.1519467113. PubMed PMID: 26884170; PubMed Central PMCID: PMCPMC4780619.

55. Higgins SJ, Purcell LA, Silver KL, Tran V, Crowley V, Hawkes M, et al. Dysregulation of angiopoietin-1 plays a mechanistic role in the pathogenesis of cerebral malaria. Sci Transl Med. 2016;8(358):358ra128. doi: 10.1126/scitranslmed.aaf6812. PubMed PMID: 27683553.

56. David S, Park JK, Meurs M, Zijlstra JG, Koenecke C, Schrimpf C, et al. Acute administration of recombinant Angiopoietin-1 ameliorates multiple-organ dysfunction syndrome and improves survival in murine sepsis. Cytokine. 2011;55(2):251-9. Epub 2011/04/30. doi: 10.1016/j.cyto.2011.04.005. PubMed PMID: 21531574.

57. Stiehl T, Thamm K, Kaufmann J, Schaeper U, Kirsch T, Haller H, et al. Lung-targeted RNA interference against angiopoietin-2 ameliorates multiple organ dysfunction and death in sepsis. Crit Care Med. 2014;42(10):e654-62. doi: 10.1097/CCM.0000000000000524. PubMed PMID: 25083983.

58. Summers C, Rankin SM, Condliffe AM, Singh N, Peters AM, Chilvers ER. Neutrophil kinetics in health and disease. Trends Immunol. 2010;31(8):318-24. doi: 10.1016/j.it.2010.05.006. PubMed PMID: 20620114; PubMed Central PMCID: PMCPMC2930213.

59. Bou Ghanem EN, Clark S, Roggensack SE, McIver SR, Alcaide P, Haydon PG, et al. Extracellular Adenosine Protects against *Streptococcus pneumoniae* Lung Infection by Regulating Pulmonary Neutrophil Recruitment. PLoS Pathog. 2015;11(8):e1005126. doi: 10.1371/journal.ppat.1005126. PubMed PMID: 26313746; PubMed Central PMCID: PMCPMC4552087.

60. Witter AR, Okunnu BM, Berg RE. The Essential Role of Neutrophils during Infection with the Intracellular Bacterial Pathogen *Listeria monocytogenes*. J Immunol. 2016;197(5):1557-65. doi: 10.4049/jimmunol.1600599. PubMed PMID: 27543669; PubMed Central PMCID: PMCPMC4995063.

61. Saffarzadeh M, Juenemann C, Queisser MA, Lochnit G, Barreto G, Galuska SP, et al. Neutrophil extracellular traps directly induce epithelial and endothelial cell death: a predominant role of histones. PLoS One. 2012;7(2):e32366. doi: 10.1371/journal.pone.0032366. PubMed PMID: 22389696; PubMed Central PMCID: PMCPMC3289648.

62. Lin SH, Fu J, Wang CJ, Gao F, Feng XY, Liu Q, et al. Inflammation elevated IL-33 originating from the lung mediates inflammation in acute lung injury. Clin Immunol. 2016. Epub 2016/10/28. doi: 10.1016/j.clim.2016.10.014. PubMed PMID: 27989898.

63. Grommes J, Soehnlein O. Contribution of neutrophils to acute lung injury. Mol Med. 2011;17(3-4):293-307. doi: 10.2119/molmed.2010.00138. PubMed PMID: 21046059; PubMed Central PMCID: PMCPMC3060975.

64. Sercundes MK, Ortolan LS, Debone D, Soeiro-Pereira PV, Gomes E, Aitken EH, et al. Targeting Neutrophils to Prevent Malaria-Associated Acute Lung Injury/Acute Respiratory Distress Syndrome in Mice. PLoS Pathog. 2016;12(12):e1006054. Epub 2016/12/07. doi: 10.1371/journal.ppat.1006054. PubMed PMID: 27926944; PubMed Central PMCID: PMCPMC5142790.

65. Rikihisa Y, Ito S. Entry of *Rickettsia tsutsugamushi* into polymorphonuclear leukocytes. Infect Immun. 1982;38(1):343-50. PubMed PMID: 6815091; PubMed Central PMCID: PMCPMC347736.

66. Girbl T, Lenn T, Perez L, Rolas L, Barkaway A, Thiriot A, et al. Distinct Compartmentalization of the Chemokines CXCL1 and CXCL2 and the Atypical Receptor ACKR1 Determine Discrete Stages of Neutrophil Diapedesis. Immunity. 2018;49(6):1062-76.e6. Epub 2018/11/13. doi: 10.1016/j.immuni.2018.09.018. PubMed PMID: 30446388; PubMed Central PMCID: PMCPMC6303217.

67. Rizvi M, Sultan A, Chowdhry M, Azam M, Khan F, Shukla I, et al. Prevalence of scrub typhus in pyrexia of unknown origin and assessment of interleukin-8, tumor necrosis factor-alpha, and interferon-gamma levels in scrub typhus-positive patients. Indian J Pathol Microbiol. 2018;61(1):76-80. doi: 10.4103/IJPM.IJPM_644_16. PubMed PMID: 29567888.

68. Chollet-Martin S, Montravers P, Gibert C, Elbim C, Desmonts JM, Fagon JY, et al. High levels of interleukin-8 in the blood and alveolar spaces of patients with pneumonia and adult respiratory distress syndrome. Infect Immun. 1993;61(11):4553-9. PubMed PMID: 8406851; PubMed Central PMCID: PMCPMC281204.

69. Allen TC, Kurdowska A. Interleukin 8 and acute lung injury. Arch Pathol Lab Med. 2014;138(2):266-9. Epub 2013/06/19. doi: 10.5858/arpa.2013-0182-RA. PubMed PMID: 23782136.

70. Astrup E, Janardhanan J, Otterdal K, Ueland T, Prakash JA, Lekva T, et al. Cytokine network in scrub typhus: high levels of interleukin-8 are associated with disease severity and mortality. PLoS Negl Trop Dis. 2014;8(2):e2648. Epub 2014/02/06. doi: 10.1371/journal.pntd.0002648. PubMed PMID: 24516677; PubMed Central PMCID: PMCPMC3916254.

71. Sônego F, Castanheira FV, Ferreira RG, Kanashiro A, Leite CA, Nascimento DC, et al. Paradoxical Roles of the Neutrophil in Sepsis: Protective and Deleterious. Front Immunol. 2016;7:155. Epub 2016/04/26. doi: 10.3389/fimmu.2016.00155. PubMed PMID: 27199981; PubMed Central PMCID: PMCPMC4844928.

72. Paris DH, Stephan F, Bulder I, Wouters D, van der Poll T, Newton PN, et al. Increased Nucleosomes and Neutrophil Activation Link to Disease Progression in Patients with Scrub Typhus but Not Murine Typhus in Laos. PLoS Negl Trop Dis. 2015;9(8):e0003990. doi: 10.1371/journal.pntd.0003990. PubMed PMID: 26317419; PubMed Central PMCID: PMCPMC4552835.

73. Park EC, Lee SY, Yun SH, Choi CW, Lee H, Song HS, et al. Clinical proteomic analysis of scrub typhus infection. Clin Proteomics. 2018;15:6. Epub 2018/02/14. doi: 10.1186/s12014-018-9181-5. PubMed PMID: 29449793; PubMed Central PMCID: PMCPMC5812041.

74. Lefrançais E, Mallavia B, Zhuo H, Calfee CS, Looney MR. Maladaptive role of neutrophil extracellular traps in pathogen-induced lung injury. JCI Insight. 2018;3(3). Epub 2018/02/08. doi: 10.1172/jci.insight.98178. PubMed PMID: 29415887; PubMed Central PMCID: PMCPMC5821185.

75. Huang X, Xiu H, Zhang S, Zhang G. The Role of Macrophages in the Pathogenesis of ALI/ARDS. Mediators Inflamm. 2018;2018:1264913. Epub 2018/05/13. doi: 10.1155/2018/1264913. PubMed PMID: 29950923; PubMed Central PMCID: PMCPMC5989173.

76. Eyal FG, Hamm CR, Parker JC. Reduction in alveolar macrophages attenuates acute ventilator induced lung injury in rats. Intensive Care Med. 2007;33(7):1212-8. Epub 2007/04/28. doi: 10.1007/s00134-007-0651-x. PubMed PMID: 17468847.

77. Narasaraju T, Yang E, Samy RP, Ng HH, Poh WP, Liew AA, et al. Excessive neutrophils and neutrophil extracellular traps contribute to acute lung injury of influenza

pneumonitis. Am J Pathol. 2011;179(1):199-210. doi: 10.1016/j.ajpath.2011.03.013. PubMed PMID: 21703402; PubMed Central PMCID: PMCPMC3123873.

78. Broug-Holub E, Toews GB, van Iwaarden JF, Strieter RM, Kunkel SL, Paine R, et al. Alveolar macrophages are required for protective pulmonary defenses in murine *Klebsiella pneumonia*: elimination of alveolar macrophages increases neutrophil recruitment but decreases bacterial clearance and survival. Infect Immun. 1997;65(4):1139-46. PubMed PMID: 9119443; PubMed Central PMCID: PMCPMC175109.

79. Benoit M, Desnues B, Mege JL. Macrophage polarization in bacterial infections. J Immunol. 2008;181(6):3733-9. PubMed PMID: 18768823.

80. Aggarwal NR, King LS, D'Alessio FR. Diverse macrophage populations mediate acute lung inflammation and resolution. Am J Physiol Lung Cell Mol Physiol. 2014;306(8):L709-25. Epub 2014/02/07. doi: 10.1152/ajplung.00341.2013. PubMed PMID: 24508730; PubMed Central PMCID: PMCPMC3989724.

81. D'Alessio FR, Craig JM, Singer BD, Files DC, Mock JR, Garibaldi BT, et al. Enhanced resolution of experimental ARDS through IL-4-mediated lung macrophage reprogramming. Am J Physiol Lung Cell Mol Physiol. 2016;310(8):L733-46. Epub 2016/02/19. doi: 10.1152/ajplung.00419.2015. PubMed PMID: 26895644; PubMed Central PMCID: PMCPMC4836113.

82. Lu HL, Huang XY, Luo YF, Tan WP, Chen PF, Guo YB. Activation of M1 macrophages plays a critical role in the initiation of acute lung injury. Biosci Rep. 2018;38(2). Epub 2018/04/27. doi: 10.1042/BSR20171555. PubMed PMID: 29531017; PubMed Central PMCID: PMCPMC5920144.

83. Vergadi E, Vaporidi K, Theodorakis EE, Doxaki C, Lagoudaki E, Ieronymaki E, et al. Akt2 deficiency protects from acute lung injury via alternative macrophage activation and miR-146a induction in mice. J Immunol. 2014;192(1):394-406. Epub 2013/11/25. doi: 10.4049/jimmunol.1300959. PubMed PMID: 24277697.

84. Cho NH, Seong SY, Huh MS, Han TH, Koh YS, Choi MS, et al. Expression of chemokine genes in murine macrophages infected with *Orientia tsutsugamushi*. Infect Immun. 2000;68(2):594-602. PubMed PMID: 10639422; PubMed Central PMCID: PMCPMC97181.

85. Koo JE, Hong HJ, Dearth A, Kobayashi KS, Koh YS. Intracellular invasion of *Orientia tsutsugamushi* activates inflammasome in asc-dependent manner. PLoS One. 2012;7(6):e39042. Epub 2012/06/18. doi: 10.1371/journal.pone.0039042. PubMed PMID: 22723924; PubMed Central PMCID: PMCPMC3377614.

86. Yun JH, Koo JE, Koh YS. Mitogen-activated protein kinases are involved in tumor necrosis factor alpha production in macrophages infected with *Orientia tsutsugamushi*. Microbiol Immunol. 2009;53(6):349-55. doi: 10.1111/j.1348-0421.2009.00127.x. PubMed PMID: 19493203.

87. Díaz FE, Abarca K, Kalergis AM. An Update on Host-Pathogen Interplay and Modulation of Immune Responses during *Orientia tsutsugamushi* Infection. Clin Microbiol Rev. 2018;31(2). Epub 2018/01/31. doi: 10.1128/CMR.00076-17. PubMed PMID: 29386235; PubMed Central PMCID: PMCPMC5967693.

88. Tsai MH, Chang CH, Tsai RK, Hong YR, Chuang TH, Fan KT, et al. Cross-Regulation of Proinflammatory Cytokines by Interleukin-10 and miR-155 in *Orientia tsutsugamushi*-Infected Human Macrophages Prevents Cytokine Storm. J Invest Dermatol. 2016;136(7):1398-407. Epub 2016/02/24. doi: 10.1016/j.jid.2015.11.034. PubMed PMID: 26921773.

89. Rodino KG, Adcox HE, Martin RK, Patel V, Conrad DH, Carlyon JA. The obligate intracellular bacterium. Infect Immun. 2018. Epub 2018/12/17. doi: 10.1128/IAI.00876-18. PubMed PMID: 30559222.

90. Tantibhedhyangkul W, Prachason T, Waywa D, El Filali A, Ghigo E, Thongnoppakhun W, et al. *Orientia tsutsugamushi* stimulates an original gene expression program in monocytes: relationship with gene expression in patients with scrub typhus. PLoS Negl Trop Dis. 2011;5(5):e1028. Epub 2011/05/17. doi: 10.1371/journal.pntd.0001028. PubMed PMID: 21610853; PubMed Central PMCID: PMCPMC3096591.

91. Drescher B, Bai F. Neutrophil in viral infections, friend or foe? Virus Res. 2013;171(1):1-7. doi: 10.1016/j.virusres.2012.11.002. PubMed PMID: 23178588; PubMed Central PMCID: PMCPMC3557572.

92. Shen XF, Cao K, Jiang JP, Guan WX, Du JF. Neutrophil dysregulation during sepsis: an overview and update. J Cell Mol Med. 2017;21(9):1687-97. doi: 10.1111/jcmm.13112. PubMed PMID: 28244690; PubMed Central PMCID: PMCPMC5571534.

93. Tantibhedhyangkul W, Ben Amara A, Textoris J, Gorvel L, Ghigo E, Capo C, et al. *Orientia tsutsugamushi*, the causative agent of scrub typhus, induces an inflammatory program in human macrophages. Microb Pathog. 2013;55:55-63. Epub 2012/10/23. doi: 10.1016/j.micpath.2012.10.001. PubMed PMID: 23088884.

94. Ogawa M, Satoh M, Kataoka M, Ando S, Saijo M. Nitric oxide enhanced the growth of an obligated intracellular bacterium *Orientia tsutsugamushi* in murine macrophages. Microb Pathog. 2017;107:335-40. Epub 2017/04/12. doi: 10.1016/j.micpath.2017.04.012. PubMed PMID: 28412201.

95. Soong L, Shelite TR, Xing Y, Kodakandla H, Liang Y, Trent BJ, et al. Type 1-skewed neuroinflammation and vascular damage associated with *Orientia tsutsugamushi* infection in mice. PLoS Negl Trop Dis. 2017;11(7):e0005765. Epub 2017/07/24. doi: 10.1371/journal.pntd.0005765. PubMed PMID: 28742087; PubMed Central PMCID: PMCPMC5542690.

96. Singer BD, Mock JR, D'Alessio FR, Aggarwal NR, Mandke P, Johnston L, et al. Flow-cytometric method for simultaneous analysis of mouse lung epithelial, endothelial, and hematopoietic lineage cells. Am J Physiol Lung Cell Mol Physiol. 2016;310(9):L796-801. Epub 2016/03/04. doi: 10.1152/ajplung.00334.2015. PubMed PMID: 26944088; PubMed Central PMCID: PMCPMC4867353.

97. Gong B, Shelite T, Mei FC, Ha T, Hu Y, Xu G, et al. Exchange protein directly activated by cAMP plays a critical role in bacterial invasion during fatal rickettsioses. Proc Natl Acad Sci U S A. 2013;110(48):19615-20. Epub 2013/11/11. doi: 10.1073/pnas.1314400110. PubMed PMID: 24218580; PubMed Central PMCID: PMCPMC3845138.

98. Heitrich M, García DM, Stoyanoff TR, Rodríguez JP, Todaro JS, Aguirre MV. Erythropoietin attenuates renal and pulmonary injury in polymicrobial induced-sepsis through EPO-R, VEGF and VEGF-R2 modulation. Biomed Pharmacother. 2016;82:606-13. Epub 2016/06/11. doi: 10.1016/j.biopha.2016.05.045. PubMed PMID: 27470403.

99. Parikh SM. The Angiopoietin-Tie2 Signaling Axis in Systemic Inflammation. J Am Soc Nephrol. 2017;28(7):1973-82. Epub 2017/05/02. doi: 10.1681/ASN.2017010069. PubMed PMID: 28465380; PubMed Central PMCID: PMCPMC5491297.

100. Soong L. Dysregulated Th1 Immune and Vascular Responses in Scrub Typhus Pathogenesis. J Immunol. 2018;200(4):1233-40. doi: 10.4049/jimmunol.1701219. PubMed PMID: 29431689; PubMed Central PMCID: PMCPMC5812358.

101. Hauptmann M, Kolbaum J, Lilla S, Wozniak D, Gharaibeh M, Fleischer B, et al. Protective and Pathogenic Roles of CD8+ T Lymphocytes in Murine *Orientia tsutsugamushi* Infection. PLoS Negl Trop Dis. 2016;10(9):e0004991. Epub 2016/09/08. doi: 10.1371/journal.pntd.0004991. PubMed PMID: 27606708; PubMed Central PMCID: PMCPMC5015871.

102. Wi YM, Woo HI, Park D, Lee KH, Kang CI, Chung DR, et al. Severe Fever with Thrombocytopenia Syndrome in Patients Suspected of Having Scrub Typhus. Emerg Infect Dis. 2016;22(11):1992-5. doi: 10.3201/eid2211.160597. PubMed PMID: 27767909; PubMed Central PMCID: PMCPMC5088014.

103. Rothlein R, Dustin ML, Marlin SD, Springer TA. A human intercellular adhesion molecule (ICAM-1) distinct from LFA-1. J Immunol. 1986;137(4):1270-4. PubMed PMID: 3525675.

104. Paris DH, Jenjaroen K, Blacksell SD, Phetsouvanh R, Wuthiekanun V, Newton PN, et al. Differential patterns of endothelial and leucocyte activation in 'typhus-like' illnesses in Laos and Thailand. Clin Exp Immunol. 2008;153(1):63-7. Epub 2008/05/23. doi: 10.1111/j.1365-2249.2008.03673.x. PubMed PMID: 18505434; PubMed Central PMCID: PMCPMC2432098.

105. Dejana E, Orsenigo F, Lampugnani MG. The role of adherens junctions and VE-cadherin in the control of vascular permeability. J Cell Sci. 2008;121(Pt 13):2115-22. doi: 10.1242/jcs.017897. PubMed PMID: 18565824.

106. Coon BG, Baeyens N, Han J, Budatha M, Ross TD, Fang JS, et al. Intramembrane binding of VE-cadherin to VEGFR2 and VEGFR3 assembles the endothelial mechanosensory complex. J Cell Biol. 2015;208(7):975-86. Epub 2015/03/23. doi: 10.1083/jcb.201408103. PubMed PMID: 25800053; PubMed Central PMCID: PMCPMC4384728.

107. Phanthanawiboon S, Limkittikul K, Sakai Y, Takakura N, Saijo M, Kurosu T. Acute Systemic Infection with Dengue Virus Leads to Vascular Leakage and Death through Tumor Necrosis Factor-α and Tie2/Angiopoietin Signaling in Mice Lacking Type I and II Interferon Receptors. PLoS One. 2016;11(2):e0148564. Epub 2016/02/04. doi: 10.1371/journal.pone.0148564. PubMed PMID: 26844767; PubMed Central PMCID: PMCPMC4742241.

108. Parikh SM, Mammoto T, Schultz A, Yuan HT, Christiani D, Karumanchi SA, et al. Excess circulating angiopoietin-2 may contribute to pulmonary vascular leak in sepsis in humans. PLoS Med. 2006;3(3):e46. doi: 10.1371/journal.pmed.0030046. PubMed PMID: 16417407; PubMed Central PMCID: PMCPMC1334221.

109. Orfanos SE, Kotanidou A, Glynos C, Athanasiou C, Tsigkos S, Dimopoulou I, et al. Angiopoietin-2 is increased in severe sepsis: correlation with inflammatory mediators. Crit Care Med. 2007;35(1):199-206. doi: 10.1097/01.CCM.0000251640.77679.D7. PubMed PMID: 17110873.

110. Nauseef WM. Myeloperoxidase in human neutrophil host defence. Cell Microbiol. 2014;16(8):1146-55. Epub 2014/06/19. doi: 10.1111/cmi.12312. PubMed PMID: 24844117; PubMed Central PMCID: PMCPMC4301731.

111. Jeyaseelan S, Young SK, Yamamoto M, Arndt PG, Akira S, Kolls JK, et al. Toll/IL-1R domain-containing adaptor protein (TIRAP) is a critical mediator of antibacterial defense in the lung against *Klebsiella pneumoniae* but not *Pseudomonas aeruginosa*. J Immunol. 2006;177(1):538-47. PubMed PMID: 16785551.

112. Garvy BA, Harmsen AG. The importance of neutrophils in resistance to pneumococcal pneumonia in adult and neonatal mice. Inflammation. 1996;20(5):499-512. PubMed PMID: 8894714.

113. Tateda K, Moore TA, Deng JC, Newstead MW, Zeng X, Matsukawa A, et al. Early recruitment of neutrophils determines subsequent T1/T2 host responses in a murine model of *Legionella pneumophila* pneumonia. J Immunol. 2001;166(5):3355-61. PubMed PMID: 11207291.

114. Källquist L, Hansson M, Persson AM, Janssen H, Calafat J, Tapper H, et al. The tetraspanin CD63 is involved in granule targeting of neutrophil elastase. Blood.

2008;112(8):3444-54. Epub 2008/07/31. doi: 10.1182/blood-2007-10-116285. PubMed PMID: 18669870.

115. Gupta AK, Joshi MB, Philippova M, Erne P, Hasler P, Hahn S, et al. Activated endothelial cells induce neutrophil extracellular traps and are susceptible to NETosis-mediated cell death. FEBS Lett. 2010;584(14):3193-7. Epub 2010/06/10. doi: 10.1016/j.febslet.2010.06.006. PubMed PMID: 20541553.

116. Aratani Y. Myeloperoxidase: Its role for host defense, inflammation, and neutrophil function. Arch Biochem Biophys. 2018;640:47-52. Epub 2018/01/11. doi: 10.1016/j.abb.2018.01.004. PubMed PMID: 29336940.

117. Goulopoulou S. Calpain: A Novel Mediator of MPO (Myeloperoxidase)-Induced Endothelial Dysfunction. Hypertension. 2018;71(4):574-6. doi: 10.1161/HYPERTENSIONAHA.118.10441. PubMed PMID: 29507102.

118. Yang Q, Ghose P, Ismail N. Neutrophils mediate immunopathology and negatively regulate protective immune responses during fatal bacterial infection-induced toxic shock. Infect Immun. 2013;81(5):1751-63. doi: 10.1128/IAI.01409-12. PubMed PMID: 23478316; PubMed Central PMCID: PMCPMC3647993.

119. Papp S, Moderzynski K, Rauch J, Heine L, Kuehl S, Richardt U, et al. Liver Necrosis and Lethal Systemic Inflammation in a Murine Model of *Rickettsia typhi* Infection: Role of Neutrophils, Macrophages and NK Cells. PLoS Negl Trop Dis. 2016;10(8):e0004935. doi: 10.1371/journal.pntd.0004935. PubMed PMID: 27548618; PubMed Central PMCID: PMCPMC4993389.

120. Prame Kumar K, Nicholls AJ, Wong CHY. Partners in crime: neutrophils and monocytes/macrophages in inflammation and disease. Cell Tissue Res. 2018;371(3):551-65. doi: 10.1007/s00441-017-2753-2. PubMed PMID: 29387942; PubMed Central PMCID: PMCPMC5820413.

121. Misharin AV, Morales-Nebreda L, Mutlu GM, Budinger GR, Perlman H. Flow cytometric analysis of macrophages and dendritic cell subsets in the mouse lung. Am J Respir Cell Mol Biol. 2013;49(4):503-10. doi: 10.1165/rcmb.2013-0086MA. PubMed PMID: 23672262; PubMed Central PMCID: PMCPMC3824047.

122. Min CK, Kim HI, Ha NY, Kim Y, Kwon EK, Yen NTH, et al. A Type I Interferon and IL-10 Induced by *Orientia tsutsuagmushi* infection supresses antigen-specific T cells and their memory responses. Front Immunol. 2018;9:2022. Epub 2018/09/04. doi: 10.3389/fimmu.2018.02022. PubMed PMID: 30233599; PubMed Central PMCID: PMCPMC6131522.

123. Buchacher T, Ohradanova-Repic A, Stockinger H, Fischer MB, Weber V. M2 Polarization of Human Macrophages Favors Survival of the Intracellular Pathogen *Chlamydia pneumoniae*. PLoS One. 2015;10(11):e0143593. Epub 2015/11/25. doi: 10.1371/journal.pone.0143593. PubMed PMID: 26606059; PubMed Central PMCID: PMCPMC4659546.

124. Ying W, Cheruku PS, Bazer FW, Safe SH, Zhou B. Investigation of macrophage polarization using bone marrow derived macrophages. J Vis Exp. 2013;(76). Epub 2013/06/23. doi: 10.3791/50323. PubMed PMID: 23851980; PubMed Central PMCID: PMCPMC3728835.

125. Wilson HM. SOCS Proteins in Macrophage Polarization and Function. Front Immunol. 2014;5:357. Epub 2014/07/28. doi: 10.3389/fimmu.2014.00357. PubMed PMID: 25120543; PubMed Central PMCID: PMCPMC4112788.

126. Jiang L, Morris EK, Aguilera-Olvera R, Zhang Z, Chan TC, Shashikumar S, et al. Dissemination of. Front Immunol. 2018;9:816. Epub 2018/04/30. doi: 10.3389/fimmu.2018.00816. PubMed PMID: 29760694; PubMed Central PMCID: PMCPMC5936984.

127. Herwig MC, Tsokos M, Hermanns MI, Kirkpatrick CJ, Muller AM. Vascular endothelial cadherin expression in lung specimens of patients with sepsis-induced acute respiratory distress syndrome and endothelial cell cultures. Pathobiology. 2013;80(5):245-51. doi: 10.1159/000347062. PubMed PMID: 23635392.

128. Park I, Kim M, Choe K, Song E, Seo H, Hwang Y, et al. Neutrophils disturb pulmonary microcirculation in sepsis-induced acute lung injury. Eur Respir J. 2019;53(3). doi: 10.1183/13993003.00786-2018. PubMed PMID: 30635296; PubMed Central PMCID: PMCPMC6437604

129. Amano K, Tamura A, Ohashi N, Urakami H, Kaya S, Fukushi K. Deficiency of peptidoglycan and lipopolysaccharide components in *Rickettsia tsutsugamushi*. Infect Immun. 1987;55(9):2290-2. PubMed PMID: 3114150; PubMed Central PMCID: PMCPMC260693.

130. Atwal S, Giengkam S, Chaemchuen S, Dorling J, Kosaisawe N, VanNieuwenhze M, et al. Evidence for a peptidoglycan-like structure in *Orientia tsutsugamushi*. Mol Microbiol. 2017;105(3):440-52. Epub 2017/06/19. doi: 10.1111/mmi.13709. PubMed PMID: 28513097; PubMed Central PMCID: PMCPMC5523937.

131. Gharaibeh M, Hagedorn M, Lilla S, Hauptmann M, Heine H, Fleischer B, et al. Toll-Like Receptor 2 Recognizes *Orientia tsutsugamushi* and Increases Susceptibility to Murine Experimental Scrub Typhus. Infect Immun. 2016;84(12):3379-87. Epub 2016/11/18. doi: 10.1128/IAI.00185-16. PubMed PMID: 27620720; PubMed Central PMCID: PMCPMC5116716.

132. Iwasaki H, Mizoguchi J, Takada N, Tai K, Ikegaya S, Ueda T. Correlation between the concentrations of tumor necrosis factor-alpha and the severity of disease in patients infected with *Orientia tsutsugamushi*. Int J Infect Dis. 2010;14(4):e328-33. Epub 2009/08/20. doi: 10.1016/j.ijid.2009.06.002. PubMed PMID: 19699129.

133. Atri C, Guerfali FZ, Laouini D. Role of Human Macrophage Polarization in Inflammation during Infectious Diseases. Int J Mol Sci. 2018;19(6). doi:

10.3390/ijms19061801. PubMed PMID: 29921749; PubMed Central PMCID: PMCPMC6032107.

134. Kramme S, An le V, Khoa ND, Trin le V, Tannich E, Rybniker J, et al. O*rientia tsutsugamushi* bacteremia and cytokine levels in Vietnamese scrub typhus patients. J Clin Microbiol. 2009;47(3):586-9. doi: 10.1128/JCM.00997-08. PubMed PMID: 19144812; PubMed Central PMCID: PMCPMC2650899.

135. Duque-Correa MA, Kuhl AA, Rodriguez PC, Zedler U, Schommer-Leitner S, Rao M, et al. Macrophage arginase-1 controls bacterial growth and pathology in hypoxic tuberculosis granulomas. Proc Natl Acad Sci U S A. 2014;111(38):E4024-32. doi: 10.1073/pnas.1408839111. PubMed PMID: 25201986; PubMed Central PMCID: PMCPMC4183271.

136. Milam KE, Parikh SM. The angiopoietin-Tie2 signaling axis in the vascular leakage of systemic inflammation. Tissue Barriers. 2015;3(1-2):e957508. Epub 2015/04/03. doi: 10.4161/21688362.2014.957508. PubMed PMID: 25838975; PubMed Central PMCID: PMCPMC4372013.

137. Thurston G, Rudge JS, Ioffe E, Zhou H, Ross L, Croll SD, et al. Angiopoietin-1 protects the adult vasculature against plasma leakage. Nat Med. 2000;6(4):460-3. doi: 10.1038/74725. PubMed PMID: 10742156.

138. Gavard J, Patel V, Gutkind JS. Angiopoietin-1 prevents VEGF-induced endothelial permeability by sequestering Src through mDia. Dev Cell. 2008;14(1):25-36. doi: 10.1016/j.devcel.2007.10.019. PubMed PMID: 18194650.

139. Lomas-Neira JL, Heffernan DS, Ayala A, Monaghan SF. Blockade of Endothelial Growth Factor, Angiopoietin-2, Reduces Indices of Ards and Mortality in Mice Resulting from the Dual-Insults of Hemorrhagic Shock and Sepsis. Shock. 2016;45(2):157-65. doi: 10.1097/SHK.0000000000000499. PubMed PMID: 26529660; PubMed Central PMCID: PMCPMC4715730.

140. Han S, Lee SJ, Kim KE, Lee HS, Oh N, Park I, et al. Amelioration of sepsis by TIE2 activation-induced vascular protection. Sci Transl Med. 2016;8(335):335ra55. doi: 10.1126/scitranslmed.aad9260. PubMed PMID: 27099174.

141. Einbond LS, Soffritti M, Esposti DD, Wu HA, Balick M, Ma H, et al. A transcriptomic analysis of black cohosh: Actein alters cholesterol biosynthesis pathways and synergizes with simvastatin. Food Chem Toxicol. 2018;120:356-66. doi: 10.1016/j.fct.2018.06.064. PubMed PMID: 29969672.

142. Ghosh CC, Thamm K, Berghelli AV, Schrimpf C, Maski MR, Abid T, et al. Drug Repurposing Screen Identifies Foxo1-Dependent Angiopoietin-2 Regulation in Sepsis. Crit Care Med. 2015;43(7):e230-40. doi: 10.1097/CCM.0000000000000993. PubMed PMID: 25855898; PubMed Central PMCID: PMCPMC4806531.

143. Merx MW, Liehn EA, Graf J, van de Sandt A, Schaltenbrand M, Schrader J, et al. Statin treatment after onset of sepsis in a murine model improves survival. Circulation. 2005;112(1):117-24. doi: 10.1161/CIRCULATIONAHA.104.502195. PubMed PMID: 15998696.

144. Kim M, Allen B, Korhonen EA, Nitschké M, Yang HW, Baluk P, et al. Opposing actions of angiopoietin-2 on Tie2 signaling and FOXO1 activation. J Clin Invest. 2016;126(9):3511-25. Epub 2016/08/22. doi: 10.1172/JCI84871. PubMed PMID: 27548529; PubMed Central PMCID: PMCPMC5004955.

145. Fuxe J, Lashnits E, O'Brien S, Baluk P, Tabruyn SP, Kuhnert F, et al. Angiopoietin/Tie2 signaling transforms capillaries into venules primed for leukocyte trafficking in airway inflammation. Am J Pathol. 2010;176(4):2009-18. Epub 2010/02/04. doi: 10.2353/ajpath.2010.090976. PubMed PMID: 20133818; PubMed Central PMCID: PMCPMC2843488.

146. Scholz A, Lang V, Henschler R, Czabanka M, Vajkoczy P, Chavakis E, et al. Angiopoietin-2 promotes myeloid cell infiltration in a beta(2)-integrin-dependent manner. Blood. 2011;118(18):5050-9. doi: 10.1182/blood-2011-03-343293. PubMed PMID: 21868579.

147. Leligdowicz A, Richard-Greenblatt M, Wright J, Crowley VM, Kain KC. Endothelial Activation: The Ang/Tie Axis in Sepsis. Front Immunol. 2018;9:838. doi: 10.3389/fimmu.2018.00838. PubMed PMID: 29740443; PubMed Central PMCID: PMCPMC5928262.

148. Smadel JE, Ley HL, Diercks FH, Paterson PY, Wisseman CL, Traub R. Immunization against scrub typhus: duration of immunity in volunteers following combined living vaccine and chemoprophylaxis. Am J Trop Med Hyg. 1952;1(1):87-99. PubMed PMID: 14903439.

149. MacMillan JG, Rice RM, Jerrells TR. Development of antigen-specific cell-mediated immune responses after infection of cynomolgus monkeys (Macaca fascicularis) with *Rickettsia tsutsugamushi*. J Infect Dis. 1985;152(4):739-49. doi: 10.1093/infdis/152.4.739. PubMed PMID: 2413138.

150. Rights FL, Smadel JE. Studies on scrib typhus; tsutsugamushi disease; heterogenicity of strains of *R. tsutsugamushi* as demonstrated by cross-vaccination studies. J Exp Med. 1948;87(4):339-51. doi: 10.1084/jem.87.4.339. PubMed PMID: 18904219; PubMed Central PMCID: PMCPMC2135778.

151. Ohashi N, Nashimoto H, Ikeda H, Tamura A. Diversity of immunodominant 56-kDa type-specific antigen (TSA) of *Rickettsia tsutsugamushi*. Sequence and comparative analyses of the genes encoding TSA homologues from four antigenic variants. J Biol Chem. 1992;267(18):12728-35. PubMed PMID: 1618776.

152. Shirai A, Catanzaro PJ, Phillips SM, Osterman JV. Host defenses in experimental scrub typhus: role of cellular immunity in heterologous protection. Infect Immun. 1976;14(1):39-46. PubMed PMID: 820646; PubMed Central PMCID: PMCPMC420841.

153. Seong SY, Huh MS, Jang WJ, Park SG, Kim JG, Woo SG, et al. Induction of homologous immune response to *Rickettsia tsutsugamushi* Boryong with a partial 56-kilodalton recombinant antigen fused with the maltose-binding protein MBP-Bor56. Infect Immun. 1997;65(4):1541-5. PubMed PMID: 9119501; PubMed Central PMCID: PMCPMC175167.

154. Jameson SC, Masopust D. Understanding Subset Diversity in T Cell Memory. Immunity. 2018;48(2):214-26. doi: 10.1016/j.immuni.2018.02.010. PubMed PMID: 29466754; PubMed Central PMCID: PMCPMC5863745.

155. Cho BA, Ko Y, Kim YS, Kim S, Choi MS, Kim IS, et al. Phenotypic characterization of peripheral T cells and their dynamics in scrub typhus patients. PLoS Negl Trop Dis. 2012;6(8):e1789. doi: 10.1371/journal.pntd.0001789. PubMed PMID: 22905277; PubMed Central PMCID: PMCPMC3419201.

156. Ha NY, Kim Y, Min CK, Kim HI, Yen NTH, Choi MS, et al. Longevity of antibody and T-cell responses against outer membrane antigens of *Orientia tsutsugamushi* in scrub typhus patients. Emerg Microbes Infect. 2017;6(12):e116. doi: 10.1038/emi.2017.106. PubMed PMID: 29259327; PubMed Central PMCID: PMCPMC5750460.

157. Min CK, Kim HI, Ha NY, Kim Y, Kwon EK, Yen NTH, et al. A Type I Interferon and IL-10 Induced by *Orientia tsutsugamushi* Infection Suppresses Antigen-Specific T Cells and Their Memory Responses. Front Immunol. 2018;9:2022. doi: 10.3389/fimmu.2018.02022. PubMed PMID: 30233599; PubMed Central PMCID: PMCPMC6131522.

158. Haddadi S, Thanthrige-Don N, Afkhami S, Khera A, Jeyanathan M, Xing Z. Expression and role of VLA-1 in resident memory CD8 T cell responses to respiratory mucosal viral-vectored immunization against tuberculosis. Sci Rep. 2017;7(1):9525. doi: 10.1038/s41598-017-09909-4. PubMed PMID: 28842633; PubMed Central PMCID: PMCPMC5573413.

159. Oja AE, Piet B, Helbig C, Stark R, van der Zwan D, Blaauwgeers H, et al. Trigger-happy resident memory CD4(+) T cells inhabit the human lungs. Mucosal Immunol. 2018;11(3):654-67. doi: 10.1038/mi.2017.94. PubMed PMID: 29139478.

160. Ray SJ, Franki SN, Pierce RH, Dimitrova S, Koteliansky V, Sprague AG, et al. The collagen binding alpha1beta1 integrin VLA-1 regulates CD8 T cell-mediated immune protection against heterologous influenza infection. Immunity. 2004;20(2):167-79. PubMed PMID: 14975239.

161. Thomas SY, Banerji A, Medoff BD, Lilly CM, Luster AD. Multiple chemokine receptors, including CCR6 and CXCR3, regulate antigen-induced T cell homing to the

human asthmatic airway. J Immunol. 2007;179(3):1901-12. doi: 10.4049/jimmunol.179.3.1901. PubMed PMID: 17641057.

162. Lee LN, Baban D, Ronan EO, Ragoussis J, Beverley PC, Tchilian EZ. Chemokine gene expression in lung CD8 T cells correlates with protective immunity in mice immunized intra-nasally with Adenovirus-85A. BMC Med Genomics. 2010;3:46. doi: 10.1186/1755-8794-3-46. PubMed PMID: 20942964; PubMed Central PMCID: PMCPMC2967494.

163. Wilk MM, Misiak A, McManus RM, Allen AC, Lynch MA, Mills KHG. Lung CD4 Tissue-Resident Memory T Cells Mediate Adaptive Immunity Induced by Previous Infection of Mice with *Bordetella pertussis*. J Immunol. 2017;199(1):233-43. doi: 10.4049/jimmunol.1602051. PubMed PMID: 28533445.

Vita

Brandon James Trent was born December 15, 1988 in Provo, Utah to parents Peter and TerraLee Trent. Brandon graduated from Liberty High School in Colorado Springs, Colorado in the spring of 2007. After high school, Brandon attended Brigham Young University for a semester before serving a two-year mission for the Church of Jesus Christ of Latter-Day Saints in Buenos Aires, Argentina. Upon return from Buenos Aires, Brandon resumed his studies at Brigham Young University, graduating with a Bachelor of Sciences in microbiology in the winter of 2013. While at Brigham Young, Brandon worked in the microbiology lab of Dr. David Erickson, studying biofilm synthesis in the bacteria *Yersinia pestis*. Brandon continued as a laboratory technician in Dr. Erickson's lab until he enrolled in the Experimental Pathology Ph.D. program at the University of Texas Medical Branch in fall 2014.

Upon entering UTMB, Brandon was awarded the Presidential Scholar Award While at UTMB, Brandon was awarded the T32 Biodefense Training Grant as well as the 2018 AAI Careers in Immunology Fellowship, which provided a combined three years of funding. Brandon also was a member of the Curriculum Development Committees for both the Graduate School of Biomedical Sciences and the Experimental Pathology programs. Brandon served as both Vice President and President of the Experimental Pathology Student Body for two years while at UTMB. Brandon was awarded two travel awards from the UTMB McLaughlin Symposium for presentation of his research. During his time at UTMB, Brandon has become a member of several scientific communities including: American Association of Immunologists (AAI), American Society of Rickettsiology (ASR), and American Society for Microbiology (ASM). Brandon's work at UTMB has allowed him to be co-author on two publications in *PLoS Neglected Tropical Diseases* (IL-33-Dependent Endothelial Activation Contributes to Apoptosis

and Renal Injury in *Orientia tsutsugamushi*-Infected Mice; Type 1-skewed neuroinflammation and vascular damage associated with *Orientia tsutsugamushi* infection in mice). Brandon has also submitted two first author publications. A mini-review article in *Frontiers in Microbiology* (Scrub Typhus Pathogenesis: Innate Immune Response and Lung Injury during *Orientia tsutsugamushi* Infection, submission # 473738), and a research paper in *PLoS Neglected Tropical Diseases* (Polarized Lung Inflammation and Tie2/Angiopoietin-Mediated Endothelial Dysfunction during Severe Orientia tsutsugamushi Infection, submission # PNTD-D-19-01266).

Brandon is married to Camille Hansen Trent since 2012. Together, they have a six month-old son named Theodore.

Permanent address: 524 S. Wisconsin Ave, League City, TX 77573

This dissertation was typed by Brandon Trent